UNIVERSITY OF KWAZULU-NATAL ™

INYUVESI YAKWAZULU-NATALI

Phase Equilibrium measurements to inform the performance and recovery of methanol/TEG mixtures as additives for natural gas dehydration treatment

By

Rahul Raghunanan

Bachelor of Science in Engineering (Chemical Engineering) (UKZN)

Submitted in fulfilment of the academic requirements for the degree of Master of Science in Engineering in the School of Engineering, University of KwaZulu-Natal

February 2024

APPROVALS FOR THESIS SUBMISSION

As the candidate's supervisor, I, Prof, Kuveneshan Moodley, have approved this thesis for submission.

…….. ….……

Prof. Kuveneshan Moodley Date

As the candidate's supervisor, I, Prof. Paramespri Naidoo, have approved this thesis for submission.

…….. ….……

Prof. Paramespri Naidoo Date

As the candidate's supervisor, I, Prof. Wayne Michael Nelson, have approved this thesis for submission.

…….. ….……

Prof. Wayne Michael Nelson Date

Abstract

Dehydration is a crucial step in the processing of raw natural gas. Water, which is naturally found in natural gas deposits, causes a significant problem during transportation, as it forms clathrate hydrates within the gas pipelines. To inhibit this formation, methanol is added to the extracted gas before piping to dehydration facilities where 2,2′-[ethane-1,2-diylbis(oxy)]di(ethan-1-ol) (triethylene glycol (TEG)) is commonly used to remove water from the natural gas. The presence of the methanol inhibitor in the gas affects the water/gas separation using TEG. This effect is not well understood due to the lack of description of the phase behaviour of the relevant multicomponent mixtures in the literature, which is required to design and optimise the gas dehydration process. This can result in ill-conditioned and inaccurate simulations for natural gas process plants, as predictions from binary VLE data alone have been shown to yield inaccurate descriptions of the separation behaviour.

This study aims to further the available knowledge in natural gas processing by conducting high-pressure phase equilibrium measurements, particularly, Pressure-liquid composition x, on novel systems of interest to the Gas Processing Association. This was performed for multicomponent mixtures commonly found in gas dehydration plants, with the measured data modelled using suitable thermodynamic models. The device employed for the vapour-liquid equilibrium measurements was a variable volume high-pressure sapphire cell apparatus. Measurements were conducted for the systems of CH_4 (1) + CH_3OH (2) and CO_2 (1) + TEG (2) + water (2) to test the experimental equipment and method. Novel data were measured for the quaternary system of CH_4 (1) + CH_3OH (2) + TEG (3) + water (4) and the senary system of CH_4 (1) + C_2H_6 (2) + C_3H_8 (3) + CH_3OH (4) + TEG (5) + water (6) at 303.15 K, 313.15 K and 323.15 K.

The verification test measurements were found to correlate well with literature data at similar conditions within the experimental expanded uncertainties of 0.06 K for temperature, 0.04 MPa for pressure, and composition uncertainty of 0.03 for the liquid phase composition. The phase behaviour showed a general proportional relationship between the pressure and light hydro-carbon composition except with the quaternary system, indicating higher solubility at higher pressures.

The data were modelled using the Cubic Plus Association (CPA) equation of state, the Perturbed Chain Statistical Association Fluid Theory model (PC-SAFT) and the Peng and Robinson equation of state (PR). For the quaternary system, the CPA model performed the best, followed by the PC-SAFT and PR models. The absolute average relative deviation (AARD) and absolute average deviation (AAD) for the simultaneous regression of all three isotherms using the CPA model were 6.56%, 3.47% and 6.02% for the AARD values and 0.405 MPa, 0.325 MPa and 0.341 MPa for the AAD(P) values. For the senary

system, the PC-SAFT model performed the best, followed by the CPA and PR models. The AARD and AAD for the simultaneous regression of all three isotherms using the PC-SAFT model were 2.46%, 3.43% and 4.24% for the AARD values and 0.043 MPa, 0.075 MPa and 0.106 MPa for the AAD(P) values. The CPA model exhibited the best performance when considering all measured systems and individual isotherms.

The result of this study contributes toward design improvements and optimization of natural gas dehydration plants using TEG and methanol. Its purpose is to fill the gap currently existing in the available phase equilibrium data of fluid mixtures containing the chemicals investigated in this work.

Declaration: Plagiarism

I, Rahul Raghunanan, declare that.

1. The research reported in this thesis, except where otherwise indicated, is my original research.

2. This thesis has not been submitted for any degree or examination at any other university.

3. This thesis does not contain other persons' data, pictures, graphs or other information, unless specifically acknowledged as being sourced from other persons.

4. This thesis does not contain other persons' writing, unless specifically acknowledged as being sourced from other researchers. Where other written sources have been quoted, then:

> a. Their words have been re-written but the general information attributed to them has been referenced.
>
> b. Where their exact words have been used, then their writing has been placed in italics and inside quotation marks and referenced.

5. This thesis does not contain text, graphics or tables copied and pasted from the Internet, unless specifically acknowledged, and the source being detailed in the thesis and in the References sections.

Signed

……

Acknowledgements

I'd like to first thank my supervisors who guided myself and the research. Special thanks go to:

- Prof P Naidoo for her expertise, knowledge and support during the duration of the study. Her years of experience greatly improved the quality of the research and this dissertation.
- Prof W Nelson for his analytical and systematic approach to all problems and solutions. His attention to detail and detailed knowledge of equipment greatly improved my own experimental efforts.
- Prof K Moodley for his hands-on knowledge, support and understanding throughout the duration of the study. As my main supervisor, Prof K Moodley always went above and beyond to accommodate any issues and was always ready and willing to lend support. His expertise in this field greatly helped the writing and modelling, and this thesis was made possible through his efforts.

Secondly, I would like to thank the members of staff and fellow researchers within the Thermodynamic Research Unit (TRU). Special thanks go to:

- Dr P Zvawanda for his training and constant support during the duration of the study.
- Mr Ayanda Khanyile for his daily help for any laboratory assistance
- Dr Marcin Durski for his support and knowledge
- Dr Phakamile Ndlovu for his support and knowledge

Thirdly I would like to thank my fellow master's students and graduate students. Special thanks go to:

- Bradley Naidoo (Masters); Nikhil Manilal (Masters); Abhay Jagdoe (Graduate); Calista Vishnu (Graduate); Navesan Govender (Undergraduate), for their support and friendship during the duration of the master's study within the TRU.
- Thanks go to a number of friends within the Chemical Engineering Discipline and outside.

Finally, thanks go to my parents Suhren and Pamela Raghunanan and brother Samir Raghunanan, for their constant love and support.

Dedication

This dissertation is dedicated to two individuals who passed away in 2022 during the start of this Master's study. Namely my beloved grandmother, Radha Ramdin, and my dog, Max. Each had a significant and positive impact on my life, and many of my achievements would not be possible without their presence.

Table of Contents

List of Figures

List of Tables

Nomenclature

English letters

Symbols	Descriptions
a	Helmholtz free energy
A_{IJ}	CPA binary interaction parameters
B_{IJ}	CPA binary interaction parameters
b	is the maximum error induced by type B uncertainty or co volume parameter
c	Gas composition uncertainty
CPAAC	Association volume for CPA
CPAAI(K)	Association energy for CPA
CPAAT	Associating type parameter for CPA.
CPAM	M parameter of the alpha function of the CPA model
CPAPC	Critical pressure for the CPA model
CPATC	Monomer critical temperature for the CPA model
Exp	Experimentally measured value
F(r)	Force of attraction or repulsion
G	Molar Gibbs free energy
H	Enthalpy
k	Coverage factor
K	Equilibrium ratio
k	Binary interaction parameter
n	number of moles
N	number of data points
n_D	refractive index
P	Pressure
PCSFAT	Associating type parameter for PC-SAFT
PCSFAU (K)	Association parameter for PC-SAFT
PCSFAV	Temperature dependent parameter for PC-SAFT
PCSFTM	Conventional component parameter for PC-SAFT
PCSFTU (K)	Critical temperature parameter for PC-SAFT
PCSFTV	Segment diameter parameter for PC-SAFT
R	Universal gas constant
S	Entropy

T	Temperature
u	Standard uncertainty
U	Expanded uncertainty
ub	Mass balance precision
v	Viscosity
V	Molar volume of a fluid
wt	Weight
x	Liquid mole fraction
y	Vapour mole fraction
z	either liquid or vapour phase
Zc	Compressibility factor

Greek letters

ρ	density
φ	Fugacity coefficient
γ	activity coefficient
μ	Chemical potential
σ	standard deviation or segment diameter
θ	parameter
α	component indicator
($\beta^{A_iB_i}$)	association volume parameter
($\varepsilon^{A_iB_i}$)	association energy parameter

Subscripts

c	critical
E	excess
i	chemical specie
j	chemical specie
max	maximum
mix	mixture
rep	repeatability
std	standard

Superscripts

assoc	association
calc	calculated
chain	chain contribution
disp	dispersion term
E-	excess property
Exp	experimental
ID	ideal solution
IG	ideal gas
hs	hard sphere
liq	liquid phase
®	registered trademark
R	Residual property
vap	vapour phase

Overbars

-	Partial molar property
^	Thermodynamic property of a component in a mixture.

Abbreviations

AAD	Absolute Average Deviation
AARD	Absolute Average Relative Deviation
APACT	Associated-Perturbed-Anisotropic-Chain Theory
CAS	Chemical abstracts service
csgm	Calibration Standard Gas Mixture
CPA	Cubic Plus Association equation
DC	Direct current
EoS	Equation of State
GC	Gas Chromatography
GC-MS	Gas Chromatography-Mass Spectrometry
HPVLE	High Pressure Vapour-Liquid Equilibria
ID	Internal diameter
LPVLE	Low pressure vapour liquid equilibrium.

MEG	Monoethylene Glycol
MSDS	Material safety data sheet
NIST	National Institute of Standard and Technology
NRTL	Nonrandom two liquid model
OD	Outer diameter
PC-SAFT	Perturbed Chain Statistical Associating Fluid Theory
PPE	Personal Protective equipment
PR	Peng-Robinson
PRWS	Peng Robinson Wong Sandler
PT	Pressure transmitter
PTFE	Polytetrafluorethylene
RMSD	Root Mean Square Deviation
ROLSI ®	Rapid Online Sampler
RSS	Root of Sum Squares
SAFT-VR	Statistical Associating Fluid Theory for potentials of Variable Range
SLE	Solid Liquid Equilibria
SRK	Soave-Redlich- Kwong
SS	Stainless Steel
TEG	Triethylene Glycol
TCD	Thermal Conductivity Detector
TRU	Thermodynamics Research Unit
UKZN	University of KwaZulu-Natal
UNIQUAC	Universal Quasichemical
VLE	Vapour Liquid Equilibria
VLLE	Vapour Liquid Liquid Equilibria
VdW	Van der Waals
WS mxr	Wong-Sandler mixing rule

Chapter 1: Introduction

Natural gas has increasingly become the premier fossil fuel used for energy and heating needs (Moore et al., 2014). This move to prominence is due to its lower carbon dioxide emission compared to coal and other liquefied petroleum-based products per unit of energy produced (McJeon et al., 2014). In addition, new extraction and refining methods, such as fracking have been developed, leading to previously ignored or unexplored gas reserves becoming viable. Alongside this growth, other industries are making strides within the energy sector. Partially within South Africa the hydrogen economy has seen significant growth alongside other renewables (Mukelabai et al., 2022). Despite this, natural gas remains an economical and reliable energy resource within South Africa through the natural gas pipelines that feed into the country from Mozambique. (Bildirici and Bakirtas, 2014) and similarly, internationally.

To maximise the heating value of natural gas and minimise the emission of other greenhouse gases such as methane, nitrous oxide and fluorinated gases, raw natural gas is subjected to several processing steps to remove the inherent impurities including water to allow for a more effective and cleaner burn by the end-users (Kidnay et al., 2019). In addition to improving the quality of the gas, removing impurities, such as water, makes transportation easier and safer as it prevents clathrate hydrate formation, which can become a process hazard if allowed to accumulate in gas pipelines (Kidnay et al., 2019).

The composition and quality of natural gas is significantly dependent on the extraction area and the extraction method used for its recovery. However, natural gas typically consists of hydrocarbons and non-hydrocarbons. The hydrocarbons mainly include methane, ethane, propane and other alkanes. The non-hydrocarbons are the impurities which are typically removed, such as hydrogen sulphide, carbon dioxide, water vapour and other minor components (Wu et al., 2017). The hydrocarbons are combustible, giving heat as a by-product of the reaction. This burn is more effective when the concentrations of these hydrocarbons are highest, increasing the heating value per unit volume of the gas. In terms of the impurities, some, such as nitrogen gas and water vapour, are non-toxic but rather have the effect of lowering the heating value of the natural gas (Faramawy et al., 2016).

Water vapour content in natural gas is of particular concern as it is almost always present in natural gas sources. Water vapour is found in the rock layers alongside natural gas and is sometimes also introduced when extraction methods such as fracking are employed. The presence of water vapour results in the formation of a hard substance known as “dirty ice” (clathrate hydrates) within gas pipelines, which occurs when water molecules encapsulate the hydrocarbons, forming cage-like solid clusters resembling ice. These clathrates form at low temperatures and high pressures and are typically a problem during cold winters where the low temperatures promote the process (O’Brien, Mejorada and PE, 2016).

If these clathrate clusters become sufficiently large, they can lead to restrictions or even blockages in the gas pipelines. In addition, when large pieces break off the pipe wall, they become projectiles within the pipelines, which can cause internal damage and possible pipeline rupture. These clathrates form within minutes, provided concentrations of saturated water are high and environmental conditions are favourable (Kidnay, Parrish and McCartney, 2019). These formations can lead to serious shutdown and production issues in addition to serious safety risks (Gipson, 2015). Thus, prevention of these clathrate formations is far more efficient than managing the consequences.

Dehydrating natural gas limits the degree of clathrate formations and prevents the above-mentioned issues. Several techniques and treatments are used to dehydrate the natural gas before it is transported to facilities for further processing. In addition, a carrier inhibitor is usually added during the transportation phase of the gas, which further inhibits the formation of clathrates. It is imperative that the dehydration process is able to reduce the amount of water vapour below the dew point of any expected temperatures, as this minimal intervention prevents the formation of clathrates.

The two most prominent chemicals/classes used in the dehydration and clathrate inhibiting processes are methanol and diols (glycols) (Kidnay, Parrish and McCartney, 2019). Methanol acts as an inhibitor by reducing the formation of hydrates by altering the clathrate formation point. Methanol is widely used throughout the gas industry, primarily in areas where weather or environmental locations make it challenging to dehydrate natural gas sufficiently, such as on ocean oil/gas rigs (Samie, 2016). There are, however, drawbacks to the use of methanol. Methanol has a higher vaporisation rate than glycols. This benefits the system by causing better solvent interaction but leads to a higher cost for solvent replacement due to vaporisation losses (Kontogeorgis and Folas, 2010). Additionally, the remaining methanol in the gas streams acts as a contaminant and must be removed before the final gas product can be sold. Environmental, health, and safety issues are also a concern, as released methanol can cause environmental contamination and is toxic to humans. Methanol additionally increases the corrosion rates within pipelines and adds to the dangers already associated with natural gas due to its high flammability. Glycols are also widely used in the gas industry to treat high water vapour concentrations in natural gas. Tri-ethylene glycol (TEG) is a common glycol; however, other glycols can be used under specific circumstances, such as for special temperature conditions, viscosity or property requirements. For instance, di-ethylene glycol is typically used when extremely low temperatures are present as it has a lower viscosity than TEG (Kidnay, Parrish and McCartney, 2019). Similar to methanol, glycols can be used as inhibitors in natural gas pipelines; however, they also have the added use of being a dehydration absorbent. These glycols are often hygroscopic and, thus are typically used in natural gas dehydration plants.

The use of glycols also has disadvantages. Due to the relatively high boiling points, glycols do not vaporise as easily as methanol; this simplifies recovery but decreases hydrate inhibition's effectiveness.

The viscosity of glycols also makes it challenging to work with at lower temperatures and, thus, in some instances, requires constant heating (Kidnay, Parrish and McCartney, 2019). Similarly, to employing methanol, all glycols have common environmental, health, and safety impacts and concerns. Using a combination of these two chemicals as a co-solvent/inhibitor is common in the gas industry. TEG is used to dehydrate the raw natural gas, and methanol is used as a further inhibitor. However, methanol is still more widely used as an inhibitor (Teixeira et al., 2018). This is simply due to the relative costs of implementing each method while meeting the minimal quality and safety specifications. The suitability of the methods used for mitigating clathrate formation also depends on the quality of the natural gas source, the water content, and the process conditions. In some cases, the cost of designing, building and operating a complicated dehydration plant outweighs the benefit (Kidnay, Parrish and McCartney, 2019). Additionally, the necessary phase equilibria data to characterise the separation behaviour of methanol-TEG-water-natural gas systems is limited in the literature, which affects the design of alternate process pathways.

Accurate thermodynamic data to describe these multicomponent chemical systems are imperative for designing and optimising process and transportation units. These process designs are costly and time-consuming endeavours, and the process can run the risk of underperforming when simulated using inaccurate modelling methods. In particular, the available data under the operating conditions for some gas industry processes (which is usually at high pressures exceeding 50 bar and temperatures exceeding ambient temperature) are rarely available due to the relative difficulty of obtaining this data, and predictions based on binary data alone have been shown to yield poor representations of the phase behaviour of the multicomponent systems (Zvawanda, 2021c). However, with the improvement in computer hardware, software and more accurate and rigorous simulations, the need for HPVLE (High-Pressure Vapour -Liquid Equilibrium) data can be addressed (Raal and Mühlbauer, 1997). This has sparked new interest in obtaining this data by developing more reliable experimental techniques.

1.1. Aims and objectives.

This project aimed to measure and model high-pressure vapour-liquid equilibrium (HPVLE) data for novel systems containing typical natural gas dehydration mixtures.

This would improve industry knowledge and allow for better design and optimisation of dehydration plants. The lack of high-pressure vapour-liquid equilibrium (HPVLE) data for multicomponent methanol, TEG, water and gas systems such as methane reveals a gap in industry knowledge. Current predictive thermodynamic models can be improved when regressed to accurate HPVLE data.

The objectives comprised:

1) To perform and measure verification systems to validate the performance of the available equipment and the testing methods.
2) To perform and measure HPVLE (P-x) data for the following novel systems at typical dehydration process temperatures:

   Methane (1) + 2,2′-[ethane-1,2-diylbis(oxy)] di(ethan-1-ol) (TEG) (2) + water (3) + methanol (4) at 303.15 K, 313.15 K and 323.15 K

   Methane (1) + ethane (2) + propane (3) + 2,2′-[ethane-1,2-diylbis(oxy)] di(ethan-1-ol) (TEG) (4) + water (5) + methanol (6) at 303.15 K, 313.15 K and 323.15 K

3) To perform thermodynamic modelling on the test and novel system data using the Cubic-Plus Association, Perturbed Chain-SAFT and Peng-Robinson models.

To achieve the aim and objectives, HPVLE experiments were proposed with the execution of Aspen Plus modelling simulations. The gaps in the literature and the call from the Gas Processing Association for expansion in this area guided the direction of this research. This study is an extension of the work conducted by Dr Paul Zvawanda during his publications (Zvawanda et al., 2022 a) and (Zvawanda et al., 2022 b) and PhD study (Zvawanda, 2022 c).

1.2. Thesis overview

This dissertation is comprised of six chapters with three appendices that outline the purpose and results of this study. The chapters are summarised below:

Chapter one presents the introduction to this study. This chapter details the importance of natural gas dehydration and the background for the chemical species used. The aims and objectives, which include the chemical systems to be investigated, are presented.

Chapter two presents the literature review of this study. The chapter reviews the available literature and background for the chemical species used, similar systems' phase equilibrium, and the models presented. Included in this review is an evaluation of the types of HPVLE equipment available and studies that have used these types of equipment.

Chapter three presents the experimental equipment and methodology used in this study. The chapter details the equipment used to conduct the calibrations, validation steps for the chemical species and HPVLE measurements.

Chapter four presents the results and discussion of this study. The chapter details the validation of chemical species, calibrations and test and novel systems. In addition, the chapter describes the modelling conducted on the experimental data using the CPA, PC-SAFT and PR EoS.

Chapters five and six present the conclusions and recommendations, respectively.

Appendices A, B, and C include additional literature; model parameters with raw data, and uncertainty calculations.

Chapter 2: Literature Review

This chapter summarises relevant information to HPVLE data measurement and modelling, namely the experimental methods and modelling approach applied in the literature to the data associated with natural gas processing method for water dehydration as investigated in this study. The dehydration process for natural gas, thermodynamic principles applied in the molecular interactions, phase equilibrium literature and modelling, followed by suitable equipment considerations, are further presented.

2.1. Methanol and TEG removal in natural gas processing

This section of the review details natural gas dehydration and adds greater context and relevance to the topic studied and the experimental results obtained.

Natural gas dehydration is essential in ensuring a final product that is safe and has a high caloric value. The compositions of natural gas can vary depending on the source location and the depth of extraction. Still, the constituents of the gas are usually similar (hydrocarbons, water, non-hydrocarbon impurities) but with varying relative quantities (Faramawy, Zaki and Sakr, 2016). Thus, the purification steps are generally uniform, entailing removing the non-hydrocarbons from the valuable hydrocarbons. The focus of this project is however natural gas dehydration, and greater detail on other natural gas purification steps can be found in Appendix A.

2.2. Error! Reference source not found.Natural gas dehydration

Saturated water vapour causes several problems within natural gas processing, such as hydrate formation, corrosion, and gas quality problems. Gas hydrates (clathrates) are the main concern and form through the interactions of water and hydrocarbons at high pressures and low temperatures. In addition, the presence of water vapour reduces the caloric value of gas per unit of volume. Thus, natural gas needs to be treated before long-term transportation and sale to end users. The natural gas must be treated to meet the dew point specifications, which is most commonly done using absorption through liquid glycols to remove water (Kidnay, Parrish and McCartney, 2019). The most commonly used glycol for this purpose is tri-ethylene glycol (TEG) (2,2′-[ethane-1,2-diylbis(oxy)]di(ethan-1-ol) due to a number of factors. Namely, TEG is hydrophilic, will not absorb heavy hydrocarbons easily and has an extensive operating range in terms of temperature (Mokhatab, Poe, William and Mak, 2015).

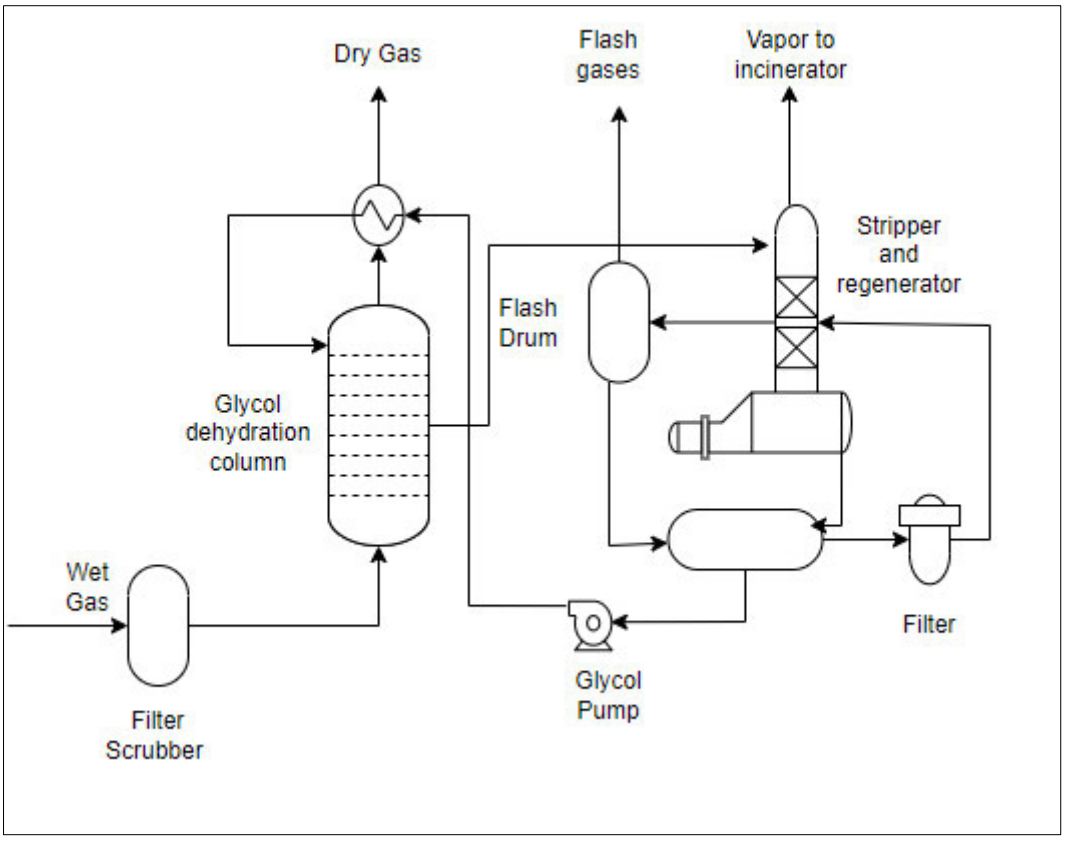

Figure 2.1 Natural Gas dehydration plant. Redrawn by R Raghunanan (Mokhatab et al., 2015)

Figure 2.1 depicts a typical TEG dehydration plant. The wet natural gas entering the plant is filtered through a separator, preventing any liquid or pipe scales from entering the scrubber. This prevents the plugging of the columns and contamination of the TEG (Mokhatab et al.,2015). Within the scrubber, wet natural gas moves up the column while lean TEG moves down. The water vapour is removed from the natural gas through absorption and the dried natural gas leaves the top of the column. The newly enriched TEG goes through a regenerator that removes the absorbed water, allowing the recycled lean TEG back to the scrubber. This is the most conventional TEG dehydration process, however, glycol injections have been preferred in more moderate-temperature regions as it is a cheaper and relatively simple process (Fan et al., 2006).

2.2.1. Methanol injections

Methanol injections are used as an alternative to TEG dehydration, while in some cases, it is used in conjunction with dehydration. When natural gas is injected with methanol, the formation point for gas hydrates shifts to make it less likely to form at the given process conditions. The use of methanol is usually limited to specific conditions, such as extremely low temperatures and offshore natural gas extraction (Mokhatab et al., 2015). TEG at very low temperatures becomes too viscous to handle efficiently; thus, methanol becomes a useful alternative for inhibition. In addition, methanol is more

volatile than TEG, allowing for more effective interactions between itself and natural gas components. For offshore natural gas operations, limited space makes the ability to dehydrate natural gas immediately after extraction difficult. Hence, methanol injections are implemented to prevent the formation of gas hydrates while the gas is transported to a suitable facility for dehydration (Kidnay et al., 2019). However, methanol must be removed before the final natural gas is sent to the end users. Due to methanol's relatively high volatility, it remains vaporized within the natural gas after the injection process. This acts as a contaminant and must be removed; otherwise, the final natural gas may not reach the required specifications. In addition, methanol can have detrimental effects on the equipment, such as poisoning catalysts in petrochemical plants and damaging molecular sieves (Teixeira et al., 2018). Hence, methanol impurities are encountered in the subsequent conventional TEG dehydration steps. Fortunately, TEG can act as an agent for the removal of methanol as well as water vapour from natural gas. This is due to TEG and methanol being soluble with each other. This rational for typically encountered TEG-methanol-water mixtures in the natural gas dehydration process forms the basis of this study.

2.3. Chemical Species of interest

This study focused on the two main components, namely methanol and tri-ethylene glycol and their interactions with water and light hydrocarbons. This section will briefly review these components and their potential interactions as well as expected phase interactions as reported in the literature. There are a number of intermolecular forces that can occur between the respective molecules found in a dehydration process. These are broken up into three main types of forces, namely dispersion, dipolar/polar and hydrogen bonding forces. Dispersion forces, or London forces, are the weakest intermolecular forces represented. These forces only occur when an induced dipole occurs in non-polar molecules. Dipolar forces represent the attraction experienced by polar molecules which have a dipole. These forces are stronger than dispersion forces but weaker than hydrogen bonding. Hydrogen bonding is the final type of intermolecular force, only occurring between molecules with hydrogen bonded to an oxygen, nitrogen or fluorine atom. Hydrogen bonding is the strongest of the three main types of intermolecular forces. More details on the specific intermolecular interactions between the studies components can be found in Appendix A.

2.3.1. Methanol

Methanol is one of the most thermodynamically effective inhibitors for preventing the formation of gas hydrates (Miroshnichenko et al., 2022). It is a colourless, volatile and light aliphatic alcohol. Methanol remains a liquid from 175.55 K to 338.15 K, making it a highly versatile solvent for low and moderate temperatures (Goodwin, 1987). The methanol molecule itself is polar due to its asymmetric shape and the high electronegativity of the oxygen atom. Figure 2.2 depicts the two methanol molecules, showing

how the negative oxygen atoms attract the positive hydrogen atoms, resulting in the potential for hydrogen bonding/polar interactions.

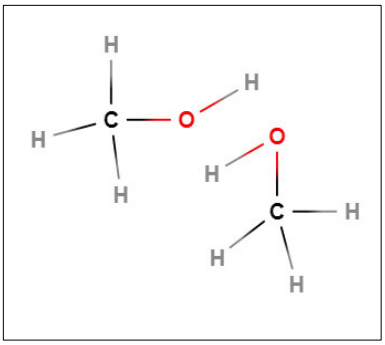

Figure 2.2 Two methanol atoms depicting hydrogen bonding. Drawn by R Raghunanan

2.3.2. Tri-ethylene glycol (TEG) (2,2′-[Ethane-1,2-diylbis(oxy)] di(ethan-1-ol)

Tri-ethylene glycol is a dihydroxy alcohol which has a transparent, colourless appearance. The compound has a high viscosity and is completely miscible with water and is hygroscopic. TEG remains a liquid from -7 ºC – 285 ºC making it a high boiling point solvent (Sun and Teja, 2003). The TEG molecule is polar due to its high electronegativity difference between the oxygen and hydrogen molecules. Figure 2.3 depicts the TEG molecule, where it can be seen that there are a number of oxygen and hydrogen molecules which causes multiple potential sites for hydrogen bonding.

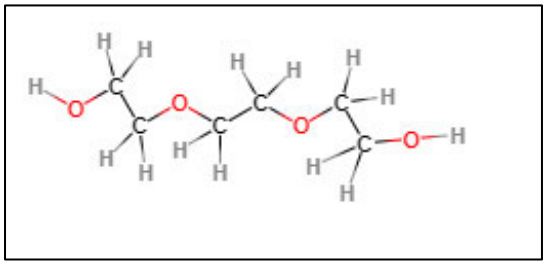

Figure 2.3 TEG molecule. Drawn by R Raghunanan

In Table 2.1 the dominant interactions expected between TEG/methanol and the proposed natural gas mixture constituents are shown.

Table 2.1 Interactions encountered in chemical mixture combinations.

Type of force	**Dispersion forces**	**Dipolar forces**	**Hydrogen bonding**	**Dispersion forces**	**Dipolar forces**	**Hydrogen bonding**
Component	**TEG**			**Methanol**		
Methane	✓	X	X	✓	X	X
Ethane	✓	X	X	✓	X	X
Propane	✓	X	X	✓	X	X
Water	✓	✓	✓	✓	✓	✓
TEG	✓	✓	✓	✓	✓	✓
Methanol	✓	✓	✓	✓	✓	✓

For this study, hydrogen bonding features prominently in the mixtures studied since many components, such as water, TEG and methanol, are known as oxygenated molecules. These molecules can self-associate, which is a type of hydrogen bonding that occurs when a molecule, such as diols, alcohols, and acids, can behave as an electron acceptor and donor (Soo, 2011). Additionally, molecules cross-associate when they hydrogen bond with molecules that are either electron acceptors or donors, typical of ketones and aldehydes (Soo, 2011). In this study, molecule combinations such as water-TEG, water-methanol and methanol-TEG would cross-associate.

2.4. High-Pressure VLE Measurements

The design and commissioning of specialised equipment for high-pressure vapour-liquid equilibrium (HPVLE) measurements is a complex process and is covered in great length by (Mühlbauer and Raal, 1993), (Nelson et al., 2021), (Ebrahiminejadhasanabadi et al., 2018) and (Zvawanda, 2022 c) to which the reader is referred for more detail. For equilibrium to be established, the system must be acceptably isolated and maintained at thermal, mechanical and chemical equilibrium. The state variables of temperature, pressure and composition of the liquid or liquid and vapor phase must then be measured accurately (in the analytical method), while composition can be determined by accurate mass balancing in the static-synthetic method. There are several difficulties that must be overcome when conducting high-pressure VLE experiments (Raal and Mühlbauer, 1997):

- Degassing the liquid components completely before loading into the equilibrium cell.
- Maintaining isothermal equilibrium conditions within the equilibrium cell.
- Estimating the contents of the equilibrium cell have reached equilibrium.
- Accurately measuring the temperature and pressure.

The following challenges are associated specifically when analytical methods are used:

- Withdrawing samples without disturbing the phase equilibrium created from both the liquid and vapour samples.
- Analysing the withdrawn samples accurately. The difficulty comes from properly calibrating the gas chromatograph and analysing the samples.

2.4.1. Methods reported for HPVLE

There are two commonly used methods for HPVLE measurements: The dynamic and static methods. In the dynamic method, a phase pass is induced, where a single vapour or the liquid and vapour phase travels through the equilibrium cell and then through an analysis network while equilibrium is achieved (Zvawanda, 2022 c). The other method that can be employed is the static method which is broken up into several subtypes. This study employed the static synthetic method. Figure 2.4 depicts the different types of methods employed in VLE research.

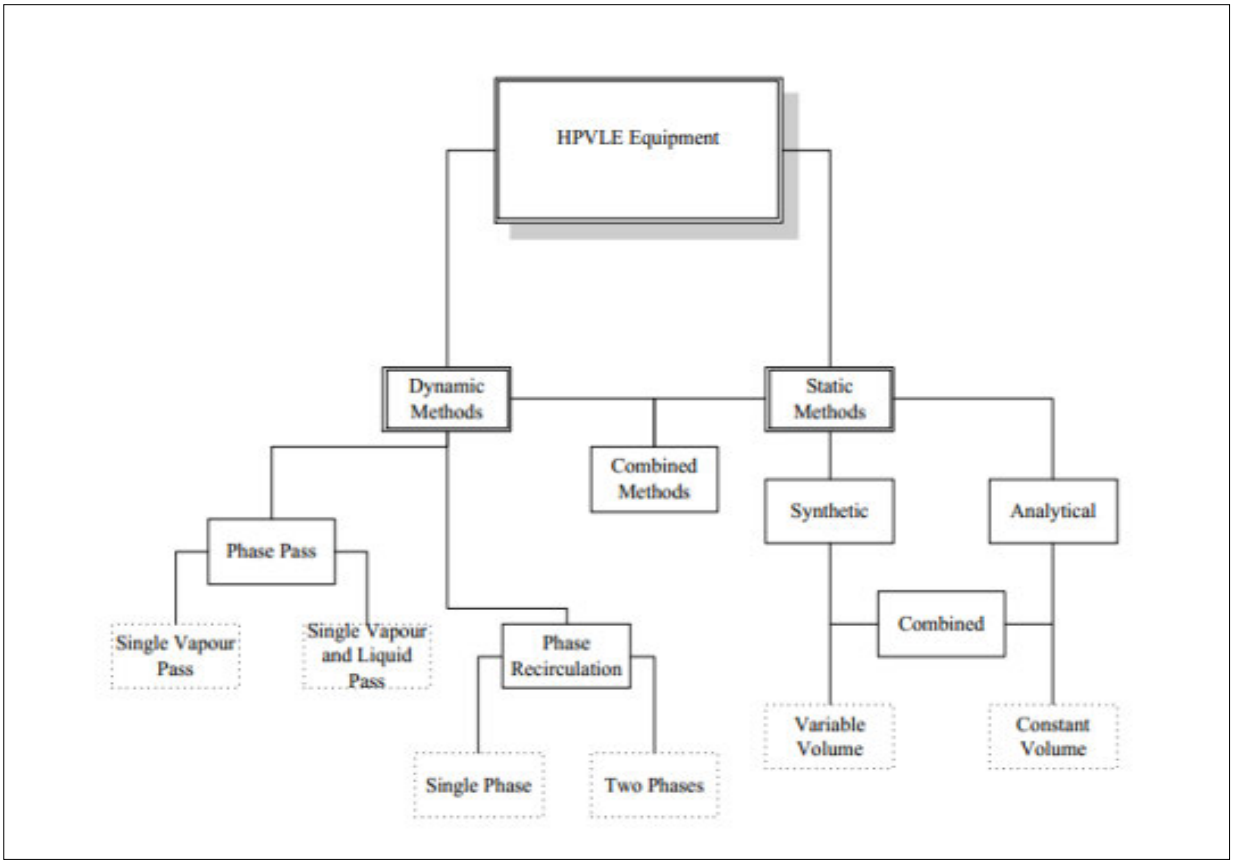

Figure 2.4 Experimental methods used for HPVLE measurements**.** extracted from (Reddy, 2006)**.**

2.4.1.1. Static methods

The static method is the more widely employed method and can be broken into three main categories: analytical, synthetic, and combined methods. The static analytical and synthetic methods are fairly similar in the loading and equilibration procedures. The methods involve charging a mixture of components into a fixed-volume equilibrium system (Knock, 2010). Generally, some form of agitation is incorporated to allow the system to reach and maintain equilibrium more effectively. Usually, magnetic (non-invasive) stirring is employed. The analytical method requires a degree of sampling from the HPVLE mixture during equilibrium. This can be either the liquid or vapour phase or both. This method allows for the gathering of Pxy data and accurate measurements for the liquid and vapour phases. The drawback of this method is the difficulty in ensuring accurate composition measurement results. The calibration of analytical components can be very technical and time-consuming (Fonseca, 2010). Thus, when accurate composition measurement is not available or deemed too complex/beyond operational limits, the synthetic method is used. The synthetic method does not require any sampling and analysis, instead, it uses other indicators to determine equilibrium, such as the visual and breaking point pressures. The phase compositions at equilibrium are established by a mass balance on the vapour and liquid phases within the cell, as the charged mixture composition is established precisely when loading the cell. The weakness of this method is that it is not simple to establish the composition of the vapour or liquid phase in the system when both the vapour and liquid phase is present. Thus, only the dew and bubble point can be determined easily for a given system. It should be noted that numerous combinations of the static, dynamic and derivatives of each of the methods have been employed in other works and modification of these methods is possible (Tshibangu, 2010).

2.4.1.1.1. The static-synthetic method

The static-synthetic method was used to obtain the results found in this paper. As previously stated, the method does not require any sampling and analysis, allowing for a greater degree of simplicity in design and operation. However, it requires the components' composition to be accurately known to produce reliable results. The method can be used to determine the isothermal or isochoric values for a known composition mixture. A major drawback of this method is that multiple components are used as only limited information from either the dew or bubble points can be determined. Additionally, the method is very slow for testing as only one composition can be tested at a time, usually with long measurement periods for HPVLE. Despite these disadvantages, the method is still widely used due to the low cost and simplicity of the apparatus. In Table 2.2 the following studies used the static synthetic method and most of the studies showed a wide range of pressures and temperatures applicable to the static synthetic method.

The static-synthetic method has been applied in the following studies:

Table 2.2 Studies using the Static Synthetic method.

Authors	**Operating range**	
	Pressure (MPa)	**Temperature (K)**
(Fischer and Gmehling, 1994)	0 – 12	303.15 - 423.15
(Raeissi and Peters, 2005)	5 – 14	293 - 349
(Kühne et al., 2008)	0 – 14	278 - 368
(Raal et al., 2011)	0 - 2	313.17 - 352.68
(Ferreira, 2018)	8 – 16.4	308 – 348

2.4.1.2. Combined methods

The combined method uses a combination of the static and dynamic method. The following studies have employed this method.

(Grigiante et al., 2008) used a static VLE apparatus using a total pressure cell which measured VLLE for ternary mixtures. The apparatus has a ROLSI ® sampler injector for analysis. Similar apparatus are found in the following studies (Lhoták and Wichterle, 1981), (Silva-Olive et al., 2006), (Paiva et al., 2008), (Gardeler et al., 2002; Chapoy et al., 2003), (Laugier and Richon, 1986), (Fourie et al., 2008) however mechanical stirring (invasive) with good sealing has also been reported in (Pfohl et al., 1997), (Chylinski et al., 2002) and (Yoon et al., 1993).

In all HPVLE measurements, the temperature and pressure are monitored with one of these variables made constant. In this study, the fixed variable was the temperature as measurements were conducted isothermally. In addition, a variable volume cell was used to enable an increase and decrease in pressure. The equipment used in this work is detailed in Chapter 3.

2.5. Published phase equilibrium data for natural systems related to this study

2.5.1. Binary Systems

2.5.1.1. TEG + methane

The phase equilibrium data available for methane + TEG are presented in Table 2.3 There is limited phase equilibrium data for methane and TEG binary systems in the open literature. Only three sources (Jou et al., 1987), (Jerinić et al., 2008) and (Zvawanda, 2022 c) provide Px isothermal data. The data found by (Jou et al., 1987) and modelled with the Peng-Robinson (PR) EoS determined that it was a poor model when applied to systems comprised of associating molecules. The study by (Jerinić et al.,2008) aimed to measure the solubility of TEG in super critical methane. The study modelled the data using the Peng-Robinson (PR) and Soave-Redlich-Kwong (SRK) EoS and determined the mean logarithmic deviation for TEG solubility. This study found that the SRK EoS performed better and there was a need for more methane-TEG data to comprehensively describe the system behaviour. Finally (Zvawanda, 2022c) measured the system using the same apparatus as used in this study for the purposes of using the data as a test system.

Table 2.3 Phase equilibrium PTx sources for methane + TEG binary system.

Reference	Temperature range (K)	Pressure (MPa)	Methane molar composition range (x_1)	Number of data points
(Jou et al., 1987)	298.15; 323.15; 348.15; 373.15; 398.15	0.11 - 20.20	0.0006 - 0.0638	51
(Jerinić et al., 2008)	298.15;316.75	0.16 - 8.61	±0.01 - ±0.062	12
(Zvawanda, 2022 c)	298.15; 323.15	1.41 - 11.29	0.0047 - 0.0460	6

2.5.1.2. Ethane + TEG

The available phase equilibrium data for ethane + TEG are presented in Table 2.4 There is only one literature source for phase equilibrium data (Px isothermal data). This source (Jou et al., 1987) employed the same technique and modelling methodology described above by the same authors.

Table 2.4 Phase equilibrium sources for ethane + TEG binary system.

Reference	Temperature range (K)	Pressure range (MPa)	Ethane molar Composition range (x_1)	Number of data points
(Jou et al., 1987)	298.15; 323.15; 348.15; 373.15; 398.15	0.11 - 20.48	0.0016 - 0.1482	59

2.5.1.3. Propane + TEG

The available phase equilibrium data for propane + TEG are presented in Table 2.5 Again, there is only one literature source for phase equilibrium data for a propane + TEG binary system that provides Px isothermal data. This source (Jou et al., 1987) employed the same technique and modelling methodology as mentioned above.

Table 2.5 Phase equilibrium sources for propane + TEG binary system.

Reference	Temperature range (K)	Pressure range (MPa)	Propane molar Composition range (x_1)	Number of data points
(Jou et al., 1987)	298.15; 323.15; 348.15; 373.15; 398.15	0.159 - 6.35	0.0007 - 0.1043	40

2.5.1.4. Water + TEG

The phase equilibrium data for water + TEG are presented in Table 2.6 There are limited literature sources for this system, with the only available data being isobaric data measured at low pressures. These sources are (Aniya et al., 2015) and (Mostafazadeh et al., 2009). The study by (Aniya et al., 2015) measured and modelled the data using the NRTL and Wilson models. The study concluded the Wilson model performed better than the NRTL model. The data in (Mostafazadeh et al.,2009) was modelled using the UNIQUAC, NRTL and Van Laar models. The study concluded that the Van Laar activity coefficient model performed the best.

Table 2.6 Phase equilibrium sources for water + TEG binary system.

Reference	Temperature range (K)	Pressure range (MPa)	Water molar Composition range (x_1)	Number of data points
(Aniya et al., 2015)	356.16 - 559.01	0.05 - 0.10	0 - 1	60
(Mostafazadeh et al., 2009)	371.55 - 421.25	0.09	0.117 - 0.410	18

2.5.1.5. TEG + methanol

There is currently no available data in the open literature for the methanol + TEG binary system to the author's knowledge. This highlights the need for such measurements as binary or constituent multicomponent systems, as these interactions are required to characterize system behaviours in natural gas dehydration plants. Due to equipment limitations this system could not be measured in this work as very low vapour pressures and high viscosities would be expected. The equipment required would need to operate at close to vacuum conditions. The equipment used to liquid vapour pressure measurements can be found in Chapter 3.3.2

2.5.1.6. Methane + methanol

The methane + methanol binary system has an abundance of literature available for Px isothermal data. Methanol is a widely used chemical solvent in several processes, including the cleaning of sour gas (Mokhatab et al., 2015). A selection of the relevant literature available is presented in Table 2.7.

Table 2.7 Phase equilibrium sources for methane + methanol binary system.

Reference	Temperature range (K)	Pressure range (MPa)	Methane molar composition range (x_1)	Number of data points
(Yarym-Agaev et al., 1985)	298.14; 313.14; 338.13	2.50 - 12.50	-	15
(Vetere, 1986)	213.2; 233.2; 273.2	1.08 - 6.97	0.0025 - 0.0900	16
(Brunner et al., 1987)	298.15; 323.15; 373.15	5.45 - 100	0.0392 - 0.6378	71
(Hong et al.,1987)	200; 220; 250; 273.15; 290; 310; 330	1.34 - 41.37	0.0095 – 0.2575	83
(Schlichting et al., 1993)	242.60; 262.00; 282.70	2.00 - 10.00	-	17
(Ukai et al.,2002)	280.15	2.11 - 11.41	0.017 - 0.051	9
(Wang et al., 2003)	283.2; 293.2; 303.2	5.05 - 40.05	0.0015 - 0.0041	24
(Frost et al., 2014)	298.87	5.24 - 18.01	0.0041 - 0.1348	9
(Frost et al., 2015)	298	3.72 - 15.51	0.0293 - 0.1221	5
(Kapateh et al.,2016)	273.15	1.71 - 46.99	0.0017 - 0.2578	10
(Zvawanda, 2022 c)	298.15; 303.15	2.63 - 10.68	0.0087 - 0.1025	5

Sources such as, (Brunner et al., 1987), (Wang et al., 2003) and (Frost et al., 2015) conducted measurements above the critical pressure of methane, while the rest typically operated across this pressure (4.595 MPa). (Schlichting et al., 1993); (Frost et al., 2014) and (Kapateh et al., 2016) modelled the data obtained using a variety of models, including the CPA and Redlich-Kwong-Soave EOS. Finally

(Zvawanda, 2022c) measured data for this system as a verification system using the same apparatus used in this study. The modelled using the PR, SRK, PRWS, CPA, and the PC-SAFT EoS, showed that the PR, SRK and PRWS models were poor in describing the system behaviour, with poor extension to the multicomponent systems. Furthermore, the choice of mixing rule had little effect on the description of the system behaviour. This study along with the two publications (Zvawanda et al., 2022 a) and (Zvawanda et al., 2022 b) are reference points for the measurements conducted in this work.

2.5.1.7. Ethane + methanol

There are a number of literature reported sources available for the ethane + methanol binary mixture for Px isothermal data. The study by (Ma and Kohn, 1964) was not publicly accessible, but data is available. The other studies found in Table 2.8 are available and were conducted for a number of reasons. The study by (Ohgaki et al., 1976) measured data which was modelled using the Redlich-Kwong EoS to determine the activity and fugacity coefficients for the liquid and vapour phases. The study by (Zeck and Knapp, 1986) used a vapour recirculation cell to investigate the VLE and VLLE for binary and ternary systems, including methanol and ethane. The study concluded the data obtained would be useful for methanol absorption units. (Ishihara et al., 1998) used a static circulation-type system to investigate the phase equilibrium properties of ethane and methanol at 298.15 K. The authors reported difficulty in correlating the data using conventional EoS due to the complex phase separation behaviours. The study by (Wang et al., 2003) investigated the solubility of a number of gas mixtures in a water-alcohol mixture. The study concluded that the data obtained would be used to improve thermodynamic modelling and prove a direct relationship between gas solubility and inhibitor concentration in the aqueous phase.

Table 2.8 Phase equilibrium sources for ethane + methanol binary system.

Reference	Temperature range (K)	Pressure range (MPa)	Ethane molar composition range (x_1)	Number of data points
(Ma and Kohn, 1964)	298;323;348;373	0.02 - 6.08	-	42
(Ohgaki et al., 1976)	298.14	1.09 - 4.12	0.0403-0.3511	5
(Zeck and Knapp, 1986)	240; 260; 273; 298	0.40 - 4.20	0.0279-1	39
(Ishihara et al., 1998)	298.15	0.96 - 4.19	0.053-1	10
(Wang et al., 2003)	283.2	0.5 - 3	0.0008-0.003	

2.5.1.8. Propane + methanol

The phase equilibrium data for propane + methanol can be found in Table 2.9. Only a few literature sources are available that provide Px isothermal data. The study by (Galivel-Solastiouk et al., 1986) presents data for a propane + methanol binary system using two static analytic and a static synthetic apparatus. The study by (Lev, et al., 1992) investigated a propane + methanol system at 310.7 K, 352.2 K, 393 K, 474.3 K. The study employed a variable-volume sapphire cylinder and concluded that the results obtained match those of other studies. Finally, the study by (Joung et al., 2004) investigated a propane + methanol system using a circulating apparatus. The study correlated the data using the PR and SRK EoS which had acceptable results.

Table 2.9 Phase equilibrium sources for propane + methanol binary system.

Reference	**Temperature range (K)**	**Pressure range (MPa)**	**Propane molar composition range (x_1)**	**Number of data points**
(Galivel-Solastiouk et al., 1986)	313.1; 343.1; 373.1	0.35-4.30	0.0252-1	31
(Lev et al., 1992)	310.7; 352.2; 393.0; 474.3	0.03-8.66	0-1	39
(Joung et al., 2004)	313.55; 327.95; 343.21	0.28-2.58	0.0192-0.1006	31

2.5.1.9. Methanol + water

There is an abundance of Px isothermal data for the water + methanol. The quantity of data available is vast and only a few relevant studies were selected and displayed in Table 2.10 The sources displayed were the most recent literature available in the desired range. The study by (Sentenac et al., 1998) used a sapphire equilibrium cell in-order to investigate the VLE from 363 K to 440 K. The data found had a good agreement with other literature. The study by (Bernatová et al., 2006) obtained data for methanol and water using a two-phase recirculating still. The data was correlated with the NRTL model and showed a good agreement.

Table 2.10 Phase equilibrium sources for methanol + water binary system.

Reference	**Temperature range (K)**	**Pressure range (kPa)**	**Methanol molar composition range (x_1)**	**Number of data points**
(Mokbel et al., 1995)	243.75; 258.69; 278.58; 288.58; 298.55; 308.57	0.29-28.28	-	36
(Sentenac et al., 1998)	363.15; 383.15; 403.15;424.15; 442.15	117-2093	0.1061-0.9061	25
(Bernatová et al., 2006)	323.15	12.35-55.61	0-1	14

2.5.2. Ternary systems

2.5.2.1. Methane + water + methanol

The phase equilibrium sources for the methane + water + methanol system can be found in Table 2.11 of which there are few literature sources for the system. The papers by (Wang et al., 2003) and (Frost, et al., 2014) have been previously mentioned. The study by (Wise et al., 2016) obtained results for the methane + water + methanol system and optimised the parameters of the CPA and SRK EoS.

Table 2.11 Phase equilibrium sources for the methane + water + methanol system

Reference	Temperature range (K)	Pressure range (MPa)	Methane molar composition range (x_1)	Number of data points
(Wang et al., 2003)	283.2; 293.2; 303.2	5.05-40.05	0-1	120
(Frost et al., 2014)	280.25; 298.77; 313.45	5.14-13.12	0.00514-0.0121	9
(Wise et al., 2016)	293.15	0.54-35.35	-	17

2.5.2.2. Ethane + water + methanol

The only available literature source for this system was the study by (Wang et al., 2003) in Table 2.12. This study has been discussed previously.

Table 2.12 Phase equilibrium sources for the ethane + water + methanol system

Reference	Temperature range (K)	Pressure range (MPa)	Ethane molar composition range (x_1)	Number of data points
(Wang et al., 2003)	283.2; 293.2; 303.2	5-40	0-1	100

2.5.2.3. Propane + water + methanol

There are two sources available for Px isothermal data as shown in Table 2.13. (Ng and Robinson, 1983) contains one data point for the system and Py data is presented by (Blanco et al., 2001).

Table 2.13 Phase equilibrium sources for the propane + water + methanol system

Reference	Temperature range (K)	Pressure range (MPa)	Ethane molar composition range (x_1)	Number of data points
(Ng and Robinson, 1983)	270.35	0.23	-	1
(Blanco et al., 2001)	254.2-282.7	0.099-0.543	-	237

2.5.2.4. Methane + methanol + TEG

The only available data in the open literature for this system was the study by (Zvawanda et al., 2022 b) as shown in Table 2.14. This study has been discussed previously.

Table 2.14- Phase equilibrium sources for the methane + methanol +TEG system

Reference	Temperature range (K)	Pressure range (MPa)	Methane molar composition range (x_1)	Number of data points
(Zvawanda et al., 2022 b)	303.16; 323.15	2.04-12.64	0.0113-0.0465	12

2.5.2.5. Methane+ propane + TEG

The only available data in the open literature for this system was the study by (Zvawanda et al., 2022 b) as shown in Table 2.15. This study has been discussed previously.

Table 2.15- Phase equilibrium sources for the methane+ propane + TEG system

Reference	Temperature range (K)	Pressure range (MPa)	Methane molar composition range (x_1)	Number of data points
(Zvawanda et al., 2022 b)	303.16; 323.15	0.78-8.58	0.0039-0.0446	10

2.5.2.6. Methane + propane + methanol

The only available data in the open literature for this system was the study by (Zvawanda et al., 2022 b) as shown in Table 2.16. This study has been discussed previously.

Table 2.16- Phase equilibrium sources for the methane + propane + methanol system

Reference	Temperature range (K)	Pressure range (MPa)	Methane molar composition range (x_1)	Number of data points
(Zvawanda et al., 2022 b)	283.16; 303.16; 323.15	1.25-9.96	0.0175-0.0871	15

Several systems of possible ternary combinations of methane, ethane, propane, water TEG and methanol have no available data found in the literature. Of the numerous combinations available, there is only data available for the above-mentioned systems.

2.5.3. Quaternary systems

2.5.3.1. Methane + propane + methanol +TEG

The only available literature source for this system was the study by (Zvawanda et al., 2022 b) as shown in Table 2.17. This study has been discussed previously.

Table 2.17- Phase equilibrium sources for the methane + propane + methanol +TEG system

Reference	Temperature range (K)	Pressure range (MPa)	Methane molar composition range (x_1)	Number of data points
(Zvawanda et al., 2022 b)	283.16; 303.16; 323.15	1.46-13.78	0.0050-0.391	15

As TEG, water, and methanol were the focus of this study, quaternary systems with these components interacting were reviewed. It was found there were no data for the methane + TEG + water + methanol; methane + TEG + water + methanol, and propane + TEG + water + methanol. Others were present but not available in open literature. The only system with open literature is the system mentioned above.

2.5.4. Quinary systems

2.5.4.1. Methane + propane +methanol + water +TEG

The only available data in open literature for this system was the study by (Zvawanda, 2022 c) as shown in Table 2.18. This study has been discussed previously.

Table 2.18- Phase equilibrium sources for the methane + propane + methanol + water + TEG system

Reference	Temperature range (K)	Pressure range (MPa)	Number of data points	Methane molar composition range (x_1)
(Zvawanda, 2022 c)	283.16; 303.16; 323.15	2.23-14.1	20	0.0074-0.0315

Similar to the quaternary systems the components TEG, water and methanol were the focus of the review. The only system available was the above-mentioned system.

2.5.5. Senary Systems

The literature review for the senary systems follows the same method as the quaternary and quinary systems and no available data was found.

2.6. Thermodynamic property methods used in this study

The intermolecular forces between the respective components of a system result in the non-ideal behaviour of the systems (Kontogeorgis and Folas, 2010). The non-ideal behaviour makes predicting system behaviours at various compositions challenging, particularly the non-idealities caused by hydrogen bonding. At moderate temperatures and low pressures, these non-ideal behaviours are minimal. However, most natural gas processes are conducted at high pressure and low temperatures where the non-ideality is most prevalent (Mokhatab et al., 2015). Thus, to model these systems accurately, an equation of state is required to describe the mixture behaviour when operating at high pressures. When specifically considering non-polar hydrocarbons, the Peng and Robinson and Soave-Redlich-Kwong (SRK) equations of state are the most popular and commonly used (Mokhatab et al., 2015). However, the Peng-Robinson EoS does not specifically consider hydrogen bonding, which makes it poor at correlating the behaviour of systems that contain water, TEG or methanol (Soo, 2011). However, its inclusion in model testing allows for the determination of the impact the missing associating parameter would have on modelling. The Cubic Plus Association (CPA) and perturbed chain

(PC) SAFT EoS do possess this consideration inherently, and are commonly used for systems that include water, glycols and methanol (Mokhatab et al., 2015).

For these reasons, this study focused on describing the phase behaviour of the measured systems with the CPA EoS, PC-SAFT model and Peng-Robinson EoS as a comparative reference to demonstrate both the abilities and limitations of these models compared to experimental data. The SRK model was omitted because the CPA is an extension of this model, including an association term, and has proved to be superior than conventional SRK for natural gas dehydration systems (Kontogeorgis and Folas, 2010).

2.6.1. Peng and Robinson equation of state

The Peng and Robinson equation of state (Peng and Robinson, 1976) has become one of the most successful models applied to phase equilibria (Walas, 1991). It improved the predictions for liquid phase behaviour by implementing an expression for volume dependency. Equations for the Peng and Robinson EoS can be found in Appendix A.

Limitations

As stated previously, the Peng and Robinson EoS has an accurate prediction ability regarding non-polar hydrocarbon molecules. However, there are limitations when highly polar and hydrogen-bonded fluids are present in the system. The lack of an association parameter causes this issue, thus, modelling that includes an association parameter has improved fits. Several studies, such as (Mathias and Copeman, 1983) and (Wu and Prausnitz, 1998), have attempted to overcome this by implementing different alpha functions and mixing rules. These have had some success in accommodating the non-idealities experienced in these systems. In addition, natural gas systems typically operate at high temperatures and pressures, which limits the accuracy of the PR EoS as it inaccurately predicts the compressibility factor. The development of newer property methods, such as the CPA and PC-SAFT has made these modifications less relevant to associating systems. The superiority of the CPA EoS and the PC-SAFT EoS to the Peng and Robinson EoS with variations in alpha function and mixing rules for natural gas dehydration systems has been shown previously in the work of (Zvawanda, 2022 c). Hence varying alpha functions and mixing rules in conjunction with the PR EoS was not considered further in this work.

Application of the PR EOS for natural gas systems

The PR EoS is applied in a number of literature sources with (Neagu and Cursaru, 2017) simulating a conventional natural gas plant. The paper concluded that the simulation was successful at simulating a natural gas plant, however this piece of literature did not make specific mention of the appropriateness or possible discrepancies associated with using the PR EoS. The paper by (Fouad and Berrouk, 2013) compared the PR EoS with the PC-SAFT EoS for application in sour natural gas system modelling.

These sour gas systems included methanol and tri-ethylene glycol alongside a number of hydrocarbons and impurities found within raw natural gas. The systems used were from available literature and typically contained either methanol or TEG and a mixture of hydrocarbon and impurities. None of the systems tested contained a methanol-TEG mixture. The study concluded that the PR EoS showed better results when the system contained a dry gas system (deviations were approximately half of that by PC-SAFT) while the PC-SAFT EoS performed better when the systems contained water or methanol by about 15-20%. This study shows there is still a relevant application for the older PR EoS while additionally showing the importance of having an EoS that considers the associating molecules. , Another study by (Saffari and Zahedi, 2013) added an original new alpha function to the PR EoS to improve its performance when predicting natural gas systems. The natural gas systems tested did not contain any liquids and were purely based on typical raw natural gas extraction composition with the exclusion of water. The study concluded the inclusion of their alpha function allowed for an accurate prediction of natural gas component behaviour, improving deviation from 3.8% to 1.4%. However, this modification has not had wide-scale application and is not typically available in commercial software. There is a shortage of recent publications applying the PR EoS, especially those that model phase data. This may be due emergence of the popular PC-SAFT and CPA EoS which could more accurately predict systems with associating components.

2.6.2. Association models

The PC-SAFT and CPA models are known as association models due to their general ability to model systems with hydrogen bonding accurately. These include systems that contain glycols, alcohols, water, acids, amines and other molecules with hydrogen bonding (Kontogeorgis and Folas, 2010). The PC-SAFT and CPA models were used in this work due to the association modelling ability and common use for modelling natural gas systems.

2.6.2.1. The Perturbed-Chain Statistical Associating Fluid Theory (PC-SAFT) model

The PC-SAFT EoS is an extension of the SAFT EoS, which uses a statistical mechanical method such as perturbation theory. There are several variations of the SAFT EoS. However, the PC-SAFT EoS differs from these by treating fluids as being connected by complex chained structures as opposed to unbound spherical particles (Kontogeorgis and Folas, 2010). Detailed explanations of the equation of state and a breakdown of their variables can be found in Appendix A.

Limitations

The PC-SAFT EoS has been widely used for mainly light hydrocarbons with some heavier hydrocarbons but has limited application in aqueous solutions (von Solms et al., 2006). This is due to the recent publishing of accurate pure water parameters for the PC-SAFT EoS and the testing of the model for aqueous systems in the literature. This is especially true for LLE aqueous systems, which the model has difficulty predicting due to a lack of a polar term within the EoS (von Solms et al., 2006).

Some authors have proposed that these limitations can be reduced by using an appropriate mixing rule such as that by Wolbach and Sandler for example (Grenner et al., 2007). This improves the fit by accounting for the induced-association interactions (Kleiner and Sadowski, 2007).

Application of the PC-SAFT model for natural gas mixtures

As previously indicated, the study by (Fouad and Berrouk, 2013) compared the Peng-Robinson EoS and the PC-SAFT EoS. The study found that PC-SAFT was a better model when predicting systems with water or methanol and PR EoS was better when predicting non-aqueous systems. The study by (Nasrifar et al., 2017) examined the prediction of natural gas containing water using the PC-SAFT EoS. The components tested were methane, ethane, hydrogen sulphide, carbon dioxide and water. There was no other association tested, such as between methanol and tri-ethylene glycol. The data used was sourced from available literature and the PC-SAFT model had accurate predictive ability. The study by (Alfradique and Castier, 2007) investigated the ability of hydrocarbon mixtures to be predicted by a number of property methods. These included PR and PC-SAFT EoS. The study used binary mixtures of hydrocarbons ranging from methane to nonane and concluded that the conventional cubic EoS provided the best representation. As the study concluded this was an unexpected outcome with the cubic EoS having the lowest deviation (%) of 1.079. Finally the study by (Kondori et al., 2018) evaluated the formation of gas hydrates in systems containing gas/water/salt/alcohol systems. These systems were evaluated using the UNIQUAC model and PC-SAFT EoS. The systems tested included the natural gas components of methane, ethane, propane, isobutane, carbon dioxide, and hydrogen sulphide, while the inhibitors used were methanol, ethanol, glycerol, NaCl, KCl, $CaCl_2$, and $MgCl_2$.The study concluded a wide range of compositions and conditions could be accurately predicted using their modelling strategy.

The above literature examples demonstrate the PC-SAFT model has a wide range of application within the natural gas research environment. However, no studies make a direct broad-scale comparison with the purpose-built CPA EoS in natural gas system applications other than the recent work of Zvawanda and coworkers. In addition, the previous studies discussed preceding the work of Zvawanda and co-workers, tend to employ associating terms with limited accuracy for TEG, water and methanol.

2.6.2.2. Cubic Plus Association (CPA) EOS

The CPA model combines the Soave-Redlich-Kwong (SRK) EoS and an association term similar to that in the SAFT model (Kontogeorgis and Folas, 2010). The model's development allows for predicting multicomponent hydrocarbon systems, including highly polar molecules such as water, glycols and alcohols. Further targets were (Kontogeorgis and Folas, 2010):

- Accurate calculations for multicomponent systems using only parameters estimated from binary data.
- Simplified mathematical formulas for describing complex compound systems.

Detailed explanations of the equation of state and a breakdown of their variables can be found in Appendix A.

Limitations

The CPA-EoS has been shown to have great versatility when dealing with both non-associating and associating compounds. It performs poorly when evaluating systems that include aromatic acids such as benzoic and terephthalic acid (Tsivintzelis and Kontogeorgis, 2012). The model has been tested in high-pressure systems where it performs satisfactorily when implemented with distinct combining rules. (Folas et al., 2006 b). However, the model has limitations in the supercritical region, where it tends to overestimate the interaction parameters (Kontogeorgis and Folas, 2010).

Application of the Cubic Plus Association (CPA) EOS for natural gas systems

The study by (Arya et al., 2014) used the CPA EoS to simulate a natural gas dehydration plant. The study aimed to demonstrate the usefulness of the CPA EoS in modelling natural gas systems. The study accomplished this by using binary parameters to simulate multicomponent systems, which included TEG, water and natural gas. The results from the simulation were agreeable with experimental data and showed the ability of the EoS to successfully simulate the dehydration process. The study by (Kontogeorgis et al., 2006) is an extension of the original CPA paper and aimed to demonstrate the improvements and greater applications of the CPA model. The authors motivated for a new focus to be placed on the estimations of pure compound parameters for alcohol-hydrocarbon VLE. The paper reiterates the usefulness of the CPA model for systems containing alcohols, glycols and water. With regard to its new focus, the study finds the model has very good correlations and predictions for alcohol-alkane VLE and SLE systems. It was also concluded that the model had not improved in terms of the 3-B TEG schemes for alcohol-alkane phase equilibrium. The study finally noted that there is still some controversy when different number of sites are attributed to water. A study by (Kruger et al., 2018) reported experimental work on a 20-component ethylene glycol, water and natural gas mixture. The study was conducted at high-pressure conditions and aimed to replicate the conditions experienced during subsea natural gas dehydration unit operations. The results were compared to a CPA EoS model in-order to evaluate the applications for this model in designing of subsea dehydration systems. The study concluded that there are benefits to using ethylene glycol as a dehydration agent especially at high pressure. The study observed the CPA model in predicting the water and MEG content in an ethylene glycol (1) + water (2) + methane (3) mixture. The study concluded this was due to the inclusion of CO_2 within the gas mixture, as the model encountered similar difficulty in previous studies. The authors did accept the modelling results with an error of 10-15% for major components and believes these can be decreased with the inclusion of additional binary VLE data in the training. Finally, a study by (Qvistgaard et al.,, 2023) conducted experimental measurements on TEG, water and natural gas mixtures at 6.9 and 12.5 MPa at a range of 15 ^{o}C-40 ^{o}C. The equation of state chosen was CPA as the

systems tested were highly associating. The CPA model was used against the experimental results while also varying its association schemes for TEG. The study concluded that the 4C association scheme remains the best-performing scheme, and subsea natural gas dehydration can be advantageous at high pressure and low temperature.

The studies using the CPA model have leveraged its advantages in predicting highly associated systems. This is especially true with the studies conducted and supervised by Kontogeorgis with whom much of the CPA natural gas modelling and testing is centred. However, there is still a lack of data for TEG and methanol mixtures with natural gas and the comparison of the CPA model with other models.

2.7. Thermodynamic modelling approach

The modelling approach taken for any phase equilibrium study requires a few key considerations. Arguably, the most significant of these is the manner in which pure component physical properties are integrated into the simulation. In-order to succeed in this venture the following important steps were considered (Carlson, 1996):

1) Choosing an appropriate physical property method for the components used.

Property methods are typically created with respect to specific component combinations. As stated previously with the PR EoS, this equation of state is generally strong at modelling and predicting natural gas systems that have non-associating components. Additional considerations such as the temperature, pressure and other properties are considered as specific methods handle non-ideal conditions better than others. For this study the physical properties methods were chosen based on previous literature for the proposed systems. Another useful tool in property method selections is the Aspen Plus: Property Method Section Assistant, which can assist in choosing an appropriate method.

2) Validating physical properties.

The validation of physical properties is a crucial step in ensuring accurate modelling. This process required experimental data to be available and compared to the modelled data. This process can be executed for the pure component and mixture component parameters. The degree of similarity between these two results will determine how accurate the models and parameters used are. In this study this was conducted for most of the components used where data was available, with the process and exceptions detailed in Chapter 3 and 5, respectively.

3) Describing the non-databank components and missing parameters

Suppose there are components missing from the available data banks or literature. In that case, it is possible to exclude these if the component is a minor constituent or exhibits a limited interactions mixture. However, if the missing component does not meet this criterion, these parameters should be estimated. Typically, similar components in terms of atomic structure will have similar properties. This

logic is sometimes used to substitute the parameters of one component for another. This study did not have this issue in terms of pure component parameters.

4) Obtaining and estimating any missing property parameters

Typically, a literature search is conducted to find any available pure and binary parameters. When these are not available, several different methods can be employed to accomplish this; however, the most accurate is regression based on experimental data. When regressing, the number of parameters should be minimized while additionally considering the standard deviation. The standard deviation should not be greater than the parameter itself; otherwise, there may be too many parameters being estimated. In addition, when there is a large temperature range, standard deviations tend to be higher. For HPVLE the phi-phi methodology for binary interaction parameter fitting is the standard practice, with fitting algorithms described in detail by Raal and Mühlbauer, (1997) for example.

These steps are taken from and given in more detail by (Carlson, 1996). However, these general steps were considered when approaching the modelling in this study. The only modification was conducted on the binary parameters regression and selection, which is expanded on in Chapter 5. The pure component parameters for the models used in this study for the PR, CPA, and PC-SAFT EoS can be found in Appendix B. The binary parameters determined can be found in Chapter 4. The algorithm used for the regression of these parameters is presented in appendix A.

2.8. Methods used to determine the suitability of models

To determine which property model was most accurate in representing the experimental data after model regression, two comparisons are used in this work to evaluate the property method fit to the experimental data.

The average absolute deviation (AAD) was used to measure deviation for various properties:

$$AAD = \frac{1}{N}\sum_{i=1}^{N}\left|\theta_i^{calc} - \theta_i^{exp}\right| \tag{2.15}$$

Where θ is the evaluated properties, and *i* is the data index and N is the number of data points.

The Absolute Average Relative Deviation (AARD)

$$AARD(\%) = \frac{1}{N}\sum_{i=1}^{N}\frac{\left|\theta_i^{calc} - \theta_i^{exp}\right|}{\theta_i^{exp}} * 100 \tag{2.16}$$

Where θ is the evaluated properties and i is the data index and N is the number of data points.

Chapter 3: Experimental Equipment and Methodology

This chapter presents the equipment used to conduct HPVLE experiments in this work as well as the methodology. The validation of the accuracy of the devices used in the measurements, experimental techniques and the purity checks of chemical components are discussed. The equipment, materials and methods employed during the study is presented. The information presented in this chapter is extracted and based on the research work from several investigative studies performed in the Thermodynamics Research Unit, such as (Nelson and Ramjugernath, 2017), (Nelson et al., 2021) and (Zvawanda, 2022 c)

3.1. Section of experimental methods

The difficulty in obtaining HPVLE experimental measurements is a major reason for the shortage of reliable data in the literature. This is due to several reasons that usually make such endeavours costly and time-consuming. To obtain accurate and reliable results, temperature and pressure must be accurately controlled or measured, and there must be no contamination during experimental runs and precise measurements/establishment of compositions of components at equilibrium in the phases. It is difficult to maintain pure liquid feed components such as methanol and TEG as they are hydrophilic, absorbing atmospheric water, and thus must be dried and their water content established prior to measurements. In addition, loading relatively small amounts of individual components/low molecular weight components makes achieving accurate mixture composition preparations difficult.

The verification systems selected in this work require singular and binary liquid mixture preparation, while the new systems involve ternary liquid systems. These mixing procedures necessitate great care and patience to ensure no air or liquid contamination occurs during preparation and filling. Therefore, the vacuum condition must be maintained during the loading process to prevent air contamination. Similar consideration and care must be taken for the preparation and loading of the singular and ternary gas mixtures. For the equilibration establishment measurements at high pressure, a great deal of care and patience must be taken to ensure accurate results. Due to the complex behaviour of high-pressure multi-component systems, inaccuracies must be prevented, and deliberate and repeatable procedures are required. Considering these difficulties, the following equipment and procedures were adopted as these were developed to ensure a reliable and accurate set of experimental results.

3.2. Experimental Equipment

3.2.1. Equilibrium cell

The central piece of the HPVLE apparatus is the equilibrium cell which was commissioned at the Thermodynamic Research Unit and supplied by Rayotek Scientific Inc. Figures 3.1 and 3.2 depict a schematic of the equilibrium cell and all relevant components. The multicomponent mixtures are charged within this cell, and phases reach equilibrium at a constant temperature. The cell comprises a hollow cylindrical sapphire tube, two stainless (SS) 316L steel flanges and several smaller components.

The equilibrium chamber comprises a synthetic sapphire tube (55mm outer diameter (OD), 32 mm inner diameter (ID), and a length of 70 mm, supplied by Rayotek Scientific Inc. (Zvawanda, 2022c). The sapphire is transparent, allowing for clear observation of the cell contents (or phases) within, making the observation of the bubble point possible. In addition, due to its material, thickness and cylindrical shape, the sapphire tube can handle extremely high pressures of up to 25 MPa (Zvawanda, 2022c).

The two stainless steel flanges are placed at either end of the cylindrical sapphire tube and are secured using two shoulder bolts with lengths of 122 mm and a shoulder size of 64 mm. These shoulder bolts are tightened using eight M8 nuts, where four are found on each of the flanges. The flange itself has a width of 99 mm, a height of 76 mm and a side thickness of 20 mm. There is a total of 5 inlet/outlet ports on the two flanges which were drilled into the flange body and sealed with 1/8" Valco SS316L compression fittings. There is one port on the flange facing the hydraulic side, which allows for the injection and removal of hydraulic fluid using an attached valve. On the flange facing the charged (mixture in equilibrium) side, there is a total of 4 ports. Two of these ports are used for charging and discharging the mixtures using a feeding valve, one was used for the pressure transducer (PT), and the final port was plugged. To ensure a hermetic seal between the flanges and cylindrical sapphire tube, two polyurethane O-rings of a diameter of 40 mm outer diameter and cross-section of 3.10 mm were inserted into grooves within the flanges. These rings were selected due to their high durability, impact strength and resistance to high pressures.

A stainless-steel piston is situated within the cylindrical sapphire tube separating the systems and hydraulic sides. This piston is moved using hydraulic fluid, which in the case of this study was water. A nitrile O-ring is installed in a groove within the piston to ensure no leakage between the hydraulic and charged side. This O-ring has an internal diameter of 20 mm and a cross-section of 4 mm, forming an airtight seal between the piston and the cylindrical sapphire. The O-rings selected were made from nitrile, which has chemical resistant to the components used in this study and is durable enough to prevent tears and abrasion damage during experimentation. In addition to this O-ring, a permanent teflon ring is placed within another piston groove. This acts as a guide ring that ensures the piston

remains stable within the sapphire tube and maintains piston alignment while applying hydraulic force. A mixer is placed within the piston which consists of an SS 316L rotary impeller, ball bearings made from ceramic and polytetrafluorethylene (PTFE) and a neodymium magnet. This device ensures that there is proper mixing within the sapphire tube, enabling faster equilibrium and good mass transfer between the respective components. The internal mixer is rotated using an external magnet connected to a DC motor placed directly above the equilibrium cell. Finally, roughly three rolls of 12 mm wide and 0.05 mm thick thread tape are placed around the cylindrical sapphire which makes contact with the steel flanges. This protects the sapphire's edges from chipping during assembly, which would affect the cell's integrity.

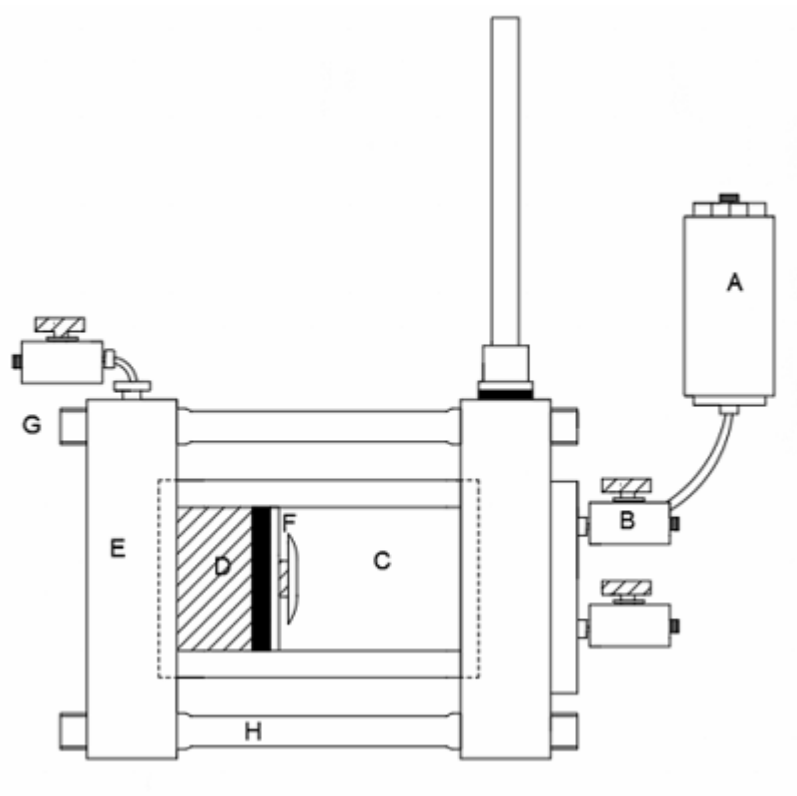

Figure 3.1 Side view Schematic of Equilibrium cell used for HPVLE measurements. Drawn by R Raghunanan. A: Pressure transducer, B: Swagelok ball valve, C: Equilibrium chamber, D-Piston, E-Flange, F: Stirrer, G:M8 Nut, H: M8 Shoulder bolt.

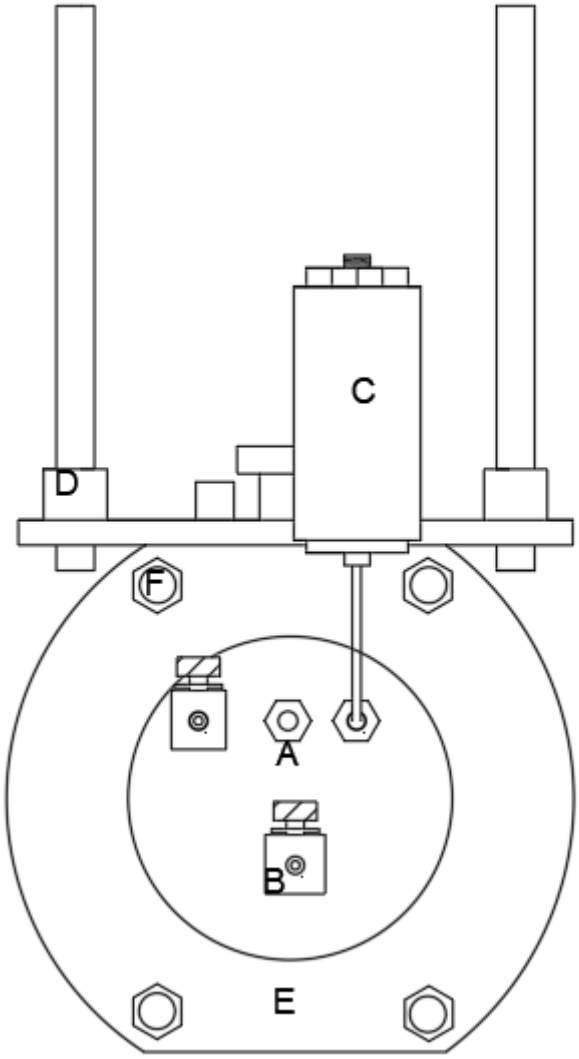

Figure 3.2 Front view Schematic of Equilibrium cell used for HPVLE measurements. Drawn by R Raghunanan. A: SS 316 Plug, B: Swagelok ball valve, C: Pressure Transducer, D: Mounting bracket, E- Front side of the flange

3.2.2. Temperature and pressure measurement devices

Two Pt-100 Ω temperature probes were used to monitor the temperature around the equilibrium cell (within an isothermal bath), which was assumed to be the temperature within the cell upon sustained thermal equilibrium. The total length of each probe was 35 cm.

One pressure-transmitter model, P-10 from WIKA was used to monitor the pressure within the equilibrium cell. This transmitter is attached to the equilibrium cell using a stainless-steel tube connected to one of the ports drilled into the flange. The pressure transducer range was 0-35 MPa gauge. The transducer had a supplier-rated accuracy of 0.05% of full scale (FS).

The pressure and temperature devices are connected to an Agilent model 34970A data logger, which tracks the signals from these devices and converts these signals into usable temperature and pressure readings. The data logger was connected to a computer (Dell I7) which uses specified software to translate these data readings into various figures, graphs and tables.

A temperature bath was used to regulate the temperature of the equilibrium cell. This consists of a bath (length 49 cm, width 36 cm and height 30 cm) filled with roughly 20 dm^2 of water, which was heated or cooled using a Grant Optima TX 150 temperature controller. The water acts as a heat transfer medium and ensures a stable temperature during experiments while the equilibrium cell is submerged. Water was selected as the heat transfer medium due to the temperatures considered in this work being well within water's melting and boiling points and because the colourless nature allowed for ease of viewing of the submerged equilibrium cell.

3.2.3. Auxiliary devices

3.2.3.1. Syringe Pump

The syringe pump used was a model 100DX ISCO pump. This device pumped water into the hydraulic side of the equilibrium cell. Carefully adjusting the settings allowed for a gradual increase in pressure while ensuring the system was in equilibrium. The 100DX has a minimum flow rate of 0.01 µl/min and a flow accuracy of ±0.3% of the set point. This relatively small flow rate allowed for the piston's gradual movement, reducing the volume within the system side of the cell and thus increasing the pressure. This allowed for the gradual change of pressure as the system moves towards the bubble point.

3.2.3.2. Mass Balance

An Ohaus model PA4202C mass balance was used to measure the mass differences of the equilibrium cell when empty, charged with a liquid, and charged with the gas and liquid. This measuring device had a maximum capacity of 4200 g and a standard uncertainty of 0.01 g. An Ohaus model PA423C mass balance was used when preparing the binary and ternary liquid mixtures, as it has a higher measurement resolution and allows for improved precision. These measuring devices allowed for the determination of mass values and, thus, the mole fraction of the synthesized mixtures within the equilibrium cell. This balance had a maximum capacity of 420 g and a standard uncertainty of 0.001 g.

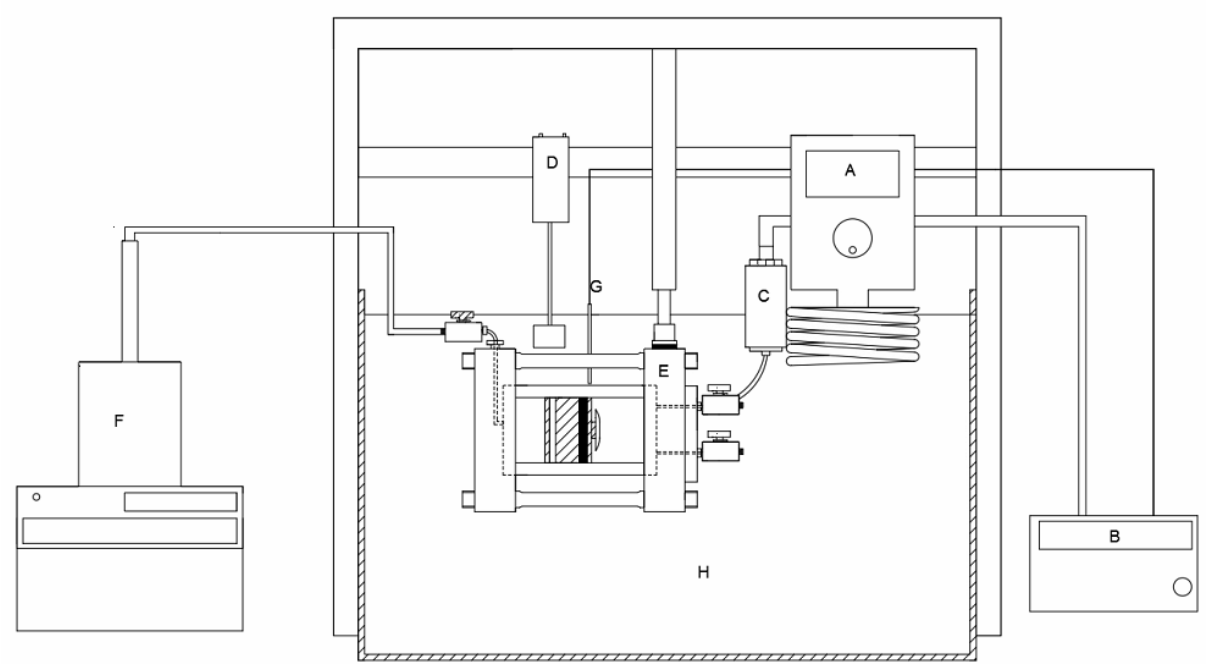

Figure 3.3 Internal Schematic of the apparatus used for HPVLE measurements. Drawn by R Raghunanan. A: Grant Optima TX 150 Temperature controller, B: Agilent Model 34970A data logger, C: Pressure transducer, D-External rod, motor and magnet, E- Equilibrium cell, F: Model 100DX Syringe pump, G: Pt-100 Ω stainless steel temperature probes (T102 & T104), H: Water Bath. This figure depicts the overall experimental set-up during HPVLE measurements.

3.3. Experimental Procedure

3.3.1. Temperature Calibration

Temperature calibration is an essential step in ensuring accurate and reliable temperature results. Thus, the two Pt-100 Ω temperature probes used in the experiment were calibrated to ensure the results were accurate to the actual temperature within the water bath. To conduct this calibration, a temperature standard was required. This acted as a known value to compare to the experimental given by the PT-100 probes. The device used for the standard was a WIKA CTH6500. The temperature was regulated using a WIKA CTB9100 stirred liquid bath. The liquid bath uses silicone oil (M20) as the medium for heating and cooling. The two Pt-100 probes and the WIKA CTH6500 standard probe were submerged in the oil at roughly the same depth, ensuring minimal temperature differences. The temperatures were selected at the lowest value of the device range of 273.15 K and were adjusted in increments of 10 K until the maximum temperature of 333.15 K was achieved. This process was repeated from the maximum temperature of 333.15 K down until the minimum temperature value of 273.15 K. Between temperature measurements; the system was allowed to stabilise until the temperature reflected by the

standard and probes were constant for over 10 minutes. At that point, the temperature of the Pt-100 probes and WIKACTB9100 temperature standard were recorded.

Upon completion of the measurement of all temperature values, a first-order linear equation and a second-order polynomial equation were used to perform the calibration. The equation with the better fit was used as the calibration equation for the Pt-100 probes labelled T102 and T104.

$$Y = mX + C \tag{3.1}$$

$$Y = lX^2 + mX + C \tag{3.2}$$

In the above equations, Y represents the newly calculated temperature, m represents the coefficient of X, C represents the y-intercept, and l represents the coefficient of X^2. The X represents the temperature observed by the probes, which, when inputted into the calibration equation, would give the calibrated temperature reading. The values for the calibration equations were determined using the LINEST function found in Microsoft Excel. This function performs the calculation by implementing the "least squares" method to find the best-fit equation for both a linear and polynomial equation. This calibration was performed before the test system experimental run, and checked periodically throughout the different experiments, as the temperature probes are sensitive to external damage, which could have affected the internal resistance of the probes and the accuracy of the resultant readings. The uncertainty determinations can be found in Appendix C

3.3.2. Pressure Calibration

Pressure calibration is essential in verifying that the pressure reflected by the device is the same as the pressure exhibited within the equilibrium cell. The device calibrated was the P-10 pressure transmitter with an operational range of 0-35 MPa. The device used as the standard for the pressure calibration was a CPC Mensor 8000 high-end pressure controller and standard. To perform the calibration, the equilibrium cell was prepared as it served as the pressurised vessel. The CPC Mensor 8000 was connected to a nitrogen (N_2) gas cylinder via the supply port, which pressurised the equilibrium cell via the control inlet on the CPC Mensor 8000. The P-10 pressure transmitter was located on the cell, sending a signal via the data logger to a nearby personal computer. The CPC Mensor 8000 results were captured via the result display. The calibration was conducted over the selected pressure range of HPVLE measurements (0-16 MPa). The pressure was initiated at 0 MPa absolute and was increased in intervals of 1MPa until 16MPa and reduced back to 0 MPa. The adjustment of the nitrogen gas cylinder controlled this increase and decrease. In between these intervals, the system was allowed to stabilise before any data was captured.

The calibration was conducted similarly to the temperature calibration, with increasing and decreasing increments, equilibration time and stabilization time. Similar equations to equations 3.1 and 3.2 were used for the first-order and second-order polynomials, and the same calculation process was used to determine the calibration.

3.3.3. Chemical Property and Composition Purity tests

Identifying and reporting the purity of the chemicals used for HPVLE measurements is of the utmost importance. Minor impurities from the supplier or via contamination can significantly impact the final results; hence the uncertainty introduced by impurities must be quantified. Several tests were conducted to verify chemical purities where possible. Tests included gas chromatography and property tests such as density, refractive index and vapour pressures. These were compared with known literature values to determine if the manufacturer's stated purities were accurate and whether the product is usable. These results can be found in Chapter 4.1.

3.3.3.1. Gas Chromatography

Gas chromatography involves the vaporisation of injected components through an adsorption column at a fixed temperature, pressure and flowrate, which registers the different components as peaks based on variations in their thermal conductivity (in this case). The instrument used in this work was a Gas Chromatogram (GC)-2010 plus supplied by Shimadzu. The GC was fitted with a Zebron capillary column of length 60 m and diameter 0.3 mm. This was used for all experimental system analyses. When used correctly, the various components of a mixture are represented as unique peaks. However, it is important to identify suitable analysis conditions so that peak separation occurs within the gas chromatograph, and the mixture components can be uniquely identified. For components that are assumed to be as close to pure as possible, only one prominent peak should be visible, as the peak area correlates with the sample purity. A specific amount was injected into the GC for all components used, namely 1 µl for liquids and 0.25 ml for gases. It should be noted that the peak area ratio is not the same as the composition of a component. However, if the peak area ratio is high enough and no other major peaks are present, the component tested is assumed to be of high purity. Components of 99% relative peak area were considered useable for this experiment, with any values below this amount requiring more testing or impurity identification.

Impurity identification was required in this work for an assumed pure propane cylinder with significant methane and ethane contamination that was procured from a reputable supplier. To characterise the mixture accurately, a calibration was conducted using known pure gases (methane, ethanol, and propane). When injected into the GC, these gases gave peak areas that were in proportion with the

number of moles injected. These ratios were used to determine each component's number of moles and, thus, the gas mixture's overall composition. This allowed for the determination of the composition shown in Chapter 4.1

3.3.3.2. Density

The densities of the liquids used in this work were measured using an Anton Paar DSA5000m densimeter. The densimeter has a measuring range of 0-3 g/cm^3 at 25^{o}C and standard uncertainty of 0.000005 g/cm^3 for density and 0.01 K for temperature. The response to changes in vibrational period of an internal U-tube within the densimeter when filled with the liquid sample, indicates the liquid density. As this vibration is induced, the tube's resonant frequency changes depending on the liquid density within the tube. Before testing began, the device was cleaned using acetone as a solvent, as the components tested were soluble in acetone. Once cleaned, the tested liquid was flushed into the inlet tube three times before results were taken, ensuring no residue remained. Once the system was prepared, a syringe of the liquid component was injected into the inlet. It was ensured that no air bubbles were present as this would cause inaccurate results. Once determined, the density was recorded, and steps were repeated two to four times, ensuring a reproducible result.

3.3.3.3. Refractive index

The refractive index was determined using an Atago-Rx7000a refractometer. The Atago-Rx7000a determines the refractive index of a liquid by measuring the change in direction that light undergoes while passing through the liquid. Before testing, the device was cleaned with acetone as a solvent as all the components tested were soluble within it. The tested liquid was loaded using a syringe which covered the lens of the device. The device then yielded the refractive index reading at a set temperature, and this procedure was repeated two to four more times to ensure repeatability. All liquid components of this study were tested at 25^{o}C with a standard uncertainty of 0.0001 n_D and 0.0002 K.

3.3.3.4. Vapour pressure measurements of gases and purchased gas mixtures

Pure component vapour pressure data are typically available for common components and is a useful verification method of component identity and purity. If any impurities are present within a gas or liquid component, it will affect the experimental vapour pressure when compared to the available literature. For this reason, any significant deviations in the measured vapour pressure from the literature, would indicate an impurity and warrant further testing.

The vapour pressure experiments for the gases used were conducted with the equilibrium cell used in the HPVLE experiments for this work. The cell was cleaned, leak-tested and evacuated before any

loading could begin. The gas was loaded into the equilibrium cell at high pressure, ensuring a liquid phase formed. If the gas struggled to form a liquid phase, the equilibrium cell was placed in an ice-water bath to lower the equilibrium chamber's temperature, assisting in forming a liquid. Once loaded with the gas-liquid mixture, the equilibrium cell was submerged inside the isothermal water bath. The pressure and temperature readings were observed using the Agilent device, and a two-phase region was ensured. The temperature of the water bath was kept constant while the pressure of the equilibrium chamber was monitored. Once stable, the pressure was recorded, and the temperature was adjusted to a new temperature. This process was repeated over a range of temperatures and multiple readings were taken to ensure repeatability.

The vapour pressure of methane was not determined due to equipment range limitations.

3.3.3.5. Liquid degassing and vapour pressure measurements

It is common for residual gases to dissolve into a liquid over time or for volatile impurities produced during chemical manufacture to dissolve in the bulk of less volatile liquids. These dissolved gases affect the vapour pressure measurements of the liquid due to their high volatility. For this reason, before vapour pressure measurements were conducted, the liquid samples used were degassed. The degassing procedure was performed as follows:

An isothermal bath was filled using a 1:1 mixture of anti-freeze and water controlled by a PolyScience temperature controller set to approximately 263.15 K. This mixture is circulated through a glass Vigreux-type column with condenser. Below the condenser, a 250 ml round bottom flask holding roughly 75ml of the testing liquid is attached via a metered Teflon plug to a Vigreux-type column and a vacuum pump. Once the glass column was evacuated, the Teflon plug was partially opened, allowing vacuum conditions within the flask. Over time the testing liquid and dissolved gases evaporated. The condenser ensured the testing liquid would condense back into a liquid but that the volatile impurities were removed by venting the gases. This process required approximately 45 minutes to complete, with the higher boiling point components taking longer to degas. The liquid vapour pressure measurements were conducted using a static non-visual cell constructed from stainless steel with a volume of 70 cm^3. Details of a similar experimental device is reported in (Naicker, 2017).

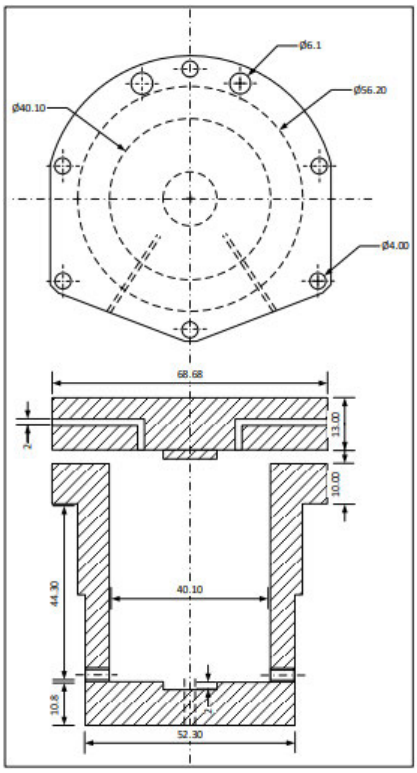

Figure 3.4 Dimensions for the Liquid vapour pressure cell (extracted from Naicker, 2017)

This cell was cleaned using the solvents ethanol and acetone to remove any residual liquids and subsequently dried and evacuated, ensuring vacuum conditions within the cell. Leak tests were conducted by monitoring the internal pressure of the cell. No leaks were observed when there were no changes in the cell pressure during vacuum conditions. Approximately 50 cm^3 of degassed liquid was loaded into the cell while ensuring vacuum conditions were maintained within the system. The pressure and temperature were monitored using a 0-100 kPa pressure transducer and one Pt-100 probe temperature probe attached to the equilibrium cell. During the vapour pressure measurements, the cell was submerged in a glycol-water mixture with a Grant TX temperature controller, which regulates the temperature of the bath and, in turn, the cell's internal temperature. Equilibrium within the cell was assumed when the temperature and pressure readings were stable for an additional 30 minutes; these measurements were then recorded. The temperature measurement range were limited to this study's experimental range, which was 303-323 K. The calibrations and uncertainties were used from recently conducted experiments using the equipment found in (Zvawanda, 2022 c).

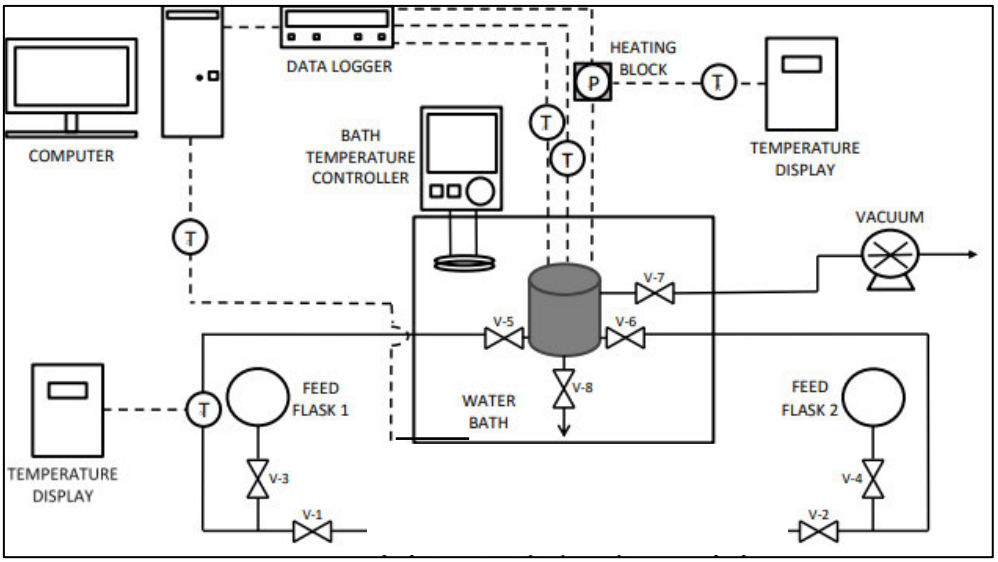

Figure 3.5 Schematic diagram of liquid vapour pressure equipment. Redrawn and modified from (Naicker, 2017).

3.3.4. Methanol moisture content

Methanol is hydrophilic, meaning it naturally attracts water molecules. As a result of this, methanol used in the experiments would theoretically absorb water from the atmosphere over time, diluting the purity of the methanol used. In order to accurately determine the moisture content of the methanol, a Karl Fischer C10S device was used for titration. This device monitors the electrical current within a methanol sample and uses a reagent which reacts with water to form a non-conductive chemical. In this test, the reactant was Karl Fischer electrolyte A. The procedure involved testing a sample of methanol where the device would automatically titrate the correct amount of reactant and determine the moisture content of the methanol. The device has a repeatability of 0.3% at > 1mg of water.

3.4. Cell preparation

Before any testing began, it was necessary to check that the equilibrium cell was free from contamination (refer to Figures 3.1-3.3). The smallest droplet or stain of any substance can compromise the final results' accuracy by altering the loaded mixture's composition. The equilibrium cell was dismantled to ensure this by removing the four bolts holding the respective flanges together. In addition, the piston, two polyurethane rings and magnetic stirrer were removed and separated. The pressure probe

was removed and checked for any liquids making its way into the probe. This is especially necessary when highly viscous fluids such as TEG were measured in the preceding run. Once fully dismantled, the flanges, piston; magnetic stirrer and cylindrical sapphire tube were washed with acetone. Acetone was chosen as the solvent used as all chemical components used are soluble in acetone, and it quickly evaporates from the equipment. It is also chemically compatible with all of the materials used in the construction of the device. Ethanol was used for cleaning the two polyurethane rings as acetone can wear down the rings over time. Subsequently, all the components are wiped using paper towels and blow-dried using compressed air. When TEG was used, the flanges, piston and magnetic stirrer were washed a second time as TEG was more challenging to remove due to its high viscosity. This is especially important as the flanges have numerous valves and fittings attached where TEG residues could remain. Before reassembly, the nitrile O-ring on the piston was replaced, and roughly three layers of polytetrafluoroethylene tape were applied to the edges of the cylindrical sapphire tube. Finally, the two polyurethane rings were inserted into the flanges, and the two halves were secured using the four bolts.

One of the major concerns in conducting any VLE experiment is sealing of the equilibrium cell. A minor leak will disturb the equilibrium in the cell as well as slowly change the composition of the components. In addition, a leak on the hydraulic side of the cell will make it difficult to maintain a constant compression pressure. For this reason, a leak test was conducted before every experimental run. The equilibrium cell was charged with 10 MPa of N_2 gas, and a surfactant solution was applied to all the nuts, O-ring points and valve connections. If any large bubbles were formed, the cell was dismantled, cleaned and reassembled with the problem area being tightened. If smaller bubbles were formed, the specific nut or valve was tightened until the leak stopped. Each area was exposed to the surfactant for roughly 10 minutes to ensure no bubbles formed. Once no leaks had been observed, the cell was evacuated, and any remaining liquid was removed using paper towels, compressed air and heated air from a blow dryer. It is imperative that all liquid is removed from the outside of the cell as this could affect the equilibrium cell's mass during composition measurements. The final step taken to prepare the cleaned and tested cell was to evacuate the cell for roughly 15-20 mins on both the hydraulic and system sides. This removed residual gases from the cleaning and leak testing procedures while also creating vacuum conditions within the cell.

3.5. Liquid Mixture Preparation

The binary liquid mixture preparation was identical to the method used by (Zvawanda, 2022 c) for preparing mixtures. The technique involved using two glass round bottom flasks with high vacuum valves. Each of these flasks were vacuumed to remove any residual air using the vacuum pump. After that, a predetermined amount of the degassed liquid components was loaded into each cell using the

measuring scale to determine the weight composition. These two glass flasks were loaded with pure components, placed under a vacuum, and remeasured to determine the amount of pure liquids. These two round bottom flasks were thereafter attached using a T connector with an incorporated valve. The flask with the lower viscosity component was placed above the other to ensure the easiest mixing. The T connector was placed under a vacuum using a vacuum pump to ensure no residual air would enter either flask. Thereafter the high vacuum valves were opened, allowing the top liquid to mix with the liquid of the bottom flask. The top flask was shaken slightly to allow as much of the top liquid to enter the bottom as possible. At this point, the bottom flask contained the system liquid mixture. The bottom flask was disconnected from the T- piece fitting and measured on the Ohaus PA423C measuring scale. The new weight of the flask was used to determine the composition of the mixture.

For ternary liquid mixtures, the process is similar, where the binary liquid mixture prepared as described above is mixed with the third component using the same procedure.

3.6. HPVLE Measurements

The HPVLE measurements were the basis of this study and followed the following procedure:

- The equilibrium cell was subjected to the above-mentioned procedure for cell preparation and was in a state of vacuum. Before any loading, the mass of the evacuated cell was measured and documented.
- The pre-made liquid component or mixture was loaded into the equilibrium cell via the ball valve found within the flange. The round bottom flask was connected to this valve using a connector, and once secured, the valve was opened, filling the cell. Once emptied, the ball valve was closed, and the round bottom flask removed. The cell mass was measured and documented.
- The gas component was added to the cell by connecting the gas line from the component cylinder to the top loading valve on the equilibrium cell. Before this connection is made, the gas line was purged, ensuring no air was trapped within the line. The cell was then filled with gas until the desired pressure. The valve was closed, and gas line removed. The mass of the completely loaded cell was then measured for a final time.
- Once fully loaded, the cell was attached to a mounting bracket. The water bath was lowered using a car jack and the cell using the mounting bracket was suspended over the water bath. Thereafter the attachments for the syringe pump model 100DX (ISCO) and pressure transducer were attached to the cell. Finally, the temperature probes were moved into place and the water bath was raised, submerging the cell in water.
- The cell was then within the water bath and the temperature controller was set to the first

experimental temperature. In addition, the magnetic drill with the neodymium magnet was placed above the cell and turned on, allowing the magnetic stirrer to start moving.

- During this process, a program monitored the temperature and pressure readings. Once the temperature and pressure had stabilized within the cell, the syringe pump was turned on at a 0.1 cm^3/minute until only a few bubbles were left. 5 minutes were allowed for stabilisation.
- If no bubbles were left, the system was refilled at a rate of 0.05 cm^3/ minute until the first bubble is observed. Thereafter the syringe pump was set to deliver 0.01 cm^3/minute of water until the bubble disappears. The bubble must be observed closely; once it disappears, the temperature and pressure are recorded.
- The stabilization, refilling and delivering process is repeated until 3 data points were captured. This is done to ensure repeatability of the equilibrium point.
- If multiple isotherms were required, the temperature controlled was changed, and the process was repeated for the new isotherm.
- Once testing was completed the syringe pump was completely refilled. The water bath was lowered, and the spinning drill, pressure and syringe pump attachments were removed. The cell was removed from the water bath and detached from the water bath.
- The cell's contents were evacuated safely and cleaned according to the above-mentioned cell preparation procedures.

3.7. Safety and Hazards

Experiments must take into consideration the safety and hazard concerns when conducted. Measurements on the high-pressure equipment were conducted at X bar and many components were highly flammable. Thus, several good practice safety procedures were followed.

3.7.1. MSDS

The MSDS for the following components: TEG, methanol, water, methane, carbon dioxide and propane can be found at (Software, 2023). These MSDS give a background for the component's safety considerations, such as hazards, health effects, etc. These were provided by the manufacturers and consulted when conducting the following experiments. The table below highlights the primary considerations for each component:

Table 3.1 MSDS summary for components used in the experiments (Software, 2023)

Component	Hazards	Health effects	Storage and Handling	Disposal methods
Methane (Gas)	• Extremely Flammable gas • Contains gas under pressure which can explode if heated.	• Suffocation is possible in a poorly ventilated room	• Within a Pressurized container. • Handle with gloves and eye protections	• Should only be dispelled in a well-ventilated room.
Ethane (Gas)	• Extremely Flammable gas • Contains gas under pressure which can explode if heated.	• Suffocation is possible in a poorly ventilated room	• Within a Pressurized container. • Handle with gloves and eye protections	• Should only be dispelled in a well-ventilated room.
Propane (Gas)	• Extremely Flammable gas • Contains gas under pressure which can explode if heated.	• Suffocation is possible in a poorly ventilated room	• Within a Pressurized container. • Handle with gloves and eye protections	• Should only be dispelled in a well-ventilated room.
Carbon Dioxide (Gas)	• Contains gas under pressure which can explode if heated.	• Suffocation is possible in a poorly ventilated room	• Within a Pressurized container.	• Should only be dispelled in a well-ventilated room.
TEG (Liquid)	• Not considered Hazardous.	• No major health effects. Typically, safety measures should be taken.	• Store in an airtight container within a cold, dry and well-ventilated room. • Handle with gloves and eye protections	• Should be disposed of in accordance with local regulations
Methanol (Liquid)	• Flammable liquids • Toxic if exposed to skin, eyes and ingested.	• Can cause eye irritation. • Can cause skin irritation. • If swallowed organ damage can occur.	• Store in an airtight container within a cold, dry and well-ventilated room • Handle with gloves and eye protections	• Should be disposed of in accordance with local regulations
Water (Liquid)	• Not considered Hazardous	• No major Health effects	• Store in an airtight container within a cold, dry and well-ventilated room	• Should be disposed of in accordance with local regulations

3.7.2. Precautions and safety measures

The hazards mentioned above are accounted for using several safety procedures and equipment. These considerations prevented the main hazards of toxic exposure, asphyxiation and flammable ignition.

3.7.2.1. Toxic Exposure

There were a number of PPE requirements that minimized the risk of toxic contact. These included lab coats, gloves and protective eyewear. In addition, steel-toed boots were worn to protect against falling objects. Contaminated disposable syringes and beakers were carefully handled and immediately disposed or cleaned during the cell preparation steps. During this cleaning process, excess liquids were poured into an airtight container for disposal. Finally, in the event of exposure there was an eye wash station, shower station and medical kit within a close distance.

3.7.2.2. Asphyxiation

For the loading of gases these were conducted within a well-ventilated room with constant venting to extractors, with the unit housed in a dedicated fume station, with shielded Perspex doors. During the disposing of the gases, this was done underneath a ventilator allowing the component gas to be safely released. Gas cylinders were stored correctly in chain-secured banks, with safety valves preventing any accidental leaks. Finally, gas masks were available in the event of an emergency which would be detected by the available oxygen detectors.

3.7.2.3. Ignition

There were no open flames allowed within the laboratory environment. In addition, there were sprinklers which would be enabled if the smoke detectors detected combustion. Finally, there were fire extinguishers which were close to the experimental area, and the experimentalist was trained in fire safety protocol.

These safety measures prevented any major incidents during the course of the experimental work and allowed for a successful and safe experimental period.

Chapter 4: Results and Discussion

The results of the high-pressure vapour liquid equilibrium experiments with validity of the measuring devices and purity of components are presented in this chapter. The results of the thermodynamic modelling for the verification measurement tests and novel multicomponent systems are also presented and discussed. These systems were modelled using the Cubic Plus Association (Kontogeorgis et al., 1996), Perturbed Chain Statistical Associating Fluid Theory (Chapman et al., 1989), and Peng and Robinson equations of state (Peng and Robinson, 1976).

As mentioned, the verification (test) systems measured were:

1) TPx data for the methane + methanol system at 303.15 K in the approximate pressure range of 2 to 13 MPa
2) TPx data for the carbon dioxide + (water + TEG) (3.5 water, 96.5 TEG mass%) system at 322.04 K in the approximate pressure range of 0.8 to 7 MPa

The two novel systems measured were:

1) TPx data for methane + (TEG + water + methanol) (91.83 TEG, 4.83 water, 3.33 methanol mass%) at 303.15 K, 313.15 K and 323.15 K in the approximate pressure range of 1 to 5.03 MPa
2) TPx data for propane + ethane + methane (96.10 propane, 0.22 ethane, 3.68 propane mass%) + TEG + water + methanol (91.83 TEG, 4.83 water, 3.33 methanol mass%) at 303.15 K, 313.15 K, 323.15 K in the approximate pressure range of 2.25 to 12.27 MPa

4.1. Chemical properties and tests

The chemicals used in this study and their respective details are presented in Table 4.1. This includes the supplier details, CAS numbers and supplier stated purities. In addition, the conductivity for the water used is presented in Table 4.1. the conductivity of water was acceptably low at 0.063 ($\mu s.cm^{-1}$) at 28 ^{o}C classifying the water as ultra-pure. In Table 4.2, the results of the various purity tests are provided. This consists of the GC relative peak areas of all components used and the physical properties (refractive index and density) for the liquid components used in the study. The comparison between the literature and experimental data for these properties shows minimal deviation within the experimental uncertainties of the measurements. Literature and experience were used to determine the ideal conditions for finding possible impurities in the components studied. As this ensured proper separation of the respective components during GC testing. This included variations of the temperature and inert gas flow where GC peaks seemed to overlap (McNair, Miller and Snow, 2019).

For the liquid components, the GC relative peak area %, though not a direct representation of the component purity, strongly indicates if significant impurities exist in the chemical considered, provided these impurities can be detected by the same column GC conditions. The operating conditions of the GC were crucial as this would ensure the separation of the components and thus an accurate characterization of the mixture components. In this case, the GC peak area values above 99% indicate the high purities of the chemical used. As can be seen, a discrepancy was detected between the supplier stated purity for propane, and the experimentally determined value found in Table 4.1 and 4.2 respectively. The details of this were be discussed in section 3.3. The results for methanol moisture content using the Karl Fischer titration are also presented in Table 4.2. Methanol is a hydrophilic compound and thus actively absorbs water from the atmosphere. This moisture content of the methanol was measured and found to be very acceptable after drying with molecular sieve, allowing the methanol to be used at a moisture content of 0.073%.

Table 4.1 Details of the chemicals used in this study.

Component	Supplier	CAS number	Supplier stated purity (mass fraction purity)	Water conductivity ($\mu s.cm^{-1}$) at 28°C
2,2'-(ethane-1,2-diylbis(oxy))diethanol) or Triethylene Glycol (TEG)	Sigma-Aldrich	112-27-6	99	N/A
Methanol (CH_3OH)	Merck	67-56-1	99.9	N/A
Water (H_2O) distilled, deionized	Processed by ELGA Purelab Option-Q apparatus	7732-18-5	N/A	0.063
Carbon dioxide (CO_2)	Afrox	124-38-9	99.9	N/A
Methane (CH_4)	Air Liquide	74-82-8	99.5	N/A
Propane (C_3H_8)	Afrox	74-98-6	99.7	N/A

Table 4.2 Purity checks for the chemicals used in this study.

Component	GC Peak Relative Area %	Density(ρ) g/cm^3 at 25°C		Refractive Index (n_D) at 25°C		Moisture Content (%)*
	Exp	Exp[1]	Lit	Exp[2]	Lit	Exp[3]
Water	99.942	0.997124	0.9971[a]	1.33239	1.33306[d]	-
TEG	99.101	1.122623	1.1225[b]	1.45419	1.4559[e]	-
Methanol	99.545	0.787151	0.7866[c]	1.32823	1.3265[d]	0.073
Methane	99.990	-	-	-	-	-
CO_2	99.584	-	-	-	-	-
Propane mixture Propane/ethane/methane	90.409/0.304/9.287	-	-	-	-	-

a: (Moosavi and Rostami, 2017); b:(Rastorguew and Gazdiev, 1969); c:(Yang et al., 2015); d:(Haynes, 2014); e:(Zvawanda et al., 2022b).

1: Anton Paar DSA5000m and uncertainty: 0.000005 g/cm^3; 2: Atago-Rx7000a and uncertainty of 0.0001 n_D; 3: Karl Fischer C10S and repeatability of 0.3% a > 1mg of water

4.2. Calibrations

The calibration of experimental equipment ensures reliable and accurate measurements. For this study, the necessary calibrations were for the pressure and temperature measuring devices, as the composition of the phases at equilibrium was not determined by sampling.

4.2.1. Temperature Calibrations

The two Pt 100 stainless steel probes were calibrated for use in the HPVLE apparatus. The procedure for this was described in Chapter 3.2.1. Table 4.3 depicts the calibration results and maximum deviations from the second-order trend, while Figures 4.2 and 4.3 depict the relationship between the temperature standard and the respective probes (T102 and T104). The Pt 100 stainless steel temperature probes were calibrated between 273 K and 333.15 K as this encapsulated the selected VLE measurement range of this study. These probes both exhibited a maximum deviation of approximately 0.043 K, and maximum expanded uncertainty of 0.050 K.

Table 4.3 Calibration polynomials for temperature probes T102 and T104[a]

Probes	Correlation	R^2 value	$\Delta T(max)$ (K)
T102	$Y = -0.000027x^2 + 1.003x - 3.124$	$R^2=1.000$	0.043
T104	$Y = -0.000022x^2 + 1.005x - 1.990$	$R^2=1.000$	0.043

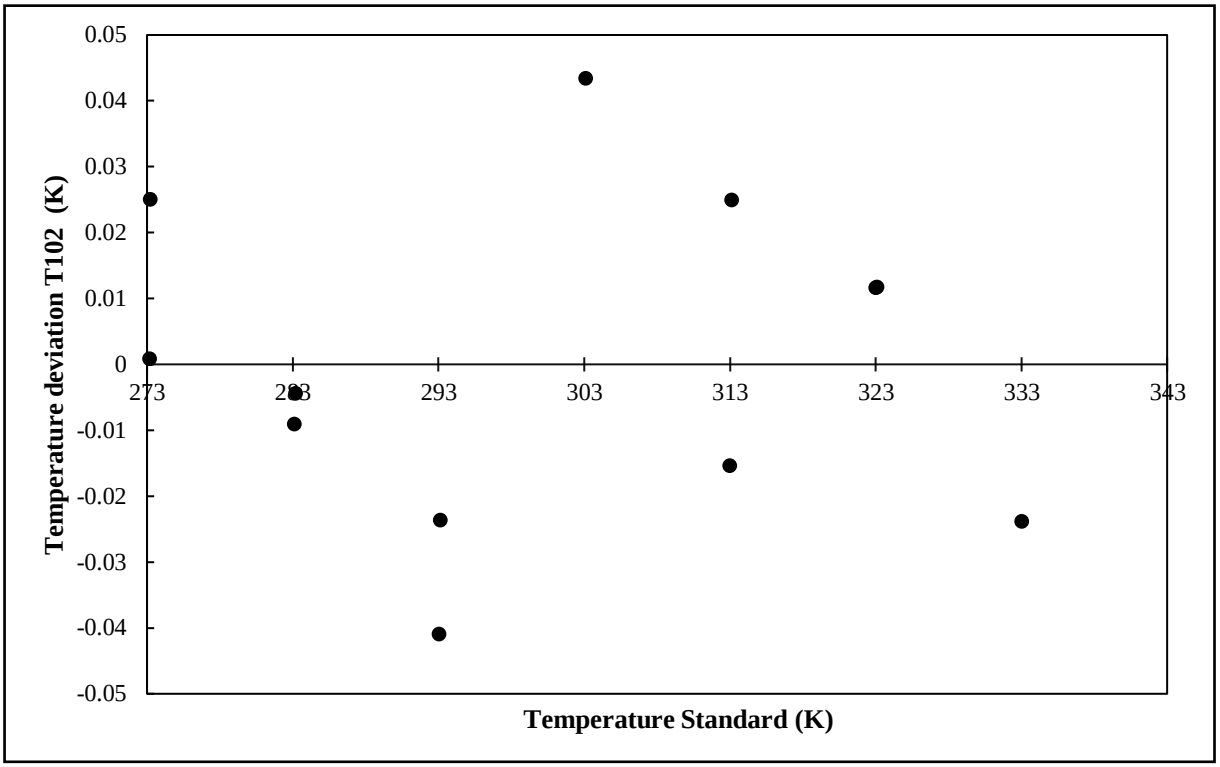

Figure 4.1 Deviation between the standard temperature and the calibrated temperature of T102.

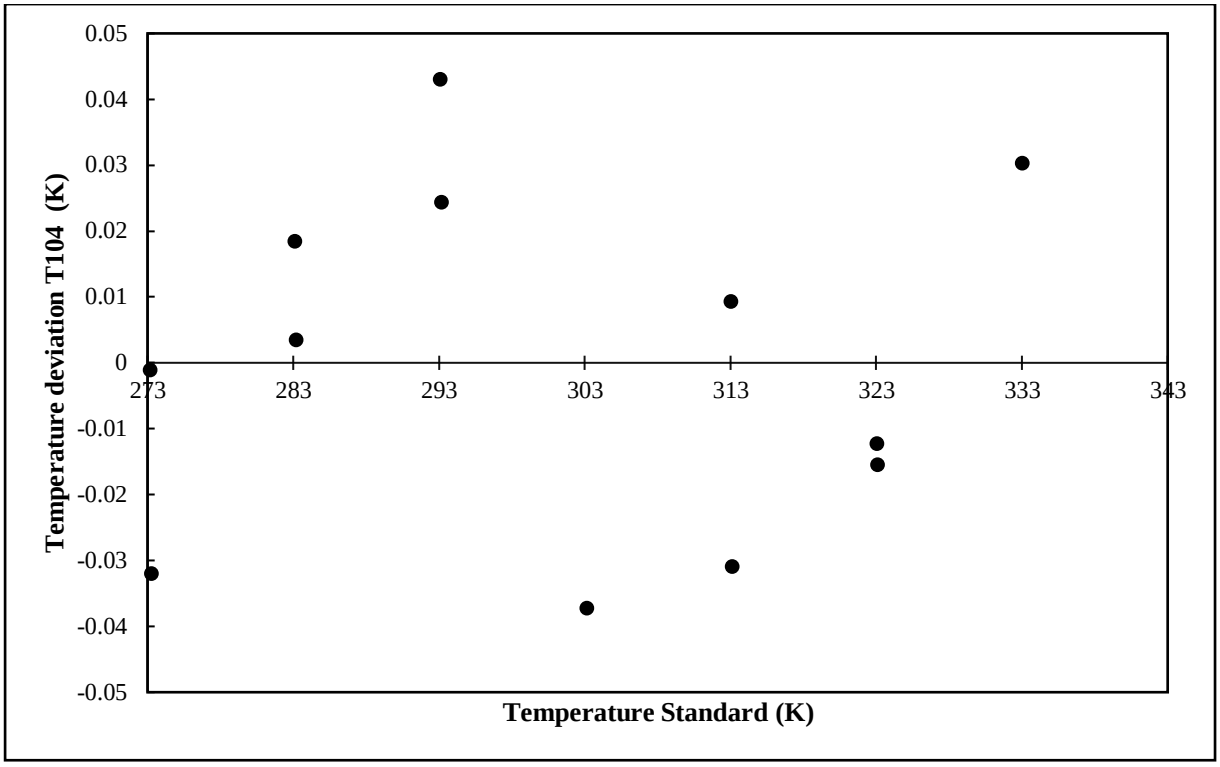

Figure 4.2 Deviation between the standard temperature and the calibrated temperature of T104.

4.2.2. Pressure Calibrations

The single WIKA P-10 pressure transducer was calibrated for use in the HPVLE apparatus. The procedure for this was described in Chapter 3.2.2. Table 4.4 depicts the calibration results and maximum deviations, while Figure 4.3 depicts the relationship between the pressure standard and the respective probe. The maximum deviation from the calibration curve was found to be 0.0016 MPa, which is within the operating range and accuracy of 0.05% full scale stated for the P-10 Pressure Transmitter (P-122) as stated by the supplier. These calibrations allowed for the calculation of the temperature and pressure uncertainties by error propagation using the methods of Joint Committee for Guides in Metrology (JCGM) as outlined in Appendix A. Thus, the maximum uncertainty was calculated as 0.028MPa for the P-10 Pressure transducer.

Table 4.4 Calibration polynomial for pressure transducer P122.

Probes	Correlation	R^2 value	$\Delta P(max)$ (10^1 MPa)
P122	$Y = -0.00000027x^2 + 1.00x + 0.043$	$R^2 = 1.000$	0.016

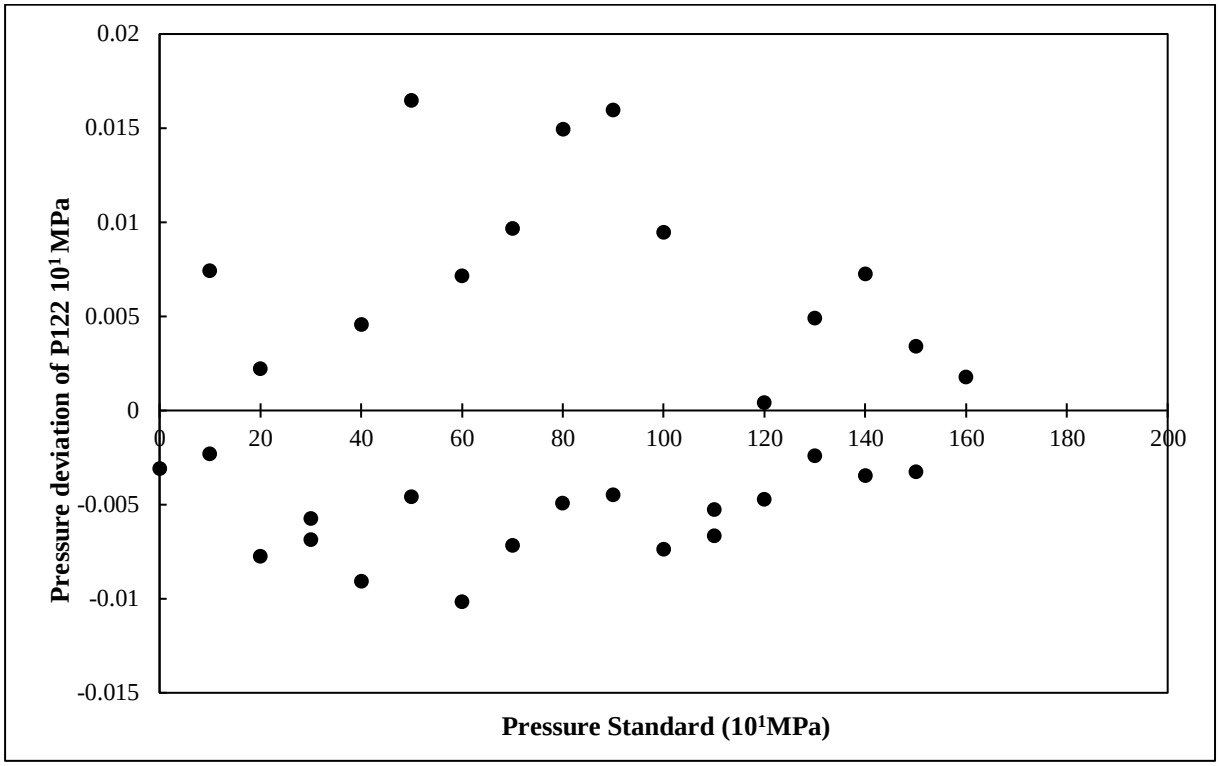

Figure 4.3 Deviation between the standard pressure and the calibrated pressure of P122.

4.3. Vapour pressures

Vapour pressure predictions using the CPA, PC-SAFT and PR equations of state (and the Antoine equation for liquids) were conducted to establish the accuracy of the models used in this work in predicting pure component VLE. This is a necessary verification before the extension of the application of the models to mixture data. These predictions were compared to literature data, as well as to experimental vapour pressure measurements performed in this work for selected components. Uncertainty calculations and value can be found in Appendix C

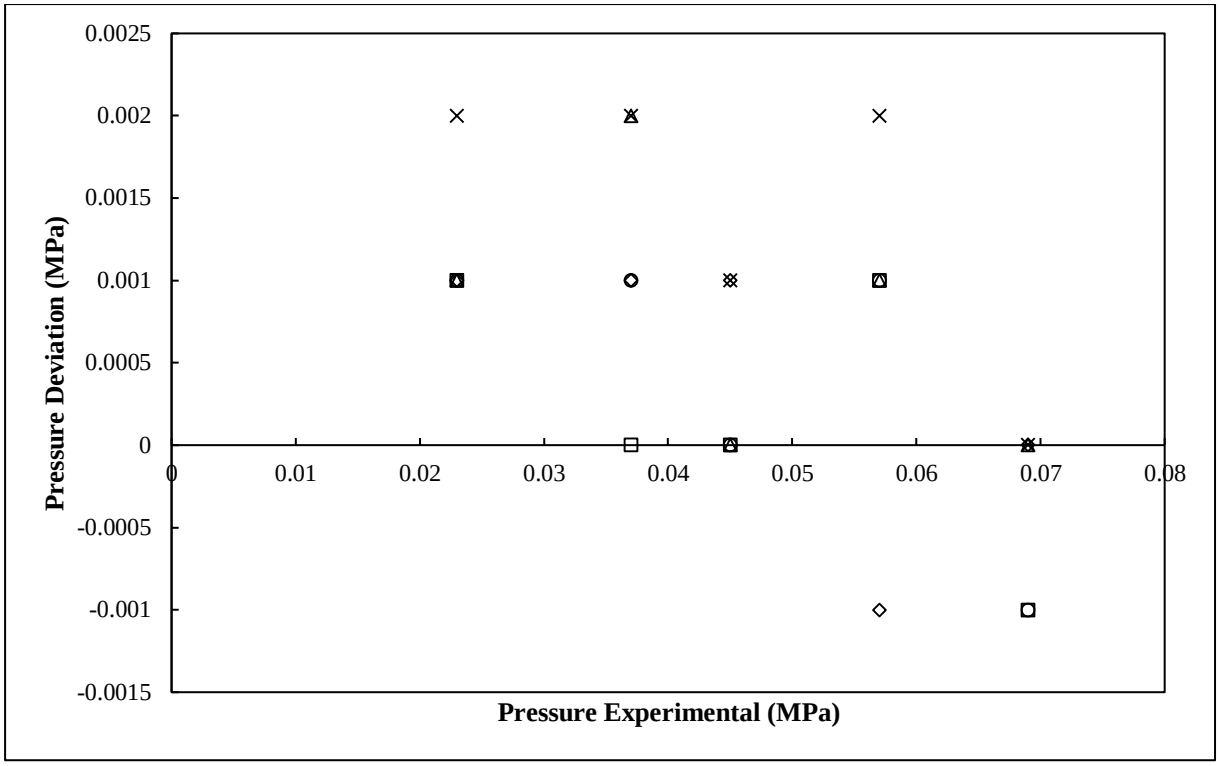

Figure 4.4 Comparison of vapour pressure data of methanol to literature deviations.; Literature (o)(Safarov et al., 2015); Predictions deviations: Antoine (□); CPA (◊); PC-SAFT (Δ); PR (X).

Table 4.5 Experimental and calculated vapour pressure deviation data with experimental uncertainty for methanol.

T_{exp} (K)[a]	P_{exp} (MPa)	$U_c(P)$[a] (MPa)	ΔP (MPa)[b]	ΔP (MPa) Antoine	ΔP (MPa) CPA	ΔP (MPa) PC-SAFT	ΔP (MPa) PR
303.24	0.023	0.0001	0.001	0.001	0.001	0.001	0.002
313.29	0.037	0.0002	0.001	0.000	0.001	0.002	0.002
318.06	0.045	0.0002	0.000	0.000	0.001	0	0.001
323.01	0.057	0.0003	0.001	0.001	-0.001	0.001	0.002
328.05	0.069	0.0004	-0.001	-0.001	0.000	0.000	0.000

[a]$U_c(T)$ = 0.04 (K) [b](Safarov et al., 2015)

Table 4.6 Pressure deviations from model data for methanol.

Deviation	Literature[a]	Antoine's	CPA	PC-SAFT	PR
AAD P(MPa)	0.0008	0.0006	0.0008	0.0008	0.0014
AARD P (%)	2.05	1.51	2.21	2.30	3.97

[a](Safarov et al., 2015)

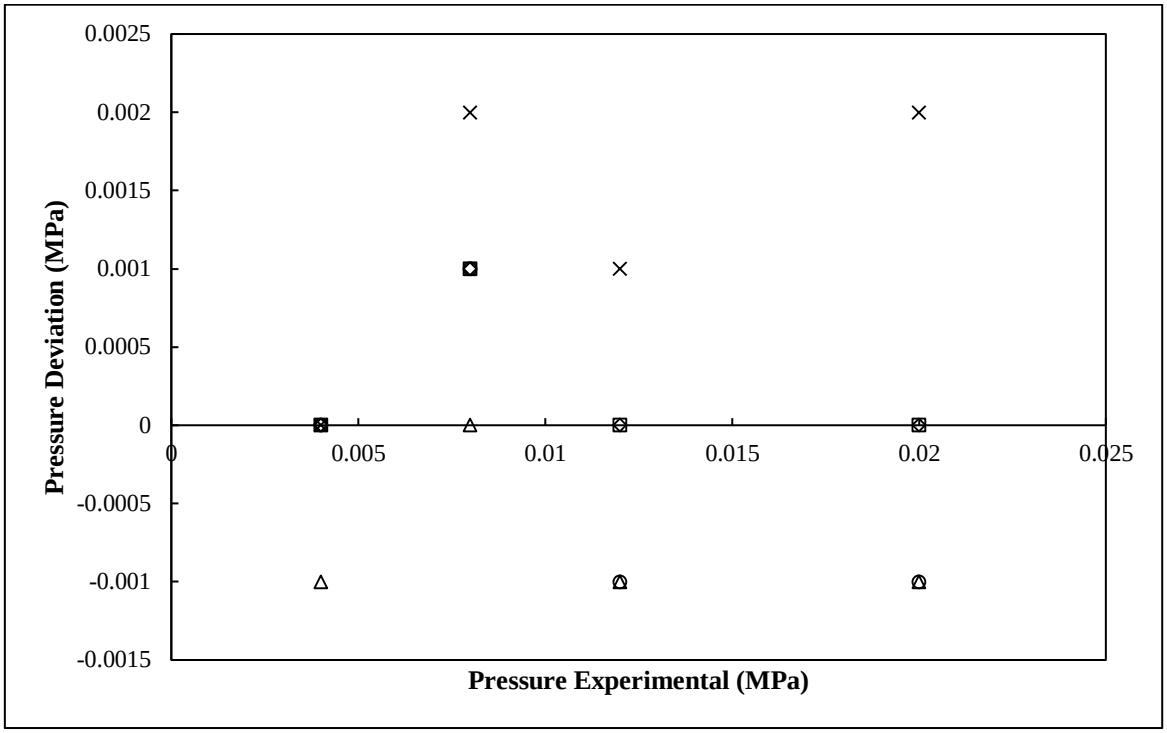

Figure 4.5 Comparison of vapour pressure data of water to literature. ; Literature (o)(Zhang et al., 2018); ; Predictions deviations: Antoine's (□); CPA (◊); PC-SAFT (Δ); PR (X).

Table 4.7 Experimental and calculated vapour pressure deviation data with experimental uncertainty for water.

T_{exp} (K)[a]	P_{exp} (MPa)	$U_c(P)$ (MPa)	P_{lit} (MPa)[b]	P (MPa) Antoine	P (MPa) CPA	P (MPa) PC-SAFT	P (MPa) PR
303.19	0.004	0.00002	0.000	0.000	0.000	-0.001	0.000
313.31	0.008	0.00004	0.001	0.001	0.001	0.000	0.002
323.26	0.012	0.00006	-0.001	0.000	0.000	-0.001	0.001
333.40	0.020	0.0001	-0.001	0.000	0.000	-0.001	0.002

[a]$U_c(T)$ =0.04(K) [b]Literature: (Zhang et al., 2018)

Table 4.8 Pressure deviations from model data for water.

Deviation	Literature[a]	Antoine	CPA	PC-SAFT	PR
AAD P(MPa)	0.0006	0.0002	0.0002	0.0006	0.0010
AARD P (%)	5.17	2.50	2.50	7.67	8.67

[a](Zhang et al., 2018)

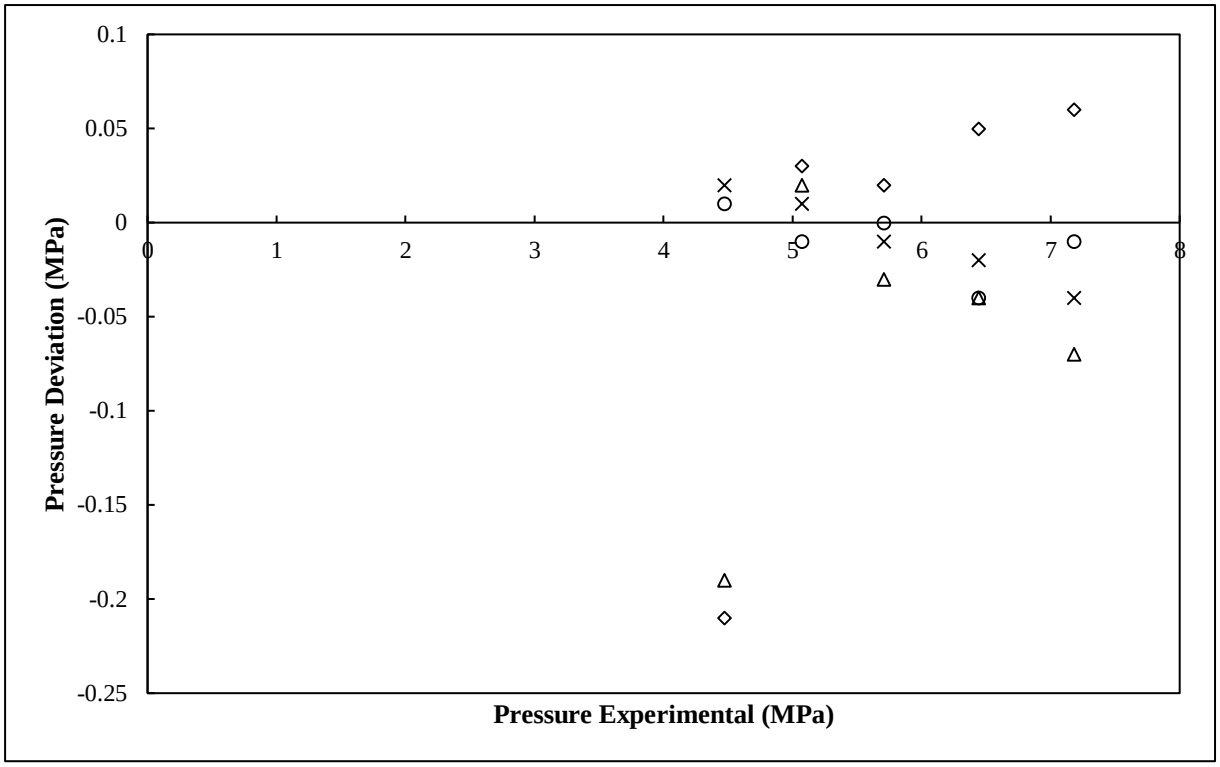

Figure 4.6 Comparison of vapour pressure deviation data of CO_2 to literature.; Literature (o) (Kim and Kim, 2005); Predictions deviations: CPA (◊); PC-SAFT (Δ); PR (X).

Table 4.9 Experimental and calculated vapour pressure deviation data with experimental uncertainty for CO_2.

T_{exp} (K)[a]	P_{exp} (MPa)	U_c(P) (MPa)	P_{lit} (MPa)[b]	P (MPa) CPA	P (MPa) PC-SAFT	P (MPa) PR
282.80	4.47	0.015	0.01	-0.21	-0.19	0.02
287.92	5.07	0.015	-0.01	0.03	0.02	0.01
293.04	5.71	0.015	0.00	0.02	-0.03	-0.01
298.27	6.44	0.015	-0.04	0.05	-0.04	-0.02
303.19	7.18	0.015	-0.01	0.06	-0.07	-0.04

[a]U_c(T) = 0.06 (K) [b]Literature: (Kim and Kim, 2005)

Table 4.10 Pressure deviations from model data for CO_2.

Deviation	Literature[a]	CPA	PC-SAFT	PR
AAD P(MPa)	0.0120	0.0620	0.052	0.0120
AARD P (%)	0.21	1.28	1.05	0.23

[a](Kim and Kim, 2005)

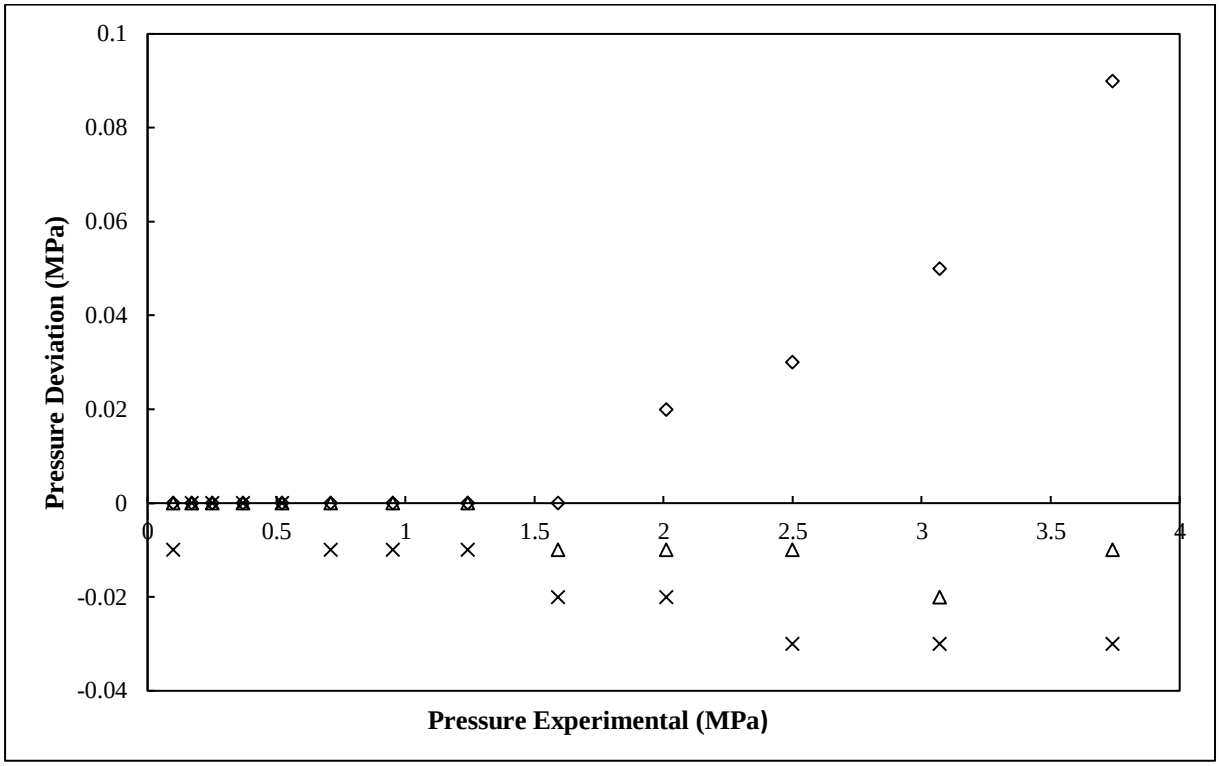

Figure 4.7 Comparison of literature vapour pressure deviation data of CH_4 to model data. Literature (o)(Haselden, 1979); Predictions deviations: CPA (◊); PC-SAFT (Δ); PR (X).

Table 4.11 Literature and calculated vapour pressure deviation data with experimental uncertainty for CH_4.

T_{exp} (K)	ΔP_{lit} (MPa)[a]	ΔP (MPa) CPA	ΔP (MPa) PC-SAFT	ΔP (MPa) PR
112	0.10	0.00	0.00	-0.01
118	0.17	0.00	0.00	0.00
124	0.25	0.00	0.00	0.00
130	0.37	0.00	0.00	0.00
136	0.52	0.00	0.00	0.00
142	0.71	0.00	0.00	-0.01
148	0.95	0.00	0.00	-0.01
154	1.24	0.00	0.00	-0.01
160	1.59	0.00	-0.01	-0.02
166	2.01	0.02	-0.01	-0.02
172	2.50	0.03	-0.01	-0.03
178	3.07	0.05	-0.02	-0.03
184	3.74	0.09	-0.01	-0.03

[a]Literature: (Haselden, 1979)

Table 4.12 Pressure deviations from model data for CH_4.

Deviation	CPA	PC-SAFT	PR
AAD P (MPa)	0.0146	0.0046	0.0131
AARD P (%)	1.15	0.188	1.423

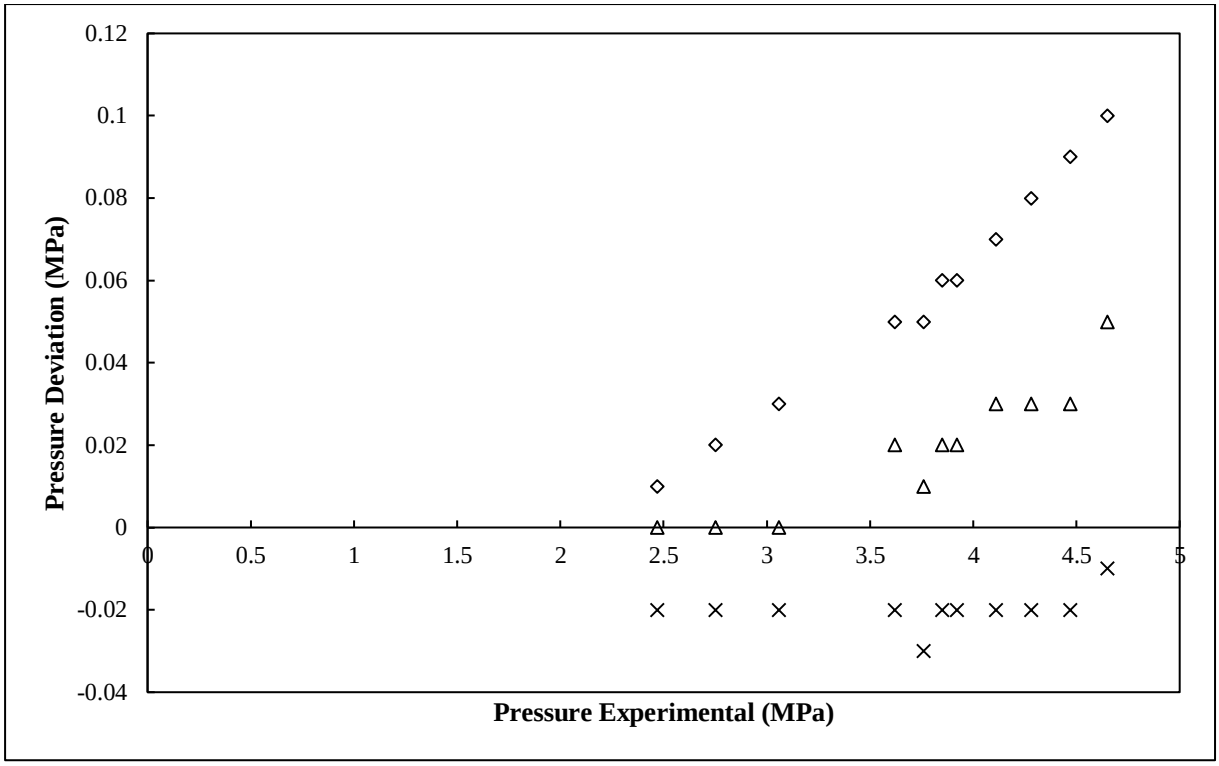

Figure 4.8 Comparison of literature vapour pressure deviations data of C_2H_6 to model data. Literature (o)(Seneviratne et al., 2017); Prediction deviations: CPA (◊); PC-SAFT (Δ); PR (X).

Table 4.13 Literature and calculated vapour pressure deviation data with experimental uncertainty for C_2H_6.

T_{exp}(K)	P_{lit}(MPa[a])	ΔP(MPa) CPA	ΔP(MPa) PC-SAFT	ΔP(MPa) PR
274.62	2.47	0.01	0.00	-0.02
279.17	2.75	0.02	0.00	-0.02
283.79	3.06	0.03	0.00	-0.02
291.25	3.62	0.05	0.02	-0.02
293.15	3.76	0.05	0.01	-0.03
294.16	3.85	0.06	0.02	-0.02
295.04	3.92	0.06	0.02	-0.02
297.19	4.11	0.07	0.03	-0.02
299.14	4.28	0.08	0.03	-0.02
301.26	4.47	0.09	0.03	-0.02
303.11	4.65	0.1	0.05	-0.01

[a](Seneviratne et al., 2017)

Table 4.14 Pressure deviations from model data for C_2H_6.

Deviation	CPA	PC-SAFT	PR
AAD P(MPa)	0.0556	0.0174	0.0190
AARD P (%)	1.40	0.42	0.53

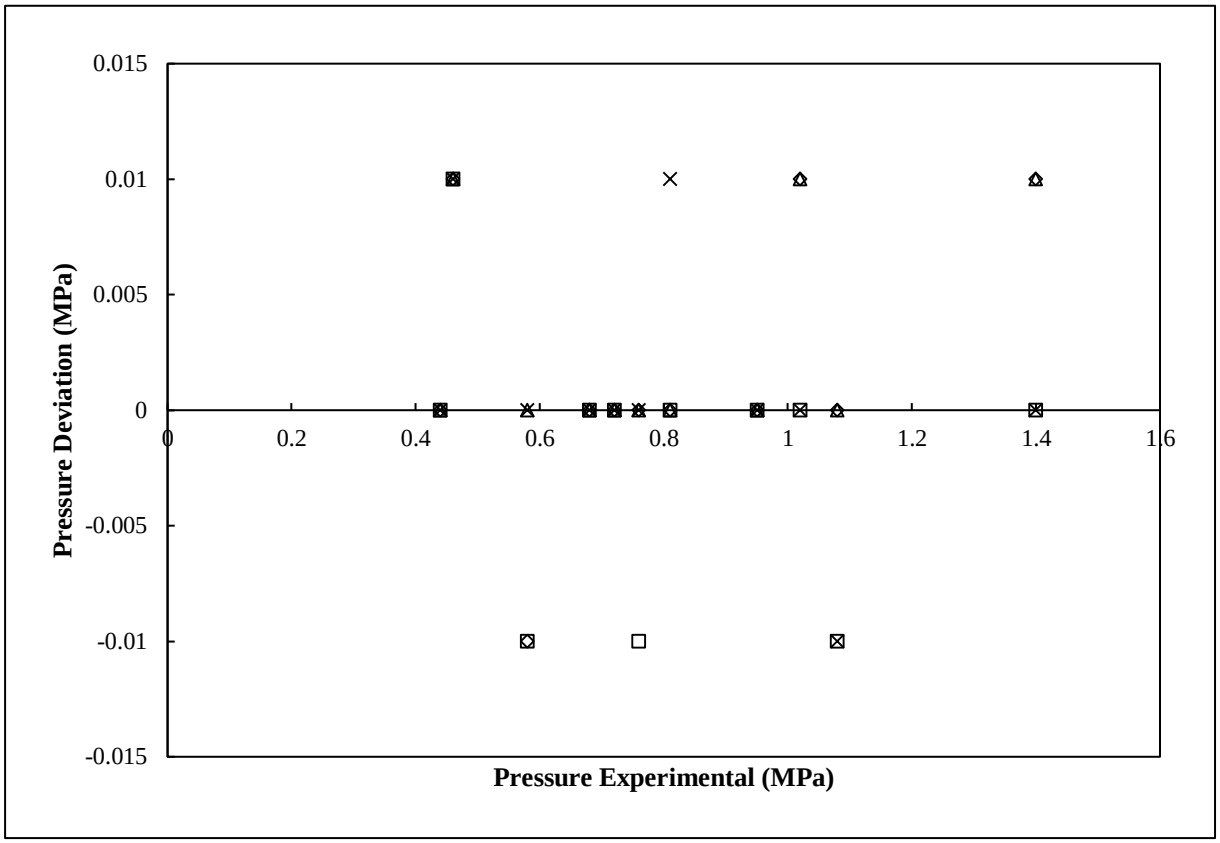

Figure 4.9 Comparison of literature vapour pressure deviations data of C_3H_8 to model data. Literature(o)(Seneviratne et al., 2017); Prediction deviations: CPA (◊); PC-SAFT (Δ); PR (X).

Table 4.15 Vapour pressure data for C_3H_8.

T_{exp} (K)	P_{lit} (MPa)[a]	P (MPa) Antoine	P (MPa) CPA	P (MPa) PC-SAFT	P (MPa) PR
270.51	0.44	0.44	0.44	0.44	0.44
271.77	0.46	0.45	0.45	0.45	0.45
280.13	0.58	0.59	0.59	0.58	0.58
285.35	0.68	0.68	0.68	0.68	0.68
287.35	0.72	0.72	0.72	0.72	0.72
289.65	0.76	0.77	0.76	0.76	0.76
291.75	0.81	0.81	0.81	0.81	0.80
297.98	0.95	0.95	0.95	0.95	0.95
300.92	1.02	1.02	1.01	1.01	1.02
303.37	1.08	1.09	1.08	1.08	1.09
314.06	1.40	1.40	1.39	1.39	1.40

[a](Seneviratne et al., 2017)

Table 4.16 Pressure deviations from model data for C_3H_8.

Deviation	Antoine	CPA	PC-SAFT	PR
AAD P(MPa)	0.0036	0.0036	0.0027	0.0027
AARD P (%)	0.56	0.51	0.35	0.39

The results are presented graphically in Figures 4.4-4.9 and in Tables 4.5-4.16, where vapour pressure experiments were undertaken with methanol and water using LPVLE equipment and CO_2 using the HPVLE equipment used in this study. The vapour pressures of methane and ethane could not be measured experimentally in this work due to the operating limits of the apparatus available for methane and due to the lack of pure ethane. In addition, ethane comprises a small part of the systems tested. Since pure propane was not available for use in this work, it was also not measured. Additionally, the vapour pressures of TEG could not be measured accurately below 373.15 K using the available equipment.

It was found that the AAD(P) for methanol, from the data presented in Table 4.5 and Figure 4.4., was 0.0008 MPa from experimental literature data, 0.0006 MPa from Antoine's equation prediction, 0.0008 from the CPA model, with the highest deviation of 0.0010 from the PR model. A similar trend was observed with the water vapour pressure data (Table 4.7 and Figure 4.5). For the CO_2 data in Table 4.9 and Figure 4.6, an acceptable correlation between the data, literature, and all models was observed, with the PR model AAD being the lowest within 0.0120 MPa.

The supercritical methane and ethane data (Tables 4.11 and 4.13) were predicted similarly by the CPA, PC-SAFT and PR models, so there is likely no superior model for these pure properties. In the methane and ethane predictions, literature values were compared with these predictions, showing a strong correlation (Figures 4.7-4.8). Similarly, for pure propane (Table 4.15), the predictions by the three models correlate well with literature data (Figure 4.9). However, the models tend to deviate from the literature with an increase of pressure in particular, the CPA model for methane and ethane. This may be an indication that the models struggle to perform well as the pressure increases. However, the AARD value for these components are relatively small.

The results show that overall, the CPA model provided a slightly better prediction of the vapour pressures followed by PC-SAFT and then PR. These results confirmed that the models were able to represent the pure component vapour pressures reasonably well.

4.4. Test system measurements

Mixture VLE measurements were performed for systems previously measured in the literature, which served as a verification method to assess the reliability of the equipment used as well as the experimental method employed. The two systems chosen were CH_4 (1) + CH_3OH (2) at 303.15 K and CO_2 (1) + TEG (2) + water (3) at 322.04 K. These systems had existing data readily available in the literature from multiple sources at the selected conditions and thus could be compared more confidently for confirmation of accurate experimental results. In addition, thermodynamic modelling was applied to these test measurement systems. These included the application of the Cubic Plus Association (CPA), Perturbed-Chain Statistical Associating Fluid Theory (PC-SAFT) and Peng Robinson (PR) models. This involved correlating the binary interaction parameters represented by k_{ij} and determining the model deviations from experimental data represented by σ. To represent a quantifiable comparison between the respective models and the experimental results, the absolute average deviation (AAD) and average relative deviations (AARD) were calculated.

4.4.1. CH_4 + CH_3OH binary test system

The first system measured was the CH_4 (1) + CH_3OH (2) binary system at 303.15 K. The results are presented in Table 4.17 and compared to the existing data of (Zvawanda et al., 2022b) and (Wang et al., 2003) graphically in Figure 4.10. It should be noted that the same set of equipment was used in the work of (Zvawanda et al., 2022b) as in this study.

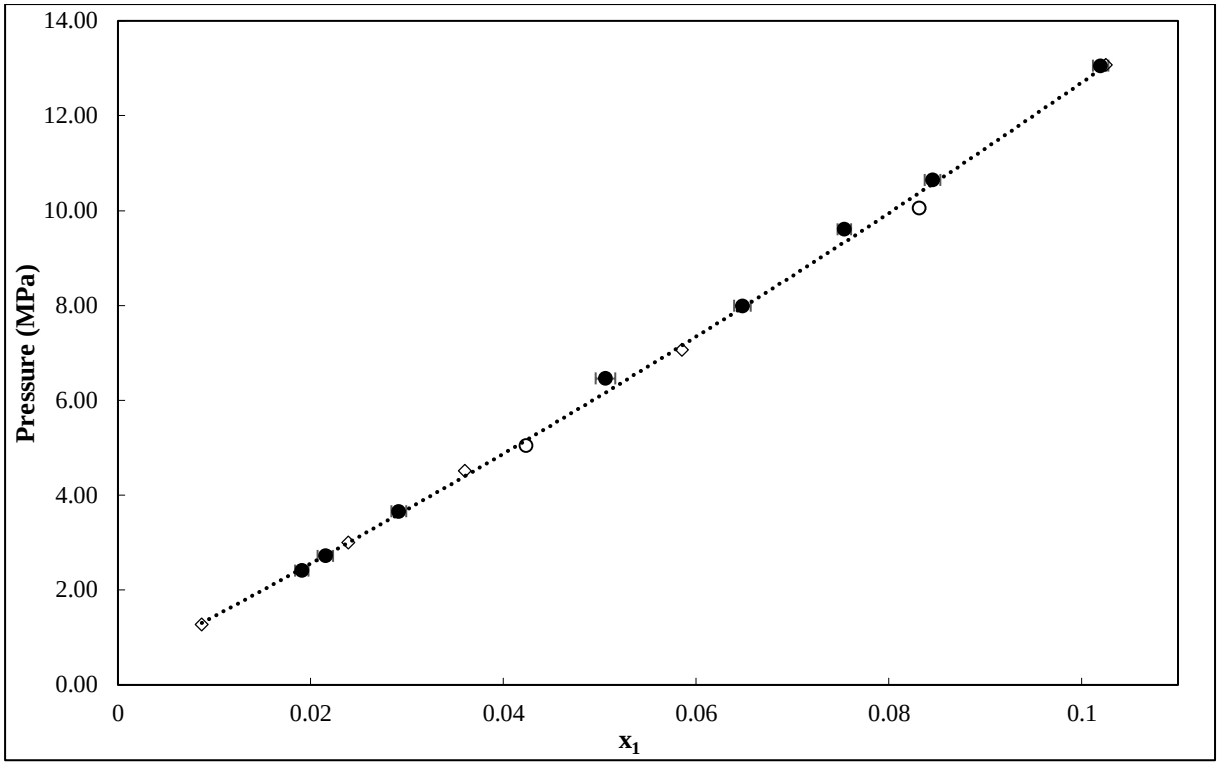

Figure 4.10 P-x data for the CH_4 (1) + CH_3OH (2) system at 303.15 K. This work (●); (Zvawanda et al., 2022b) (◊) and (Wang et al., 2003) (○). Polynomial trendline for data of (Wang et al., 2003) (••••••).

Table 4.17 P-x data and uncertainty for the CH_4 (1) + CH_3OH (2) system at 303.15 K.

T_{exp} (K)[a]	P_{exp} (MPa)	Liquid mole composition (x_1)	U_c (P) (MPa)	U_c (x_1)
303.18	2.410	0.019	0.025	0.0009
303.18	2.721	0.022	0.025	0.0009
303.17	3.076	0.026	0.025	0.009
303.17	3.661	0.029	0.025	0.009
303.16	6.463	0.051	0.026	0.0012
303.18	7.994	0.065	0.025	0.009
303.17	9.701	0.075	0.083	0.009
303.16	10.690	0.085	0.025	0.001
303.15	13.060	0.1	0.026	0.001

[a]$U_c(T) = 0.06$ (K)

The deviation found between the data points and the general trend is accommodated by the uncertainty for the experimental point and the literature data. The point measured at 9.7 MPa shows the highest deviation from the literature trend, but again is within the uncertainties of this work and the literature studies. Considering this, the experimental results show a close relationship with the work of (Zvawanda et al., 2022b) and (Wang et al., 2003). This validates the equipment's ability to produce accurate and reliable VLE results for a binary gas-liquid system at their respective conditions.

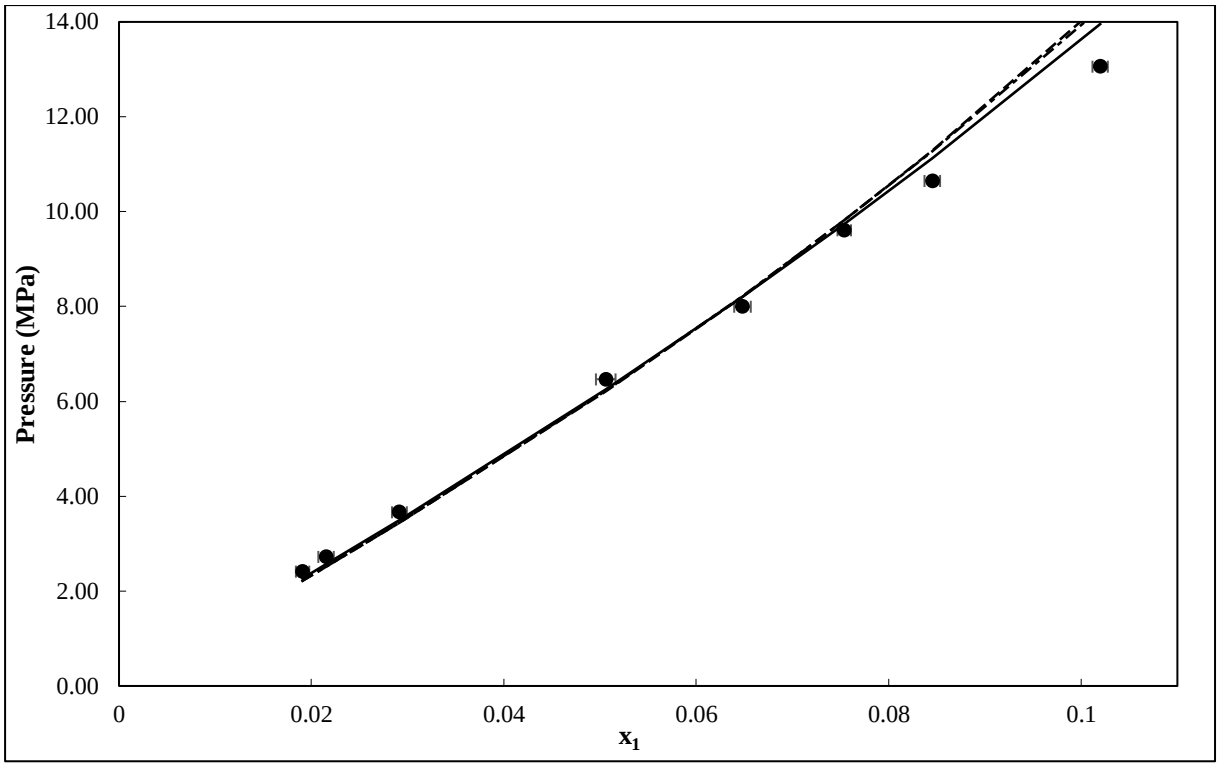

Figure 4.11 P-x data for the CH_4 (1) + CH_3OH (2) system at 303.15 K with comparison to regressed property models. Experimental (●), CPA model (----), PC-SAFT model (– – –), PR model (- · - · -).

Table 4.18 Experimental and regressed isothermal P-x data for the CH_4 (1) + CH_3OH (2) system at 303.15 K.

$x_{1, exp}$	P_{exp}(MPa)	Pressure (MPa)		
		CPA	PC-SAFT	PR
0.019	2.41	2.27	2.22	2.22
0.022	2.72	2.57	2.51	2.51
0.029	3.66	3.50	3.44	3.44
0.051	6.46	6.26	6.21	6.22
0.065	7.99	8.21	8.21	8.23
0.075	9.61	9.73	9.81	9.82
0.085	10.65	11.12	11.29	11.27
0.102	13.06	13.95	14.37	14.27

Table 4.19- Regressed binary parameters and deviations for models employed for the CH_4 (1) + CH_3OH (2) system at 303.15 K.

Parameters	CPA	PC-SAFT	PR
k_{12}	0.048	-0.033	-0.019
σ_{K12}	0.005	0.003	0.004
AAD P(MPa)	0.280	0.388	0.376
AARD (%)	4.14	5.61	5.54

The measured VLE data were regressed using the CPA, PC-SAFT, and PR models by fitting them to the objective function presented in appendix A. These results are presented graphically in Figure 4.11. The corresponding results for this modelling are presented in Tables 4.18 to 4.19 and show that the CPA model performed best with the lowest AAD and AARD, with the PR model being second and the PC-SAFT model performing the worst. These model correlations had AARD values of 4.14%, 5.54% and 5.61%, respectively. The CPA and PC-SAFT models were expected to perform well for this type of system due to their applicability for natural gas systems and for systems containing associating molecules. However, it is likely that these advantages are not observed entirely due to the simplicity of this binary system and the limited expected association. Although hydrogen bonding exists, it is only expected to occur significantly between CH_3OH molecules that are self-associating, limiting the PC-SAFT model's correlative benefits for cross-associating systems. This is the likely reason that the PR model performs better than the PC-SAFT model for the system.

4.4.2. CO_2 (1) +TEG (2) + water (3) test system

The second test system measured was the CO_2 (1) +TEG (2) + water (3) system at 322.04 K, which is presented in Table 4.20. The experimental results were compared to the data of (Zvawanda et al., 2022b) and (Wise and Chapoy, 2016). This comparison is presented graphically in Figure 4.12. In this figure, there is a small deviation from the general trend of (Wise and Chapoy, 2016) and (Zvawanda et al., 2022b)*;* however, this is accommodated by the experimental uncertainty of 0.02 - 0.03 MPa. In addition, the results from the experiments exhibit a satisfactory trend. This validates the equipment's ability to produce accurate and reliable VLE results for multiple component mixtures with a viscous liquid phase.

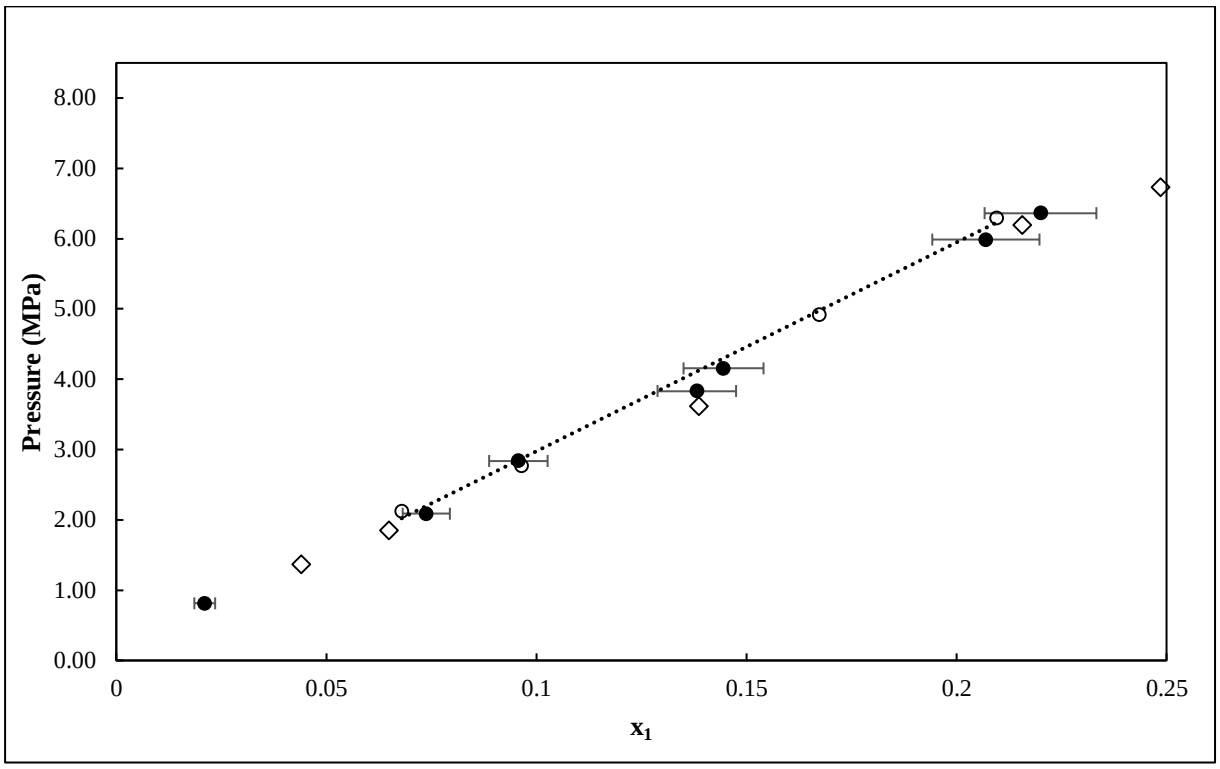

Figure 4.12 P-x data for the CO_2 (1) + TEG-water (96.5/3.5 wt.%) system at 322.04 K. This work (●); (Zvawanda et al., 2022b) at 322.04 K(◊); (Wise and Chapoy, 2016) 322.04 K (○). Polynomial trendline for data of (Wise and Chapoy, 2016) (•••••).

Table 4.20 P-x data for the CO_2 (1) + TEG-water (96.5/3.5 wt.%) system at 322.04 K.

T_{exp} (K)[a]	P_{exp} (MPa)	$x_{1,exp}$	U_c (P) (MPa)	U_{x_1}
322.03	0.81	0.021	0.02	0.002
322.03	2.09	0.074	0.02	0.006
322.04	2.84	0.096	0.02	0.007
322.02	3.83	0.138	0.03	0.009
322.05	4.15	0.142	0.04	0.010
322.03	5.99	0.207	0.03	0.013
322.04	6.36	0.220	0.03	0.013

[a]$U_c(T) = 0.06$ (K)

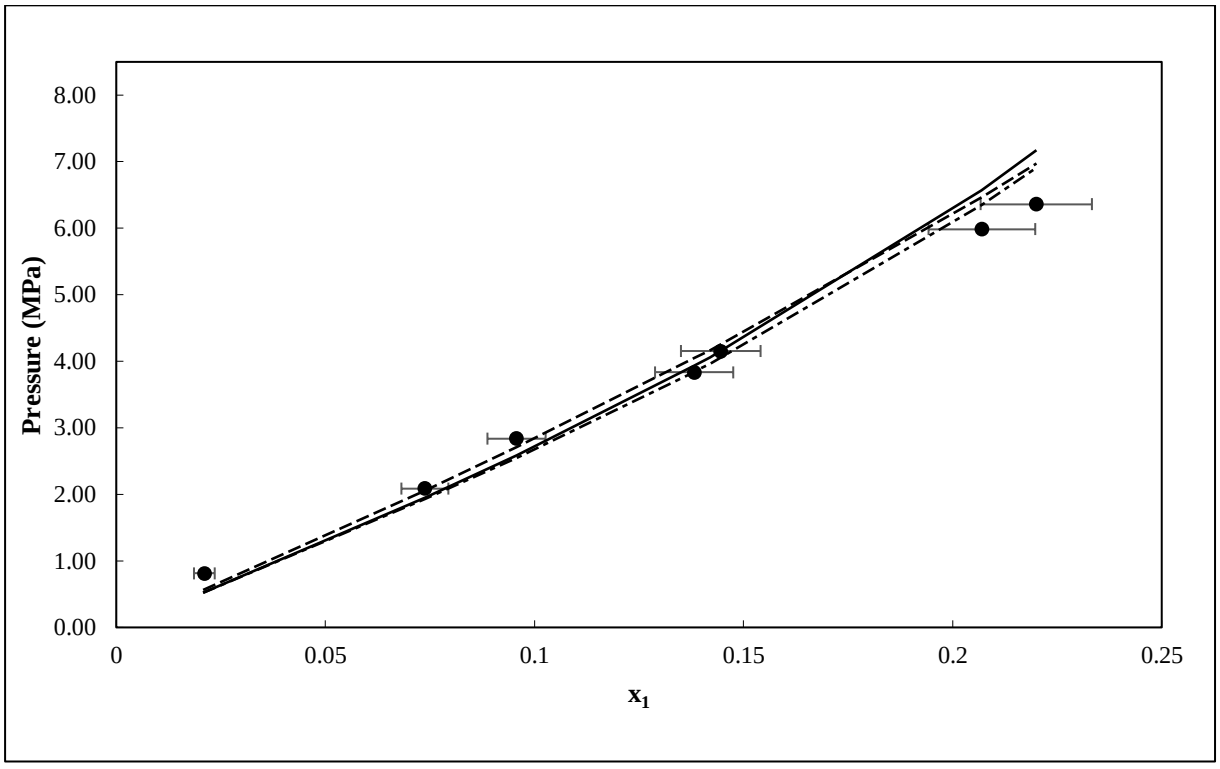

Figure 4.13 P-x data for the CO_2 (1) + TEG (2)-water (3) (96.5/3.5 wt.%) system at 322.04 K with comparison to regressed property models. Experimental (●), CPA model (▪▪▪▪), PC-SAFT model (----), PR model (- ▪ - ▪ -)

Table 4.21 P-x data for the CO_2 (1) + TEG (2)-water (3) (96.5/3.5 wt.%) system at 322.04 K with comparison to regressed property models.

$x_{1, exp}$	P_{exp}(MPa)	Pressure (MPa)		
		CPA	PC-SAFT	PR
0.019	2.41	2.27	2.22	2.22
0.022	2.72	2.57	2.51	2.51
0.029	3.66	3.16	3.44	3.44
0.051	6.46	3.51	6.21	6.22
0.065	7.99	6.27	8.21	8.23
0.075	9.61	8.22	9.81	9.82
0.085	10.65	7.61	11.29	11.27
0.102	13.06	9.76	14.37	14.27

Table 4.22 Regressed binary parameters, deviations and model errors for models employed in the CO_2 (1) + TEG (2)-water (3) (96.5%/3.5) system at 322.04 K.

Parameters	CPA	PC-SAFT	PR
k_{12}	0.140	0.327	0.225
σ_{K12}	0.019	0.167	0.019
k_{13}	-0.041	-0.607	-1.080
σ_{K13}	0	3.491	0
k_{23}	-0.094	0.051	-0.221
σ_{K23}	0.250	0.161	0.128
AAD(MPa)	0.313	0.260	0.251
AARD(%)	10.56	8.63	9.60

These test system results were also regressed using the CPA, PC-SAFT and PR models, with regression results presented in Tables 4.21 to 4.22. These results are compared to the experimental data graphically in Figure 4.13. The results showed that the PC-SAFT model performed the best, with the PR model next, and the CPA model performing the worst. These had AARD values of 8.63%, 9.60 and 10.56%, respectively. The reasons for this are likely due the representation of the complex associating behaviour in the liquid phase for the TEG-water interaction, as well as the interaction of the quadrupole CO_2 molecule with the polar TEG and water molecules. This is seemingly better represented by the PC-SAFT model in this case, despite Aspen Plus ® treating the CO_2 molecule as dipolar.

4.5. Novel system measurements

4.5.1. CH_4 (1) + (CH_3OH (2) + TEG (3) + water (4) quaternary system

Novel VLE data were measured for the system of CH_4 (1) + (CH_3OH (2) + TEG (3) + water (4) 3.33 (2)/91.84 (3)/4.83 (4) wt%) at 303.15 K, 313.15 K and 323.15 K. The results of these measurements are presented graphically in Figures 4.14 – 4.17 and tabulated in Tables 4.23 – 4.25. The single isotherms are presented and discussed first, followed by the combination of all data into a single plot and analyses of the model results.

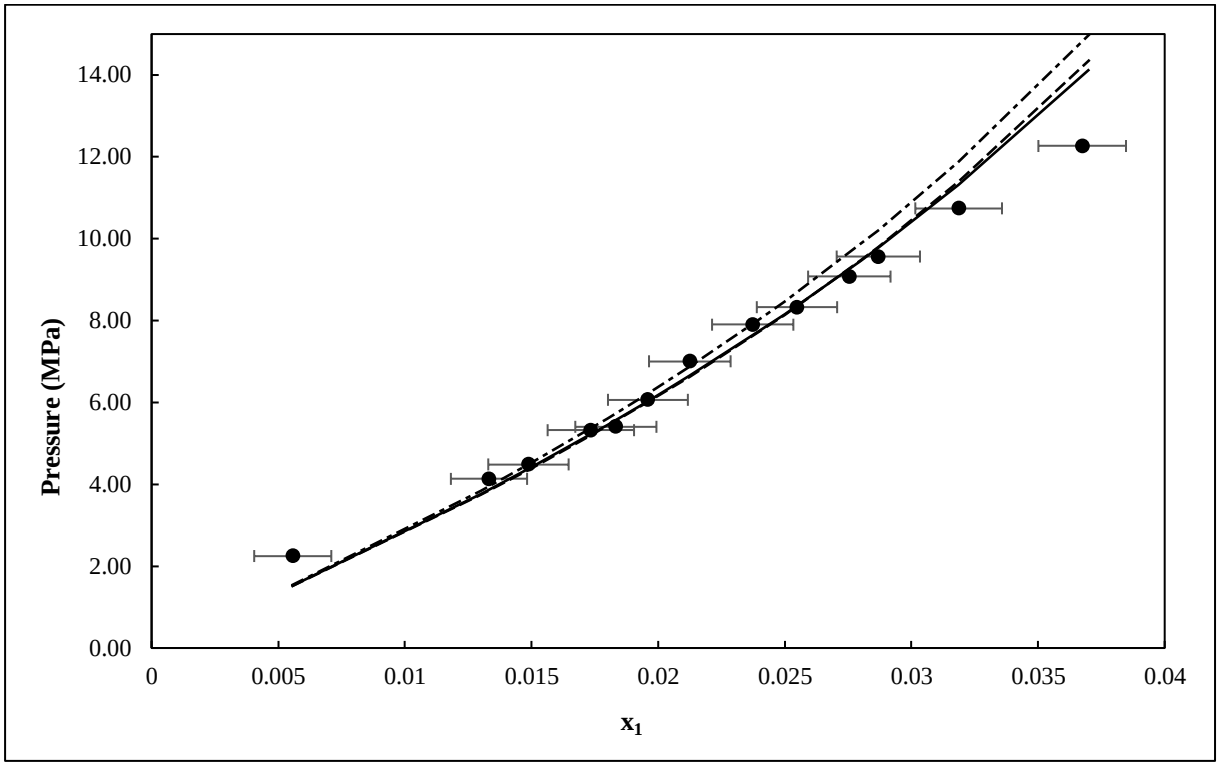

Figure 4.14 P-x data for the CH_4 (1) + (CH_3OH (2) /TEG (3)/Water (4) 3.33/91.84/4.83 wt%) system at 303.15 K with comparison to regression results by various models. Experimental (●), CPA model (·····), PC-SAFT model (----), PR model (- ▪ - ▪ -).

Table 4.23 P-x data) and model results for the CH_4 (1) + (CH_3OH (2) /TEG (3)/Water (4) 3.33/91.84/4.83 wt%) system at 303.15 K

T_{exp} (K)[a]	$x_{1,exp}$[b]	P_{exp} (MPa)	U_c (P)	ΔPressure (MPa)		
				CPA	PC-SAFT	PR
303.16	0.006	2.25	0.02	0.73	0.73	0.71
303.15	0.013	4.11	0.03	0.35	0.37	0.26
303.14	0.015	4.49	0.03	0.07	0.1	-0.04
303.16	0.017	5.32	0.03	0.22	0.24	0.08
303.14	0.018	5.40	0.07	-0.05	-0.03	-0.21
303.15	0.020	6.06	0.06	0.03	0.05	-0.16
303.15	0.021	7.01	0.06	0.36	0.38	0.14
303.14	0.024	8.00	0.08	0.25	0.27	-0.03
303.14	0.025	8.33	0.07	0.18	0.18	-0.14
303.13	0.028	9.07	0.03	-0.38	-0.41	-0.8
303.13	0.029	9.56	0.06	-0.22	-0.24	-0.65
303.14	0.032	10.74	0.03	-0.57	-0.65	-1.14
303.14	0.037	12.27	0.05	-1.85	-2.08	-2.71

[a]$U_c(T) = 0.06$ (K) ; [b] $U_c(x_1) = 0.002$; $\Delta P = (P_{exp} - P_{calc})$ where P_{calc} was determined using the model

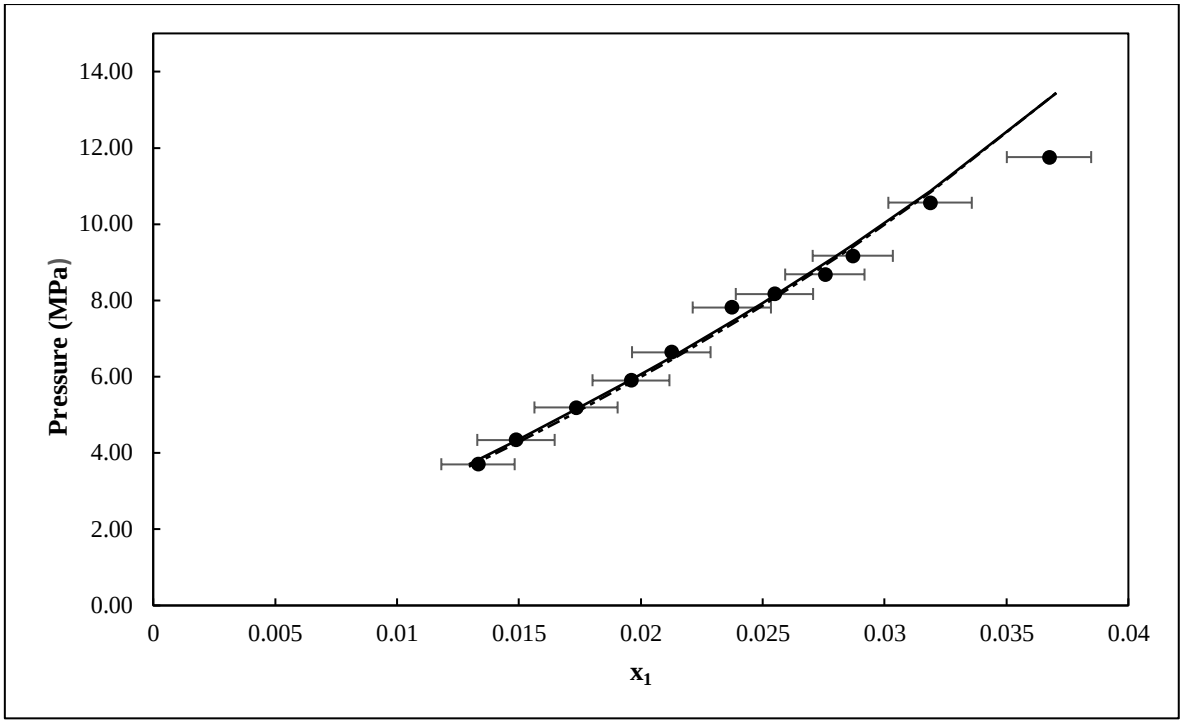

Figure 4.15 P-x data for the CH_4 (1) + (CH_3OH (2) /TEG (3)/Water (4) 3.33/91.84/4.83 wt%) system at 313.15 K with comparison to regression results by various models. Experimental (●), CPA model (·····), PC-SAFT model (----), PR model (- ▪ - ▪ -).

Table 4.24 P-xand modelg results for the CH_4 (1) + (CH_3OH (2) /TEG (3)/Water (4) 3.33/91.84/4.83 wt%) system at 313.15 K

T_{exp} (K)	$x_{1,exp}$	P_{exp} (MPa)	U_c (P) (MPa)	ΔPressure (MPa)		
				CPA	PC-SAFT	PR
313.15	0.013	3.70	0.08	-0.02	0	0.04
313.14	0.015	4.34	0.06	-0.02	0.01	0.05
313.15	0.017	5.19	0.04	0.17	0.2	0.24
313.16	0.020	5.91	0.03	0	0.02	0.06
313.15	0.021	6.64	0.05	0.13	0.16	0.2
313.16	0.024	7.81	0.04	0.26	0.29	0.33
313.15	0.025	8.17	0.03	0.23	0.26	0.3
313.15	0.028	8.68	0.03	-0.48	-0.48	-0.42
313.15	0.029	9.17	0.06	-0.29	-0.29	-0.23
313.16	0.032	10.56	0.04	-0.31	-0.35	-0.28
313.14	0.037	11.76	0.03	-1.66	-1.78	-1.66

[a]$U_c(T) = 0.06$ (K) ; [b]$U_c(x_1) = 0.002$; $\Delta P = (P_{exp} - P_{calc})$ where P_{calc} was determined using the mode

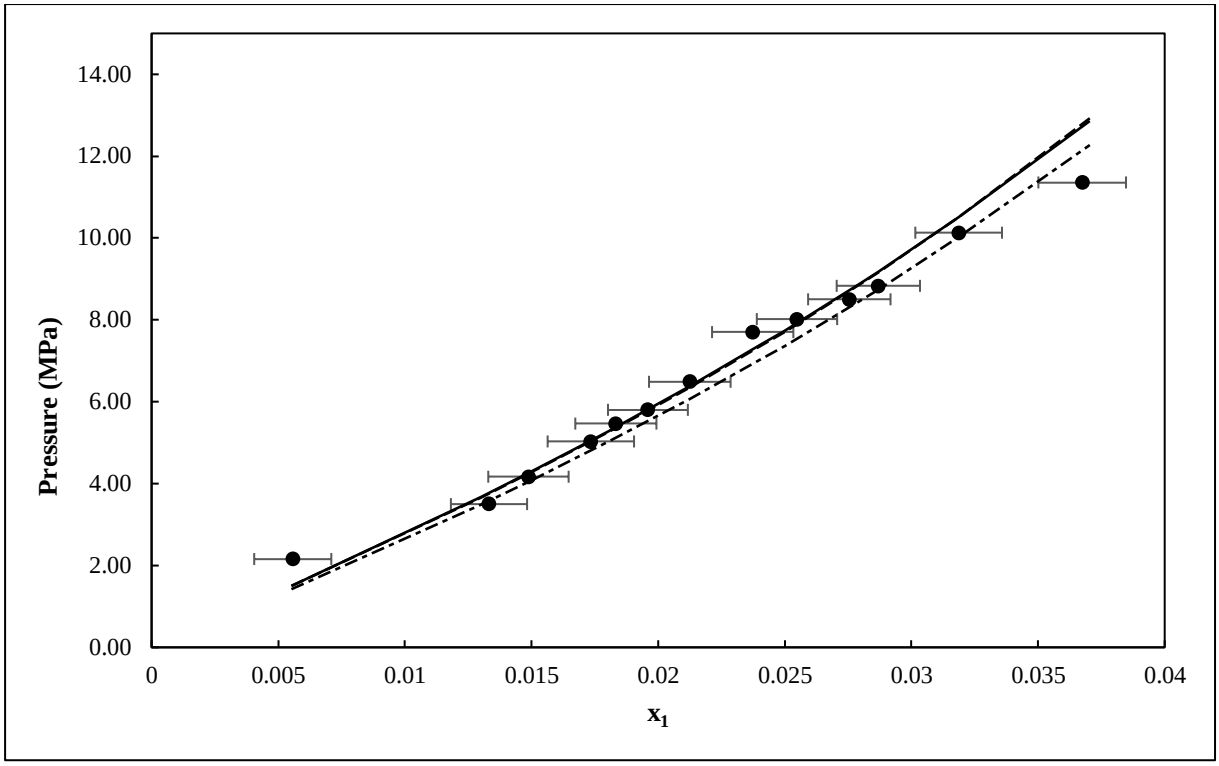

Figure 4.16 P-x for the CH_4 (1) + (CH_3OH (2) /TEG (3)/water (4) 3.33/91.84/4.83 wt%) system at 323.15 K with comparison to regression results by various models. Experimental (●), CPA model (·····), PC-SAFT model (----), PR model (- ▪ - ▪ -).

Table 4.25 Experimental P-x and model results for the CH_4 (1) + (CH_3OH (2) /TEG (3)/Water (4) 3.33/91.84/4.83 wt%) system at 323.15 K

T_{exp} (K)	$x_{1, exp}$	P_{exp} (MPa)	U_c (P) (MPa)	ΔPressure (MPa)		
				CPA	PC-SAFT	PR
323.14	0.006	2.16	0.03	0.64	0.65	0.73
323.15	0.013	3.50	0.03	-0.18	-0.16	0.01
323.16	0.015	4.17	0.04	-0.13	-0.1	0.09
323.15	0.017	5.03	0.04	0.09	0.11	0.33
323.14	0.018	5.47	0.03	0.2	0.22	0.46
323.14	0.020	5.80	0.13	-0.01	0.02	0.27
323.16	0.021	6.49	0.03	0.11	0.14	0.42
323.15	0.024	7.70	0.03	0.32	0.36	0.68
323.15	0.025	8.02	0.03	0.28	0.31	0.65
323.15	0.028	8.50	0.03	-0.4	-0.38	0.02
323.15	0.029	8.83	0.04	-0.35	-0.33	0.08
323.15	0.032	10.13	0.03	-0.37	-0.38	0.11
323.15	0.037	11.36	0.03	-1.48	-1.55	-0.89

[a]$U_c(T) = 0.06$ (K) ; [b]U_c (x_1) = 0.002; $\Delta P = (P_{exp} - P_{calc})$ where P_{calc} was determined using the model

The pressure in all three isotherms was shown to increase with increasing methane concentration, which is expected within the studied range.

In Figure 4.17, the three isotherms are presented on a single set of axes. It can be observed that there is crossover of the isotherms at the lower methane compositions, where an inversion of the temperature trend occurs. At compositions greater than the inflection composition (> 0.023 mole fraction methane), the distinction between the isotherms becomes more apparent. At this point, it is clear that the mixture pressure increases with decreasing temperature.

Table 4.26 Regressed binary interaction parameters and deviations for the modelling of the CH_4 (1) + (CH_3OH (2) /TEG (3)/Water (4) 3.33/91.84/4.83 wt%) system between 303.15 K and 323.15 K for simultaneous regression of all 3 isotherms.

Parameters	CPA	PC-SAFT	PR
k_{12}	-0.12	0.35	0.35
σ_{K12}	0	0.41	0.48
k_{13}	0.32	0.16	0.46
σ_{K13}	0.05	0.05	0.05
k_{14}	-1.04	-0.56	-0.82
σ_{K14}	0.90	0.59	0.48
k_{23}	0.16	0.11	0.01
σ_{K23}	0	0.14	0.05
k_{24}	0.85	1	0.70
σ_{K24}	0	1.85	0
k_{34}	0.10	0.08	-0.21
σ_{K34}	0.11	0.09	0.06

Table 4.27 Results of model errors for the CH_4 (1) + (CH_3OH (2) /TEG (3)/Water (4) 3.33/91.84/4.83 wt%) system between 303.15 K and 323.15 K for simultaneous regression of all 3 isotherms.

Model	CPA			PC-SAFT			PR		
Temperature (K)	**303.15**	**313.15**	**323.15**	**303.15**	**313.15**	**323.15**	**303.15**	**313.15**	**323.15**
AAD P(MPa)	0.405	0.325	0.351	0.442	0.348	0.362	0.543	0.348	0.365
AARD (%)	6.56	3.47	6.02	6.98	3.69	6.14	7.61	3.93	6.86

The data were modelled with the CPA, PC-SAFT and PR models considering all temperatures simultaneously. This was done as a significant number of binary interaction parameters were fitted and insufficient data was measured in a single isotherm to obtain truly independent model fit parameters.

In order to determine if all binary interaction parameters were significant and system-dependent, three different regression scenarios were applied. In the first scenario, all the binary parameters were regressed based on the experimental data in this work. In the second scenario, only the binary parameters involving associating components were regressed, assuming that these would be more significant and that binary interactions between non-polar components in the mixture would be far less non-ideal and justifiably set to 0. In the third scenario, binary interaction parameters from binary

systems for the components comprising the system were sourced from literature where available and fixed in the equation of state, with only the unavailable parameters determined by regression of the data from this work. This process was only conducted on the CPA Model as there was a lack of literature binary parameters for the PC-SAFT and PR models for these systems. By limiting the number of parameters regressed, more precise solutions were expected. The results for these regression scenarios are presented in Table 4.28, with scenario 1 performing the best, scenario 3 second and scenario 2 performing the worst. Hence, the scenario with the highest number of non-zero binary interaction parameters provided the best fit of the data, and the scenario with the lowest number of non-zero interaction parameters performed poorly. The differences in AARD between the scenarios is significant. Scenario one is therefore necessary for an accurate fit of the data and these parameters are presented in Table 4.32. This method was necessary as there was a general lack of binary interaction parameters available in literature and those that were available seemed to perform very poorly in predicting the behaviour of a particular binary pair in a multicomponent system when compared to the experimental data obtained.

The results are presented in Tables 4.23 to 4.27 for scenario one. The CPA model performed the best, with the PC-SAFT model second and the PR model performing the worst. The AARD for these fits is presented in Tables 4.26 and 4.27, where the CPA model is shown to have the lowest AARD for all temperatures. This result would be expected as the CPA model has had success in modelling the VLE data associated with natural gas systems. The ability to predict/correlate the behaviour of systems with many associating terms is an advantage of the model due to its associating term. The regressed binary parameters in Table 4.26 are generally greater in magnitude than their standard deviations. This indicates that the fitting resulted in a model that is acceptably well-conditioned. The poorer performance of the PC-SAFT model is attributed to the presence of water in the mixture, which the model has difficulty describing the behaviour of in multicomponent mixtures. The PR model performance is expected as the model lacks a specialized term to account for associating mixtures. All models replicated the unique temperature dependence of the data. It should also be noted that the performance of the models seems to deviate from the experimental data the most at the highest-pressure point. This indicates that the models may be reaching their limitations regarding predictive ability at these conditions.

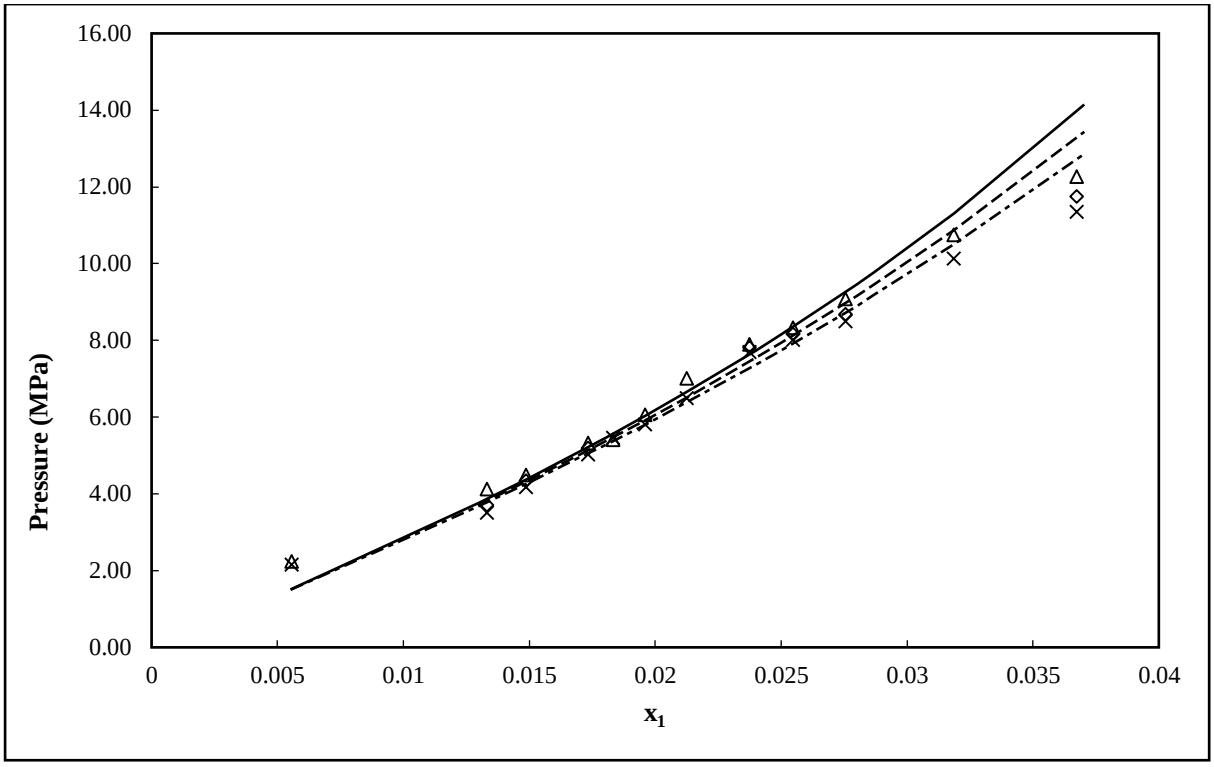

Figure 4.17 -A P-x for the CH_4 (1) + (CH_3OH (2) /TEG (3)/Water (4) 3.33/91.84/4.83 wt%) system. Δ- 303.15 K ; ◊- 313.15 K; × - 323.15 K; lines represent the CPA model fits at 303.15 K (·····), 313.15 K (----), 323.15K (- ▪ - ▪ -).

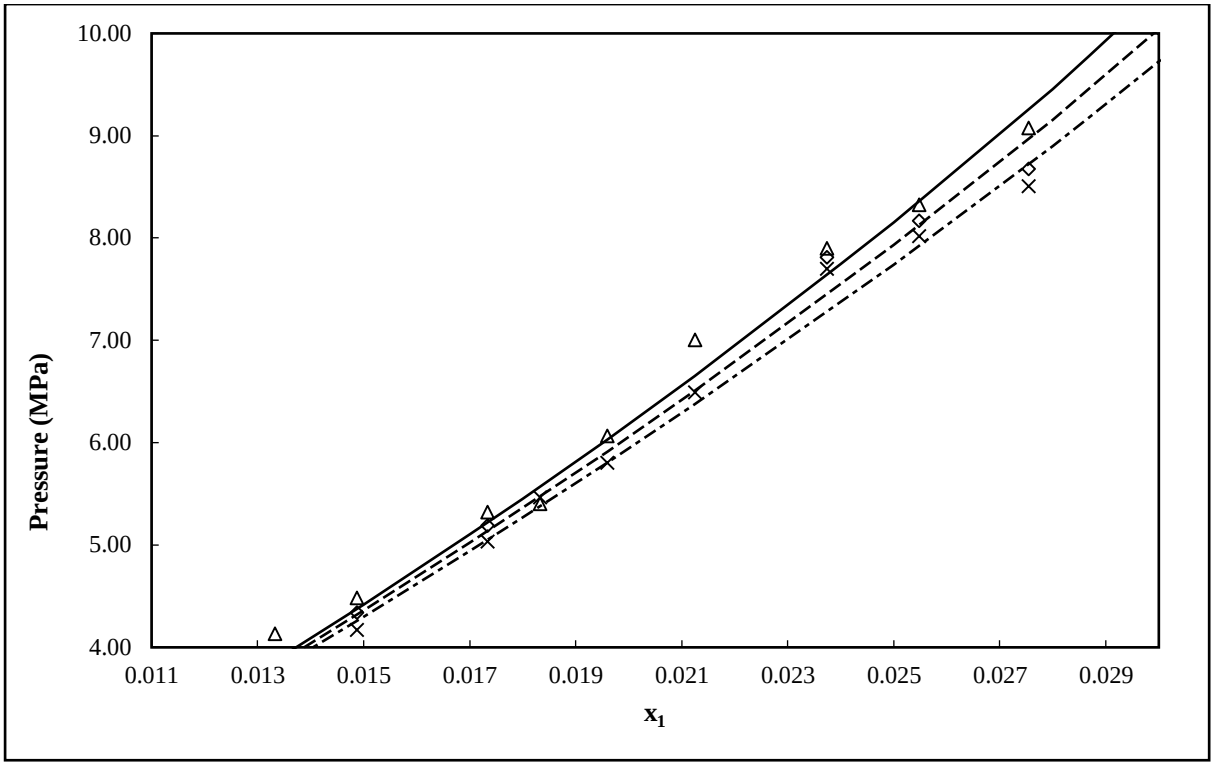

Figure 4.17 -B P-x data for the CH_4 (1) + (CH_3OH (2) /TEG (3)/Water (4) 3.33/91.84/4.83 wt%) system. Δ- 303.15 K ; ◊- 313.15 K; × - 323.15 K; lines represent the CPA model fits at 303.15 K (·····),313.15 K (----),323.15K (- ▪ - ▪ -).

Table 4.28 Average absolute deviation of models employed for the (CH_4 (1)) + (CH_3OH (4) /TEG (5)/Water (6) 3.33/91.84/4.83 wt%) system between 303.15 K and 323.15K for simultaneous regression of all 3 isotherms.

Model	**CPA**			**PC-SAFT**			**PR**		
Temperature (K)	**303.15**	**313.15**	**323.15**	**303.15**	**313.15**	**323.15**	**303.15**	**313.15**	**323.15**
	Regression of all binary interaction parameters								
AAD P(MPa)	0.405	0.325	0.351	0.442	0.348	0.362	0.543	0.348	0.365
AARD (%)	6.56	3.47	6.02	6.98	3.69	6.14	7.61	3.93	6.86
	Regression of binary interaction parameters for only the associating components								
AAD P(MPa)	0.934	0.8091	0.715						
AARD (%)	14.903	10.62	11.44						
	Employing existing binary interaction parameters from literature for available pairs and regressing for only the unavailable parameter pairs.								
AAD P(MPa)	0.744	0.6219	0.565						
AARD (%)	12.25	8.164	9.23						

4.5.2. (CH_4 (1)/C_2H_6(2)/C_3H_8(3) 3.68/0.22/96.10 wt%) + (CH_3OH (4) /TEG (5)/Water (6) 3.33/91.84/4.83 wt%) senary system

The second novel system measured was the (CH_4 (1)/C_2H_6(2)/C_3H_8(3) 3.68/0.22/96.10 wt%) + (CH_3OH (4) /TEG (5)/Water (6) 3.33/91.84/4.83 wt%) senary system at 303.15 K, 313.15 K and 323.15 K. The data are presented graphically in Figures 4.18-4.21 and in Tables 4.29-4.31. The single isotherms are presented and discussed first, followed by the combination of all data into a single plot and analyses of the model results.

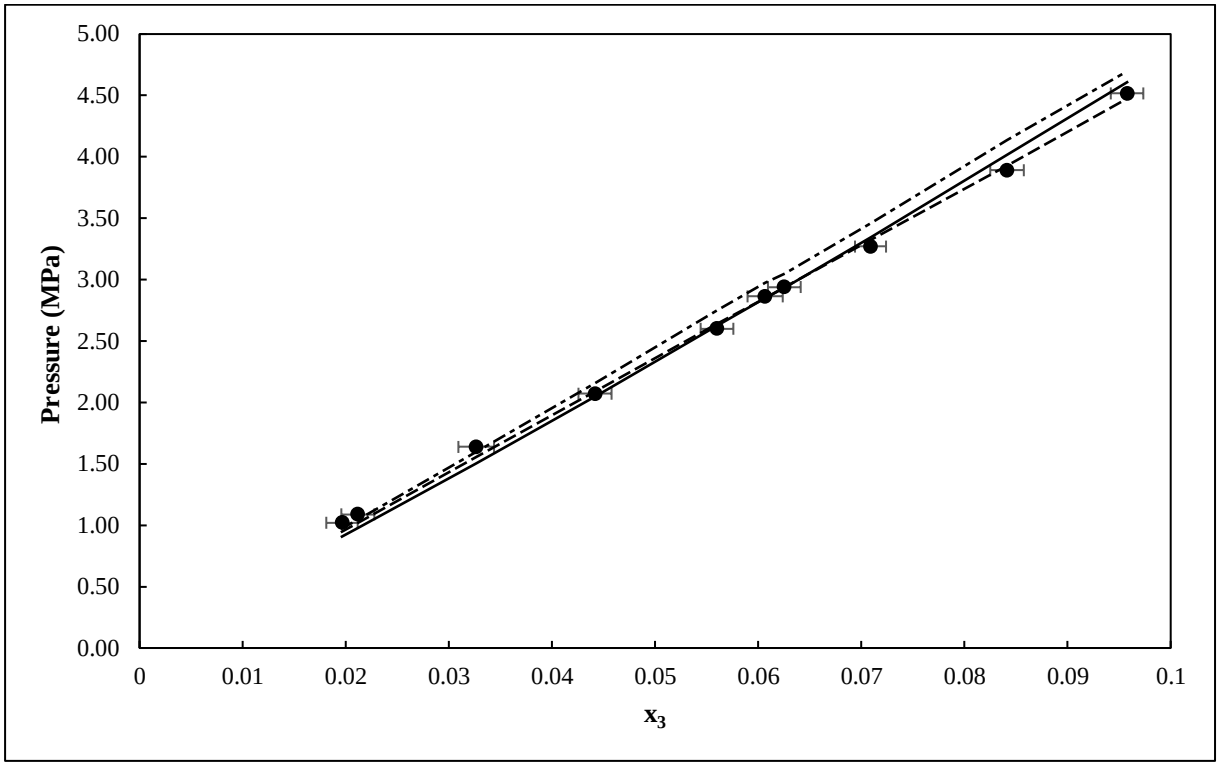

Figure 4.18 P-x data for the (CH_4 (1)/C_2H_6 (2)/C_3H_8 (3) 3.68/0.22/96.10 wt%) + (CH_3OH (4) /TEG (5)/Water (6) 3.33/91.84/4.83 wt%) system at 303.15K with comparison to regression results by various models. Experimental (●), CPA model (·····), PC-SAFT model (----), PR model (- ▪ - ▪ -).

Table 4.29 P-x data and model results for the (CH_4 (1)/C_2H_6 (2)/C_3H_8 (3) 3.68/0.22/96.10 wt%) + (CH_3OH (4)/TEG (5)/Water (6) 3.33/91.84/4.83 wt%) system at 303.15 K

T_{exp} (K)	$x_{3,exp}$	P_{exp} (MPa)	U_c (P) (MPa)	ΔPressure (MPa)		
				CPA	PC-SAFT	PR
303.15	0.020	1.02	0.03	0.11	0.07	0.05
303.15	0.021	1.09	0.03	0.11	0.07	0.04
303.16	0.033	1.64	0.03	0.13	0.08	0.04
303.15	0.044	2.07	0.03	0.02	-0.02	-0.09
303.14	0.056	2.60	0.04	-0.02	-0.04	-0.15
303.15	0.061	2.86	0.05	0.01	0.01	-0.11
303.14	0.063	2.94	0.03	0.01	0	-0.11
303.15	0.071	3.27	0.04	-0.08	-0.05	-0.19
303.16	0.084	3.89	0.03	-0.13	-0.04	-0.25
303.14	0.096	4.52	0.03	-0.09	0.05	-0.18

[a] $U_c(T) = 0.06$ (K) ; [b] $U_c(x_3) = 0.002$; $\Delta P = (P_{exp} - P_{calc})$ where P_{calc} was determined using the model

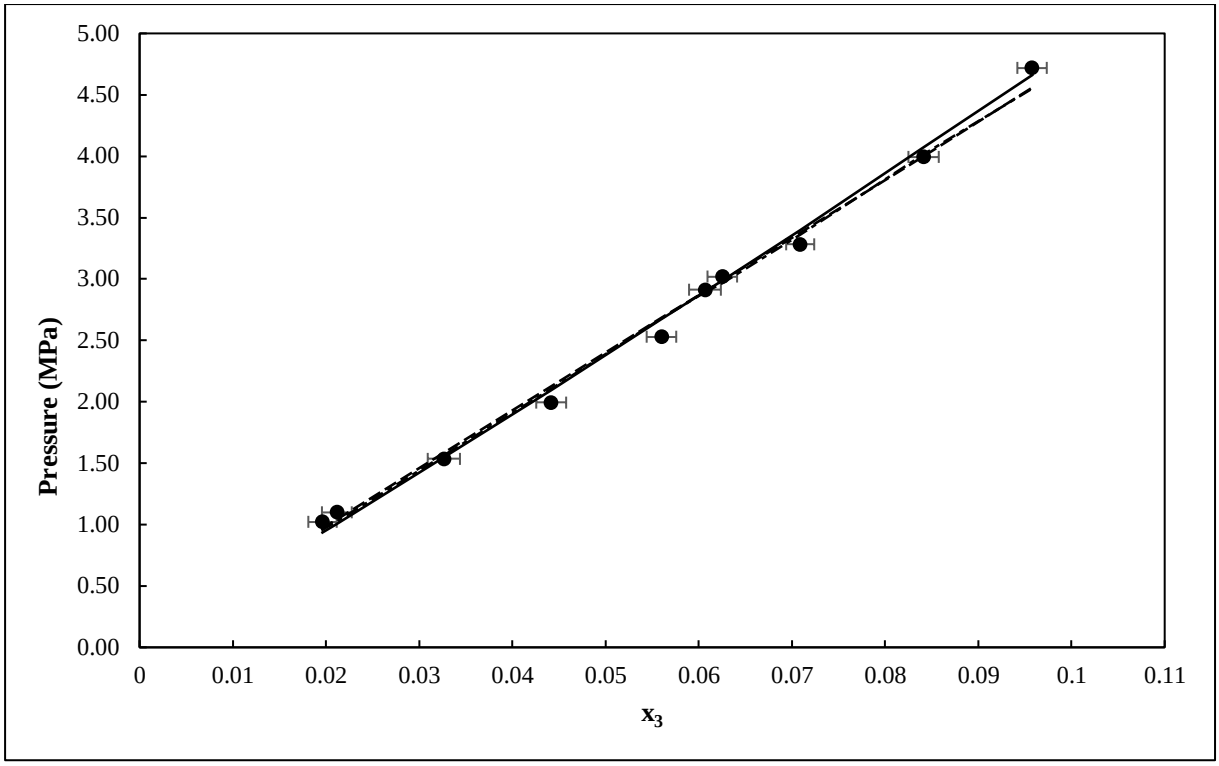

Figure 4.19 P-x data for the (CH_4 (1)/C_2H_6 (2)/C_3H_8 (3) 3.68/0.22/96.10 wt%) + (CH_3OH (4) /TEG (5)/Water (6) 3.33/91.84/4.83 wt%) system at 313.15 K with comparison to regression results by various models. Experimental (●), CPA model (·····), PC-SAFT model (----), PR model (- ▪ - ▪ -).

Table 4.30 Experimental P-x and model results for the (CH_4 (1)/C_2H_6 (2)/C_3H_8 (3) 3.68/0.22/96.10 wt%) + (CH_3OH (4) /TEG (5)/Water (6) 3.33/91.84/4.83 wt%) system at 313.15 K

T_{exp} (K)	$x_{3,exp}$	P_{exp} (MPa)	U_c (P)	ΔPressure (MPa)		
				CPA	PC-SAFT	PR
313.16	0.020	1.02	0.03	0.08	0.05	0.06
313.16	0.021	1.10	0.06	0.09	0.06	0.07
313.16	0.033	1.53	0.03	-0.01	-0.06	-0.03
313.16	0.044	1.99	0.03	-0.1	-0.13	-0.11
313.16	0.056	2.53	0.06	-0.14	-0.15	-0.15
313.15	0.061	2.91	0.07	0.01	0.01	0.02
313.15	0.063	3.02	0.04	0.03	0.03	0.05
313.16	0.071	3.28	0.03	-0.12	-0.1	-0.08
313.15	0.084	3.99	0.03	-0.08	-0.01	-0.02
313.15	0.096	4.72	0.03	0.06	0.16	0.17

[a] $U_c(T) = 0.06$ (K) ; [b] $U_c(x_3) = 0.002$; $\Delta P = (P_{exp} - P_{calc})$ where P_{calc} was determined using the model

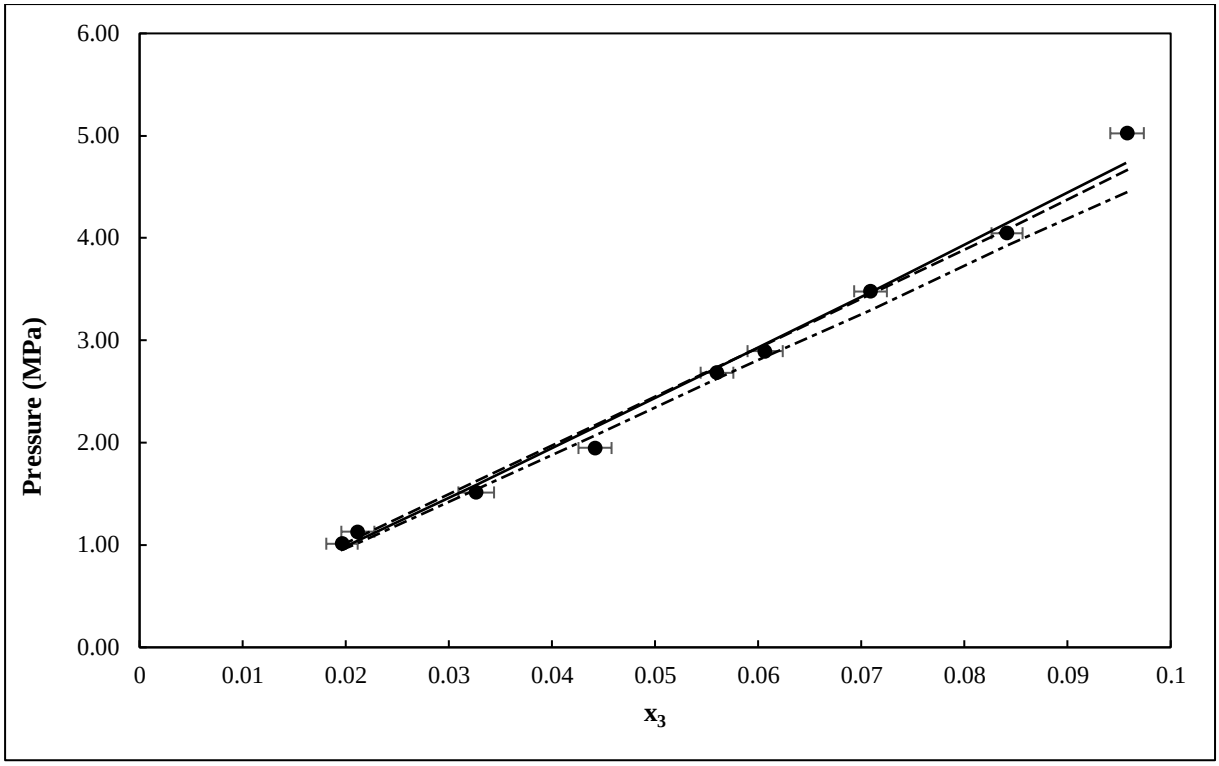

Figure 4.20 P-x data for the (CH_4 (1)/C_2H_6 (2)/C_3H_8 (3) 3.68/0.22/96.10 wt%) + (CH_3OH (4) /TEG (5)/Water (6) 3.33/91.84/4.83 wt%) system at 323.15 K with comparison to regression results by various models. Experimental (●), CPA model (·····), PC-SAFT model (----), PR model (- ▪ - ▪ -).

Table 4.31 P-x data and model results for the (CH_4 (1)/C_2H_6 (2)/C_3H_8 (3) 3.68/0.22/96.10 wt%) + (CH_3OH (4) /TEG (5)/Water (6) 3.33/91.84/4.83 wt%) system at 323.15 K

T_{exp} (K)	$x_{3,exp}$	P_{exp} (MPa)	U_c (P) (MPa)	ΔPressure (MPa)		
				CPA	PC-SAFT	PR
323.15	0.020	1.01	0.03	0.04	0.01	0.06
323.15	0.021	1.13	0.05	0.09	0.05	0.11
323.14	0.033	1.51	0.02	-0.08	-0.11	-0.03
323.16	0.044	1.95	0.02	-0.2	-0.22	-0.12
323.16	0.056	2.68	0.03	-0.06	-0.06	0.05
323.15	0.061	2.89	0.03	-0.08	-0.07	0.05
323.15	0.071	3.48	0.03	0.01	0.03	0.19
323.15	0.084	4.05	0.03	-0.1	-0.04	0.12
323.16	0.096	5.03	0.03	0.29	0.37	0.58

[a] $U_c(T) = 0.06$ (K) ; [b] $U_c(x_3) = 0.002$

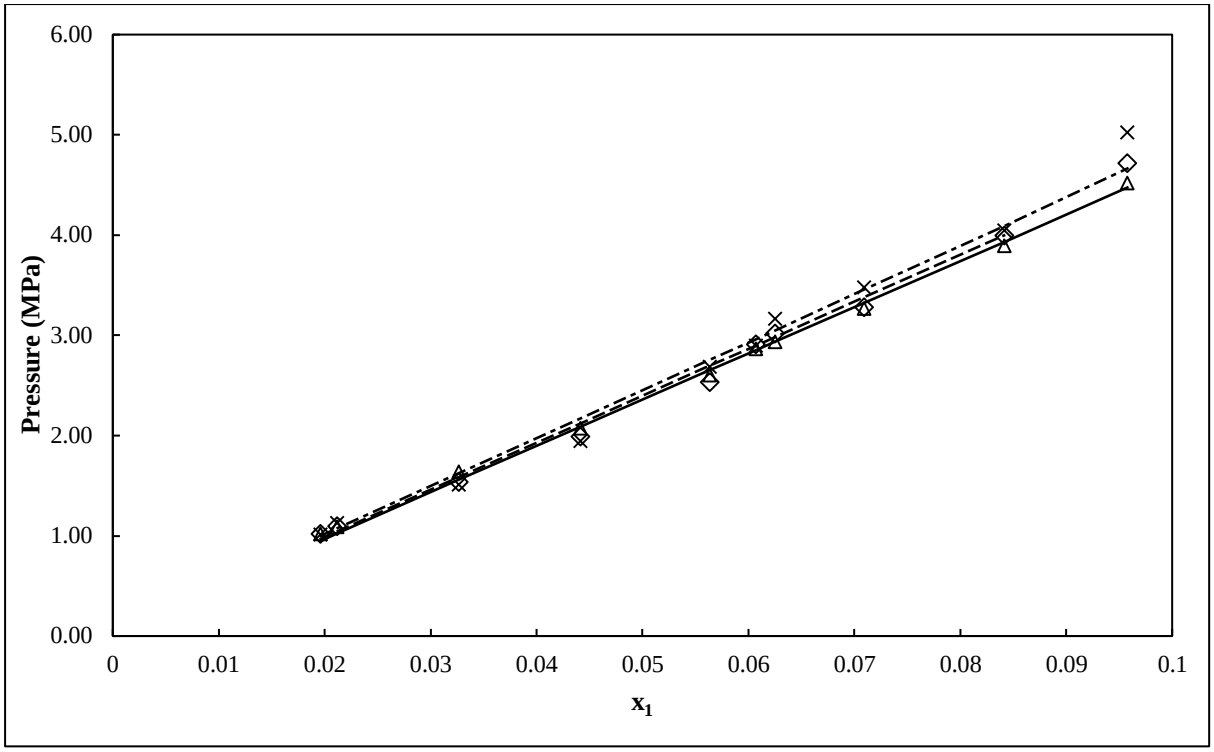

Figure 4.21 P-x data for the CH_4 (1)/C_2H_6 (2)/C_3H_8 (3) (3.68/0.22/96.10 wt%) + (CH_3OH (4) /TEG (5)/Water (6) 3.33/91.84/4.83 wt%) system Δ- 303.15 K ; ◊- 313.15 K; × - 323.15 K. ; PC-SAFT model 303.15 K (·····), PC-SAFT model 313.15 K (----), PC-SAFT model 323.15 K (- ▪ - ▪ -).

Note that the initial pressures of the gas mixtures loaded into the cell for these measurements were limited in this case by the low cylinder supply pressure of the propane gas mixture available.

In Figure 4.21, all three isotherms are presented on a single set of axes. A temperature trend inversion results in a cross-over of the isotherms at approximately 0.056 mole fraction propane. At compositions of methanol above this point, a more significant dependence of the isotherms on temperature is observed.

Table 4.32- Regressed binary interaction parameters and deviations for the modelling of the (CH_4 (1)/C_2H_6 (2)/C_3H_8 (3) 3.68/0.22/96.10 wt%) + (CH_3OH (4) /TEG (5)/Water (6) 3.33/91.84/4.83 wt%) system between 303.15 K and 323.15 K for simultaneous regression of all 3 isotherms.

Parameters	**CPA**	**PC-SAFT**	**PR**
k_{12}	2.87	1.05	0.02
σ_{k12}	4.55	12.66	0.00
k_{13}	0.88	0.05	0.15
σ_{k13}	0.28	0.29	0.00
k_{14}	-0.12	0.33	1.07
σ_{k14}	0.00	3.53	2.04
k_{15}	0.08	0.30	0.28
σ_{k14}	0.15	0.47	0.39
k_{16}	4.05	-0.72	0.71
σ_{k16}	2.53	5.45	2.97
k_{23}	3.94	0.89	-0.01
σ_{k23}	4.11	12.04	0.00
k_{24}	-0.25	0.91	0.30
σ_{k24}	16.12	183.86	0.00
k_{25}	-0.22	0.09	0.54
σ_{k25}	0.68	10.23	18.77
k_{26}	6.02	-0.13	-2.93
σ_{k26}	0.00	201.95	156.31
k_{34}	0.65	-0.07	0.56
σ_{k34}	0.00	5.88	10.67
k_{35}	0.13	0.05	-0.47
σ_{k35}	0.15	0.88	1.42
k_{36}	-1.02	0.10	4.51
σ_{k36}	2.22	10.61	10.72
k_{45}	0.16	0.60	0.27
σ_{k45}	0.00	0.13	0.05
k_{46}	0.85	-4.19	-0.86
σ_{k46}	0.00	1.29	0.00
k_{56}	0.39	0.47	0.02
σ_{k56}	0.11	0.07	0.05

Table 4.33 Average absolute deviation of models employed for the (CH_4 (1)/C_2H_6 (2)/C_3H_8 (3) 3.68/0.22/96.10 wt%) + (CH_3OH (4) /TEG (5)/Water (6) 3.33/91.84/4.83 wt%) system between 303.15 K, 313.15 K and 323.15 K for simultaneous regression of all 3 isotherms.

Model	**CPA**			**PC-SAFT**			**PR**		
Temperature (K)	**303.15**	**313.15**	**323.15**	**303.15**	**313.15**	**323.15**	**303.15**	**313.15**	**323.15**
	Regression of all binary interaction parameters								
AAD P(MPa)	0.078	0.073	0.103	0.043	0.075	0.106	0.120	0.076	0.146
AARD (%)	3.97	3.66	4.47	2.46	3.43	4.24	4.47	3.50	5.27
	Regression of binary interaction parameters for only the associating components								
AAD P(MPa)	0.957	1.240	1.443						
AARD (%)	35.70	47.05	55.34						
	Employing existing binary interaction parameters from literature for available pairs and regressing for only the unavailable parameter pairs.								
AAD P(MPa)	0.206	0.113	0.216						
AARD (%)	9.91	5.30	8.35						

The data were modelled with the CPA, PC-SAFT and PR models considering all temperatures simultaneously. Due to the number of components comprising the system, a large number of binary parameters were required to be calculated from a limited number of experimental points. The same three regression scenarios were tested in this system as the previous novel system. The results for these regression scenarios are presented in Table 4.33, with scenario one performing the best, followed by scenario 3 second and scenario 2. Hence, the scenario with the highest number of non-zero binary interaction parameters provided the best fit of the data and the scenario with the lowest number of non-zero interaction parameters performed poorly. The differences in AARD between the scenarios are of multiples of 3 to 12. Scenario one is therefore necessary for an accurate fit of the data and these parameters are presented in Table 4.32. Note that for many of the binary interaction parameters regressed, the standard deviation value for the parameter exceeded the magnitude of the parameter. Attempts were made to omit those parameter combinations with larger standard deviations from the final regression, such as setting the non-associating binary parameters to zero; however, these resulted in a poor correlation of the P-x data. Furthermore, in many cases it was not possible to formulate a consistent method of elimination. For example, it is not consistent to omit the interaction between ethane and methanol without omitting the interaction between propane and methanol, as ethane and propane are similar non-polar molecules and the interactions with methanol should therefore be similar. Hence, due to the large number of parameters required to represent the phase behaviour accurately, some

physical meaning of the interaction parameters has been lost. An additional contributing factor may also be the limitation of the commercial regression software employing optimization tools that search for the local minimum instead of the global minimum for solutions. This could possibly be resolved by incorporating more complex global optimization regression tools such as stochastic algorithms. This requires extensive programming application and computing time and is regarded as beyond the scope of this work. The trend in temperature was predicted.

Interestingly, the CPA model mostly exhibits a better AAD for the systems, while the PC-SAFT model has a lower AARD%. This indicates that CPA is performs better at the higher-pressure values than at the lower, where PC-SAFT is superior. Noting that the pressure range measured for this system is within 6 MPa, the superior performance of the CPA model at higher pressures correlates with the results from the first new system within the region of 2-12 MPa. Other factors that affect the performance difference in CPA and PC-SAFT between the quaternary new system above and this senary system may be the description of methane vs. propane as the bulk vapour phase constituent by the two models, as well as the difference in the description of 6 component systems as opposed to 4. Again, the PR model mostly performed worse than the other two models but still yielded qualitative results.

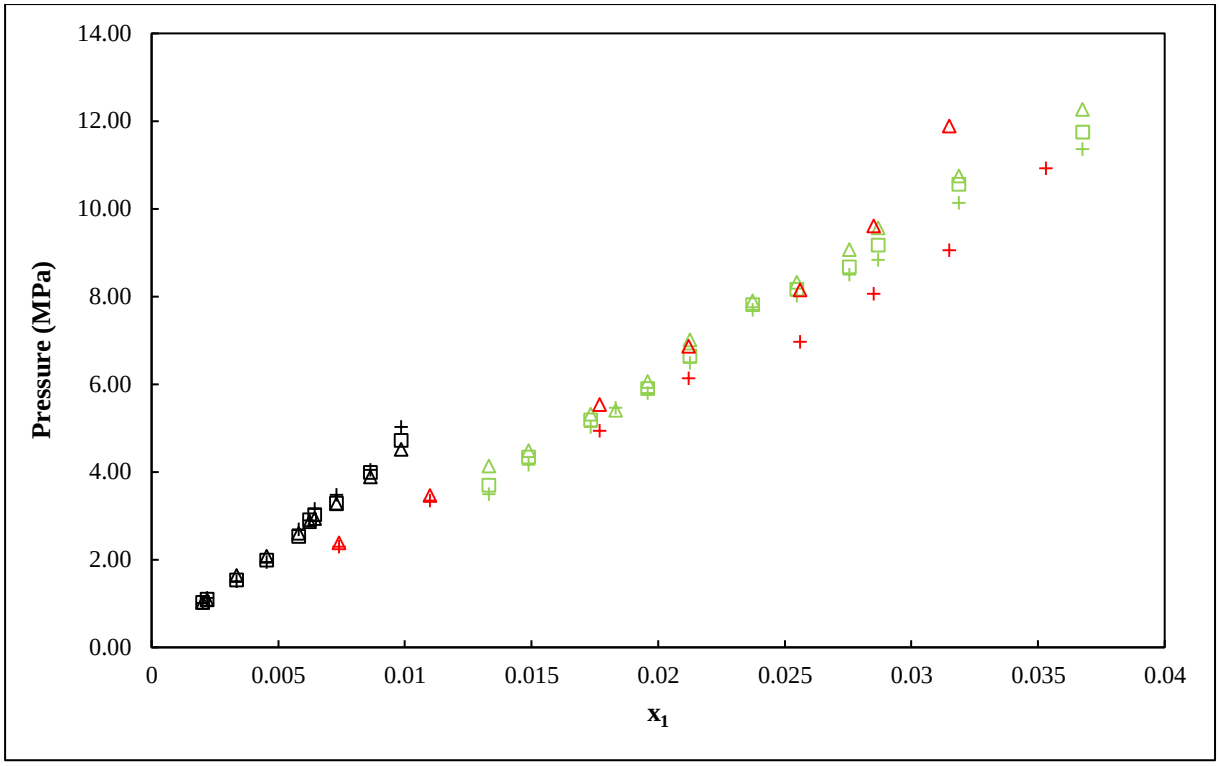

Figure 4.22 System-x data for systems of CH_4 (1)/C_2H_6 (2)/C_3H_8 (3) + (CH_3OH (4) /TEG (5)/Water (6) This work, CH_4 (1)+ (CH_3OH (2) /TEG (3)/Water (4) 3.33/91.84/4.83 wt%), Δ- 303.15 K ; □- 313.15 K; + - 323.15 K. Data of (Zvawanda et al., 2022b) (CH4 (1)/C3H8 (2) 87.36/12.64 wt%) + (CH_3OH (4) /TEG (5)/Water (6) 3.33/91.84/4.83 wt%). Δ- 303.15 K ; +- 323.16 K. This work, CH_4 (1)/C_2H_6 (2)/C_3H_8 (3) 3.68/0.22/96.10 wt%) + (CH_3OH (4) /TEG (5)/Water (6) 3.33/91.84/4.83 wt%) system, Δ- 303.15 K ; □- 313.15 K; + - 323.15 K.

In Figure 4.22, the results of both novel systems (methane in aqueous solvent mixture and propane-rich gas with methane and ethane in aqueous solvent mixture) are compared along with the results of (Zvawanda et al., 2022b) (methane-rich gas with propane in aqueous solvent mixture). This comparison shows that in the methane-rich mixtures, the total pressure of the mixture decreases with increasing temperature. This trend of methane behaviour is not observed in the propane-rich gas mixture in the aqueous solvent mixture, where the system pressure increases with temperature. This is an indication that a directly proportional relationship exists between temperature and solubility in methane rich systems. This suggests that the loss of natural gas to the aqueous solvent is more likely in methane rich systems at higher temperature than in propane rich systems. There is also a distinct difference in the shape of the phase behaviour of methane in the pure methane gas-aqueous solvent mixture system, the methane-rich gas-aqueous solvent mixture and the propane-rich gas-aqueous solvent mixture, which may indicate that the dehydration behaviours using TEG may vary with the relative composition of methane and propane in these mixtures.

Chapter 5: Conclusions

Overall, high-quality HPVLE P-x data was measured for two verification systems with 15 data points and, 66 data points for the new systems. This contributes to the increasing data base and thermodynamic knowledge of multicomponent phase equilibrium behaviour. The relevance and suitability of the CPA and PC-SAFT EoS for the prediction/correlation of natural gas systems were also demonstrated through the regression and modelling of this newly enquired data.

P-x phase data for the two test systems, namely, CH_4(1) + CH_3OH (2) binary system at 303.15 K and the CO_2 (1) +TEG (2) + water (3) system at 322.04 K showed an acceptable comparison to literature data. This confirmed the accuracy of the equipment and techniques employed. These systems had model errors (AARD) of 4.14% and 8.63% for their best-performing models, the CPA and PR EoS.

For the quaternary and senary system of CH_4 (1) + (CH_3OH (2) + TEG (3) + water (4) (3.33 (2), 91.84 (3), 4.83 (4) wt%)) and (CH_4 (1) + C_2H_6 (2) + C_3H_8 (3) 3.68 (1), 0.22 (2), 96.10 (3) wt%) + (CH_3OH (4) + TEG (5) + water (6) 3.33 (4), 91.84 (5), 4.83 (6) wt%)), phase data were measured over three isotherms 303.15 K ; 313.15 K and 323.15 K. The quaternary system showed an inversion of the trends of the isotherms with temperature at the 0.056-mole fraction of propane, while the senary system showed a directly proportional relationship with temperature. This indicated a direct relationship between methane system's solubility and temperature while showing the inverse for propane-rich systems.

Thermodynamic modelling of the quaternary and senary phase behaviour revealed that the scenario where all parameter combinations were regressed yielded the most accurate fit, with a 10% difference between the regression of all parameters and the regression of all unknown parameters. In the quaternary system, the CPA model performed the best with AAD values of 0.405 MPa, 0.325 MPa and 0.351 MPa and AARD of 6.56% 3.47% and 6.02% respectively for the temperatures of 303.15 K, 313.15 K and 323.15 K. The next best performing model was PC-SAFT followed by the PR model. This result was expected due to the speciality of the CPA model in predicting the phase behaviour of highly associating systems. Different results were observed in the senary system, with the PC-SAFT model yielding a lower AARD values of 2.46%, 3.43% and 4.24% but the CPA exhibiting a better AAD of 0.078 MPa, 0.073 MPa and 0.103 MPa, indicating the CPA model performs better at higher pressures. These results can be explained by the limited lower pressure range considered for the senary system and the complexity of the system.

The results from this work, both the generation of new phase equilibrium data and model parameters, with standard deviations provides valuable data and trends for process design. The model results show the difficulty in modelling multi-component systems using conventional software and optimization algorithms. The model results further reinforce the agility and suitability of the CPA and PC-SAFT models for these process fluids.

Chapter 6: Recommendations

The phase equilibrium data for the dehydration of natural gas systems become scarcer as these systems increase in complexity due to additional constituents such as ethane and propane, etc. Available data is often limited in range and not measured at high pressures and temperatures, limiting their applicability. Thus, several further combinations of compositions over a wide temperature range should be tested with the components considered in this study, namely TEG, methanol, water, methane, ethane, and propane. An evaluation of the available literature was reviewed in Chapter 2.3.

There are several substances found in natural gas that are not present in the systems tested in this study, such as hydrogen sulphide and heavier hydrocarbons. Thus, it is recommended that these compounds be included in future studies. In addition, TEG may be a common glycol used for dehydration, but other glycols, such as MEG are employed in certain process scenarios for natural gas dehydration. Hence it is recommended that the measurements conducted in this work be repeated with other dehydrating agents such as MEG, to obtain the phase equilibrium data to make more informed comparisons between the performances of TEG and MEG for dehydration.

The vapour pressure measurements excluded values for methane, ethane and TEG. Thus, it is recommended that these values be measured and included in future studies. This would require the development of new equipment and would allow for the complete evaluation of the equations of states used.

Due to some equipment limitations, measurements were not possible above 15 MPa. Thus, it is recommended that the equipment be improved so that the measurements can be extended to pressures greater than 15 MPa.

The pressures measured for the propane/ethane/methane (96.10/0.22/3.68 mass%) + TEG/Water/Methanol (91.83/4.83/3.33 mass%) were relatively low due to the cylinder pressure of the propane gas mixture source. Thus, it is recommended that a larger, higher pressure propane cylinder be used in future studies to reach equilibrium compositions greater than those achieved in this study.

The modelling conducted in this study showed the usefulness of the CPA, PC-SAFT and PR equations of states; however, these models should be used in simulations to gain the best benefit of the parameters determined. Thus, it is recommended that the parameters obtained be used in a natural dehydration plant simulation. This is currently ongoing in another study within the research group.

References

Ahlrichs, R., Penco, R. and Scoles, G. (1977) 'Intermolecular forces in simple systems', Chemical Physics, 19, pp. 119–130. Available at: https://doi.org/10.1016/0301-0104(77)85124-0.

Ahmed, T. (2010) Working Guide to Vapor-liquid Phase Equilibria Calculations. Elsevier. Available at: https://doi.org/10.1016/C2009-0-30576-0.

Alfradique, M.F. and Castier, M. (2007) 'Critical points of hydrocarbon mixtures with the Peng–Robinson, SAFT, and PC-SAFT equations of state', Fluid Phase Equilibria, 257, pp. 78–101. Available at: https://doi.org/10.1016/j.fluid.2007.05.012.

Aniya, V., Singh, A., De, D., Reddy, R. and Satyavathi, B. (2015) 'Experimental isobaric vapor–liquid equilibrium at sub-atmospheric and local atmospheric pressures, volumetric properties and molar refractivity from 293.15 to 313.15K of water+triethylene glycol', Fluid Phase Equilibria, 405, pp. 132–140. Available at: https://doi.org/10.1016/j.fluid.2015.07.030.

Arya, A., Maribo-Mogensen, B., Tsivintzelis, I. and Kontogeorgis, G.M. (2014) 'Process Design of Industrial Triethylene Glycol Processes Using the Cubic-Plus-Association (CPA) Equation of State', Industrial & Engineering Chemistry Research, 53, pp. 11766–11778. Available at: https://doi.org/10.1021/ie501251d.

Austrheim (2006) Experimental Characterization of High-Pressure Natural Gas Scrubbers. The University of Bergen. Available at: https://bora.uib.no/bora-xmlui/handle/1956/2007.

Bernatová, S., Aim, K. and Wichterle, I. (2006) 'Isothermal vapour–liquid equilibrium with chemical reaction in the quaternary water+methanol+acetic acid+methyl acetate system, and in five binary subsystems', Fluid Phase Equilibria, 247, pp. 96–101. Available at: https://doi.org/10.1016/j.fluid.2006.06.005.

Besford, Q.A., Van den Heuvel, W. and Christofferson, A.J. (2022) 'Dipolar Dispersion Forces in Water–Methanol Mixtures: Enhancement of Water Interactions upon Dilution Drives Self-Association', The Journal of Physical Chemistry B, 126, pp. 6231–6239. Available at: https://doi.org/10.1021/acs.jpcb.2c04638.

Bildirici, M.E. and Bakirtas, T. (2014) 'The relationship among oil, natural gas and coal consumption and economic growth in BRICTS (Brazil, Russian, India, China, Turkey and South Africa) countries', Energy, 65, pp. 134–144. Available at: https://doi.org/10.1016/j.energy.2013.12.006.

Blanco, S., Velasco, I., Rauzy, E. and Otín, s. (2001) 'Dew Points of Ternary Propane + Water + Methanol: Measurement and Correlation.', JOURNAL OF CHEMICAL ENGINEERING OF JAPAN, 34, pp. 971–978. Available at: https://doi.org/10.1252/jcej.34.971.

Brunner, E., Hültenschmidt, W. and Schlichthärle, G. (1987) 'Fluid mixtures at high pressures IV. Isothermal phase equilibria in binary mixtures consisting of (methanol + hydrogen or nitrogen or methane or carbon monoxide or carbon dioxide)', The Journal of Chemical Thermodynamics, 19, pp. 273–291. Available at: https://doi.org/10.1016/0021-9614(87)90135-2.

Carlson, E.C. (1996) Don't gamble with physical properties for simulations. American Institute of Chemical Engineers.

Chapman, W.G., Gubbins, K.E., Jackson, G. and Radosz, M. (1989) 'SAFT: Equation-of-state solution model for associating fluids', Fluid Phase Equilibria, 52, pp. 31–38. Available at: https://doi.org/10.1016/0378-3812(89)80308-5.

Chapoy, A., Coquelet, C. and Richon, D. (2003) 'Measurement of the Water Solubility in the Gas Phase of the Ethane + Water Binary System near Hydrate Forming Conditions', Journal of Chemical & Engineering Data, 48, pp. 957–966. Available at: https://doi.org/10.1021/je0202230.

Chylinski, K., Cebola, M.., Meredith, A., Saville, G. and Wakeham, W.. (2002) 'Apparatus for phase equilibrium measurements at high temperatures and pressures', The Journal of Chemical Thermodynamics, 34, pp. 1703–1728. Available at: https://doi.org/10.1016/S0021-9614(02)00233-1.

Dahm, K.D. and Visco, D.P. (2014) Fundamentals of Chemical Engineering Thermodynamics, SI Edition. SI. Stamford.

Dai, C., Hu, Y., Wu, Y., Zhao, M. and Yue, T. (2020) 'Effects of structural properties of alcohol molecules on decomposition of natural gas hydrates: A molecular dynamics study', Fuel, 268, p. 117322. Available at: https://doi.org/10.1016/j.fuel.2020.117322.

Ebrahiminejadhasanabadi, M., Nelson, W.M., Naidoo, P., Mohammadi, A.H. and Ramjugernath, D. (2018) 'Experimental measurement of carbon dioxide solubility in 1-methylpyrrolidin-2-one (NMP) + 1-butyl-3-methyl-1H-imidazol-3-ium tetrafluoroborate ([bmim][BF4]) mixtures using a new static-synthetic cell', Fluid Phase Equilibria, 477, pp. 62–77. Available at: https://doi.org/10.1016/j.fluid.2018.08.017.

Fan, S., Zhang, Y., Tian, G., Liang, D. and Li, D. (2006) 'Natural Gas Hydrate Dissociation by Presence of Ethylene Glycol', Energy & Fuels, 20, pp. 324–326. Available at: https://doi.org/10.1021/ef0502204.

Faramawy, S., Zaki, T. and Sakr, A.A.-E. (2016) 'Natural gas origin, composition, and processing: A review', Journal of Natural Gas Science and Engineering, 34, pp. 34–54. Available at: https://doi.org/10.1016/j.jngse.2016.06.030.

Ferreira, M. (2018) Phase Equilibria & thermodynamic modelling of the ternary system CO2 + 1-decanol + N-Tetradecane. Stellenbosch University. Master's thesis Available at:

https://scholar.sun.ac.za/items/ad53bab4-19cc-42a4-9947-5154de3d39b4.

Fischer, K. and Gmehling, J. (1994) 'P-x and .gamma..infin. Data for the Different Binary Butanol-Water Systems at 50.degree.C', Journal of Chemical & Engineering Data, 39, pp. 309–315. Available at: https://doi.org/10.1021/je00014a026.

Folas, G.K., Berg, O.J., Solbraa, E., Fredheim, A.O., Kontogeorgis, G.M., Michelsen, M.L. and Stenby, E.H. (2007) 'High-pressure vapor–liquid equilibria of systems containing ethylene glycol, water and methane', Fluid Phase Equilibria, 251, pp. 52–58. Available at: https://doi.org/10.1016/j.fluid.2006.11.001.

Folas, G.K., Kontogeorgis, G.M., Michelsen, M.L. and Stenby, E.H. (2006a) 'Application of the Cubic-Plus-Association (CPA) Equation of State to Complex Mixtures with Aromatic Hydrocarbons', Industrial & Engineering Chemistry Research, 45, pp. 1527–1538. Available at: https://doi.org/10.1021/ie050976q.

Folas, G.K., Kontogeorgis, G.M., Michelsen, M.L. and Stenby, E.H. (2006b) 'Application of the Cubic-Plus-Association Equation of State to Mixtures with Polar Chemicals and High Pressures', Industrial & Engineering Chemistry Research, 45, pp. 1516–1526. Available at: https://doi.org/10.1021/ie0509241.

Fonseca, J. (2010) Design, Development and Testing of New Experimental Equipment for the Measurement of Multiphase Equilibrium. Centre for Energy Resources Engineering (CERE).

Fouad, W.A. and Berrouk, A.S. (2013) 'Phase behavior of sour natural gas systems using classical and statistical thermodynamic equations of states', Fluid Phase Equilibria, 356, pp. 136–145. Available at: https://doi.org/10.1016/j.fluid.2013.07.029.

Fourie, F.C. v. N., Schwarz, C.E. and Knoetze, J.H. (2008) 'Phase equilibria of alcohols in supercritical fluids', The Journal of Supercritical Fluids, 47, pp. 161–167. Available at: https://doi.org/10.1016/j.supflu.2008.07.001.

Frost, M., Karakatsani, E., von Solms, N., Richon, D. and Kontogeorgis, G.M. (2014) 'Vapor–Liquid Equilibrium of Methane with Water and Methanol. Measurements and Modeling', Journal of Chemical & Engineering Data, 59, pp. 961–967. Available at: https://doi.org/10.1021/je400684k.

Frost, M., von Solms, N., Richon, D. and Kontogeorgis, G.M. (2015) 'Measurement of vapor–liquid–liquid phase equilibrium—Equipment and results', Fluid Phase Equilibria, 405, pp. 88–95. Available at: https://doi.org/10.1016/j.fluid.2015.07.009.

Galivel-Solastiouk, F., Laugier, S. and Richon, D. (1986) 'Vapor-liquid equilibrium data for the propane-methanol and propane-methanol-carbon dioxide system', Fluid Phase Equilibria, 28, pp. 73–85. Available at: https://doi.org/10.1016/0378-3812(86)85069-5.

Gardeler, H., Fischer, K. and Gmehling, J. (2002) 'Experimental Determination of Vapor−Liquid Equilibrium Data for Asymmetric Systems', Industrial & Engineering Chemistry Research, 41, pp. 1051–1056. Available at: https://doi.org/10.1021/ie0103456.

Gipson, S. (2015) Gas Hydrates. Available at: https://naturalgasindustryhub.com/natural-gas-hydrates/ (Accessed: 4 July 2022).

Goodwin, R.D. (1987) 'Methanol Thermodynamic Properties From 176 to 673 K at Pressures to 700 Bar', Journal of Physical and Chemical Reference Data, 16, pp. 799–892. Available at: https://doi.org/10.1063/1.555786.

Grenner, A., Kontogeorgis, G.M., von Solms, N. and Michelsen, M.L. (2007) 'Application of PC-SAFT to glycol containing systems – PC-SAFT towards a predictive approach', Fluid Phase Equilibria, 261, pp. 248–257. Available at: https://doi.org/10.1016/j.fluid.2007.04.025.

Grigiante, M., Stringari, P., Scalabrin, G., Ihmels, E.C., Fischer, K. and Gmehling, J. (2008) '(Vapour + liquid + liquid) equilibria and excess molar enthalpies of binary and ternary mixtures of isopropanol, water, and propylene', The Journal of Chemical Thermodynamics, 40, pp. 537–548. Available at: https://doi.org/10.1016/j.jct.2007.12.002.

Haselden, G.C. (1979) 'Methane: international thermodynamic tables of the fluid state', Cryogenics, 19, p. 365. Available at: https://doi.org/10.1016/0011-2275(79)90163-2.

Haynes, W.M. (2014) CRC Handbook of Chemistry and Physics. Edited by W.M. Haynes. CRC Press. Available at: https://doi.org/10.1201/b17118.

Hong, J.H., Malone, P. V., Jett, M.D. and Kobayashi, R. (1987) 'The measurement and interpretation of the fluid-phase equilibria of a normal fluid in a hydrogen bonding solvent: the methane+ methanol system', Fluid Phase Equilibria, 38, pp. 83–96. Available at: https://doi.org/10.1016/0378-3812(87)90005-7.

Hunter, C.A. (2004) 'Quantifying Intermolecular Interactions: Guidelines for the Molecular Recognition Toolbox', Angewandte Chemie International Edition, 43, pp. 5310–5324. Available at: https://doi.org/10.1002/anie.200301739.

Ishihara, K., Tanaka, H. and Kato, M. (1998) 'Phase equilibrium properties of ethane+methanol system at 298.15 K', Fluid Phase Equilibria, 144, pp. 131–136. Available at: https://doi.org/10.1016/S0378-3812(97)00251-3.

JCGM/WG, (2008) Evaluation of Measurement Data-Guide to the Expression of Uncertainty in Measurement. Stand Geneva.

Jerinić, D., Schmidt, J., Fischer, K. and Friedel, L. (2008) 'Measurement of the triethylene glycol

solubility in supercritical methane at pressures up to 9MPa', Fluid Phase Equilibria, 264, pp. 253–258. Available at: https://doi.org/10.1016/j.fluid.2007.11.017.

Jou, F.-Y., Deshmukh, R.D., Otto, F.D. and Mather, A.E. (1987) 'Vapor liquid equilibria for acid gases and lower alkanes in triethylene glycol', Fluid Phase Equilibria, 36, pp. 121–140. Available at: https://doi.org/10.1016/0378-3812(87)85018-5.

Joung, S.N., Shin, H.Y., Kim, H.S. and Yoo, K.-P. (2004) 'High-Pressure Vapor−Liquid Equilibrium Data and Modeling of Propane + Methanol and Propane + Ethanol Systems', Journal of Chemical & Engineering Data, 49, pp. 426–429. Available at: https://doi.org/10.1021/je0340506.

Kapateh, M.H., Chapoy, A., Burgass, R. and Tohidi, B. (2016) 'Experimental Measurement and Modeling of the Solubility of Methane in Methanol and Ethanol', Journal of Chemical & Engineering Data, 61, pp. 666–673. Available at: https://doi.org/10.1021/acs.jced.5b00793.

Kidnay, A.J., Parrish, W.R. and McCartney, D.G. (2019) Fundamentals of Natural Gas Processing. 3rd edn, Fundamentals of Natural Gas Processing. 3rd edn. Edited by C. Press. Boca Raton. Available at: https://doi.org/10.1201/9780429464942.

Kim, J.H. and Kim, M.S. (2005) 'Vapor–liquid equilibria for the carbon dioxide + propane system over a temperature range from 253.15 to 323.15 K', Fluid Phase Equilibria, 238, pp. 13–19. Available at: https://doi.org/10.1016/j.fluid.2005.09.006.

Kleiner, M. and Sadowski, G. (2007) 'Modeling of Polar Systems Using PCP-SAFT: An Approach to Account for Induced-Association Interactions', The Journal of Physical Chemistry C, 111, pp. 15544–15553. Available at: https://doi.org/10.1021/jp072640v.

Knock, J. (2010) Modification, Reconstruction And Commissioning Of A Vapour Recirculation Apparatus For High-Pressure Lowtemperature Vapour-Liquid Equilibrium Measurements. University of KwaZulu -Natal, Master Thesis.

Kondori, J., Zendehboudi, S. and James, L. (2018) 'Evaluation of Gas Hydrate Formation Temperature for Gas/Water/Salt/Alcohol Systems: Utilization of Extended UNIQUAC Model and PC-SAFT Equation of State', Industrial & Engineering Chemistry Research, 57, pp. 13833–13855. Available at: https://doi.org/10.1021/acs.iecr.8b03011.

Kondori, J., Zendehboudi, S. and James, L. (2019) 'New insights into methane hydrate dissociation: Utilization of molecular dynamics strategy', Fuel, 249, pp. 264–276. Available at: https://doi.org/10.1016/j.fuel.2019.02.125.

Kontogeorgis, G.M. and Folas, G.K. (2010) Thermodynamic Models for Industrial Applications. Wiley. Available at: https://doi.org/10.1002/9780470747537.

Kontogeorgis, G.M., Michelsen, M.L., Folas, G.K., Derawi, S., von Solms, N. and Stenby, E.H. (2006) 'Ten Years with the CPA (Cubic-Plus-Association) Equation of State. Part 1. Pure Compounds and Self-Associating Systems', Industrial & Engineering Chemistry Research, 45, pp. 4855–4868. Available at: https://doi.org/10.1021/ie051305v.

Kontogeorgis, G.M., Voutsas, E.C., Yakoumis, I. V. and Tassios, D.P. (1996) 'An Equation of State for Associating Fluids', Industrial & Engineering Chemistry Research, 35, pp. 4310–4318. Available at: https://doi.org/10.1021/ie9600203.

Kruger, F.J., Danielsen, M. V., Kontogeorgis, G.M., Solbraa, E. and von Solms, N. (2018) 'Ternary Vapor–Liquid Equilibrium Measurements and Modeling of Ethylene Glycol (1) + Water (2) + Methane (3) Systems at 6 and 12.5 MPa', Journal of Chemical & Engineering Data, 63, pp. 1789–1796. Available at: https://doi.org/10.1021/acs.jced.8b00115.

Kruger, F.J., Kontogeorgis, G.M., Solbraa, E. and von Solms, N. (2018) 'Multicomponent Vapor–Liquid Equilibrium Measurement and Modeling of Ethylene Glycol, Water, and Natural Gas Mixtures at 6 and 12.5 MPa', Journal of Chemical & Engineering Data, 63, pp. 3628–3639. Available at: https://doi.org/10.1021/acs.jced.8b00495.

Kühne, E., Calvo, E.S., Witkamp, G.J. and Peters, C.J. (2008) 'Fluid phase behaviour of the ternary system bmim[BF4]+1-(4-isobutylphenyl)-ethanol+carbon dioxide', The Journal of Supercritical Fluids, 45, pp. 293–297. Available at: https://doi.org/10.1016/j.supflu.2008.01.007.

Laugier, S. and Richon, D. (1986) 'New apparatus to perform fast determinations of mixture vapor–liquid equilibria up to 10 MPa and 423 K', Review of Scientific Instruments, 57, pp. 469–472. Available at: https://doi.org/10.1063/1.1138909.

Lev, A.-D., Robinson, D.B., Chung, S.Y.-K. and Chen, C.-J. (1992) 'The equilibrium phase properties of the propane-methanol and n -Butane-methanol binary systems', The Canadian Journal of Chemical Engineering, 70, pp. 330–334. Available at: https://doi.org/10.1002/cjce.5450700217.

Lhoták, V. and Wichterle, I. (1981) 'Vapour-liquid equilibria in the ethane-n-butane system at high pressures', Fluid Phase Equilibria, 6, pp. 229–235. Available at: https://doi.org/10.1016/0378-3812(81)85006-6.

LibreTexts (2022) London Dispersion Interactions, LibreTexts Chemistry. Available at: https://chem.libretexts.org/Bookshelves/Physical_and_Theoretical_Chemistry_Textbook_Maps/Supplemental_Modules_%28Physical_and_Theoretical_Chemistry%29/Physical_Properties_of_Matter/Atomic_and_Molecular_Properties/Intermolecular_Forces/Specific_Interaction.

Liu, X. (2022) 2.6 Intermolecular Force and Physical Properties of Organic Compounds. Available at: https://kpu.pressbooks.pub/organicchemistry/chapter/2-6-intermolecular-force-and-physical-

properties-of-organic-compounds/ (Accessed: 29 November 2022).

Liwanth, H. (2014) Vapour-Liquid Equilibrium Measurements at Moderate Pressures using a Semi-Automatic Glass Recirculating Still. University of Kwa-Zulu Natal. Available at: https://ukzn-dspace.ukzn.ac.za/bitstream/handle/10413/11208/Lilwanth_Hitesh_2014.pdf?sequence=1&isAllowed=y.

Lopez-Echeverry, J.S., Reif-Acherman, S. and Araujo-Lopez, E. (2017) 'Peng-Robinson equation of state: 40 years through cubics', Fluid Phase Equilibria, 447, pp. 39–71. Available at: https://doi.org/10.1016/j.fluid.2017.05.007.

Ma, Y.. and Kohn, J.P.. (1964) 'Multiphase and Volumentric Equilibrtia of the Ethane-Methanol System at Temperatures Between -40 and 100 C', Chem Eng Data, 9, pp. 3–5.

Mathias, P.M. and Copeman, T.W. (1983) 'Extension of the Peng-Robinson equation of state to complex mixtures: Evaluation of the various forms of the local composition concept', Fluid Phase Equilibria, 13, pp. 91–108. Available at: https://doi.org/10.1016/0378-3812(83)80084-3.

McJeon, H., Edmonds, J., Bauer, N., Clarke, L., Fisher, B., Flannery, B.P., Hilaire, J., Krey, V., Marangoni, G., Mi, R., Riahi, K., Rogner, H. and Tavoni, M. (2014) 'Limited impact on decadal-scale climate change from increased use of natural gas', Nature, 514, pp. 482–485. Available at: https://doi.org/10.1038/nature13837.

Miroshnichenko, D., Teplyakov, V. and Shalygin, M. (2022) 'Recovery of Methanol during Natural Gas Dehydration Using Polymeric Membranes: Modeling of the Process', Membranes, 12, p. 1176. Available at: https://doi.org/10.3390/membranes12121176.

Mokbel, I., Kasehgari, H., Rauzy, E. and Jose, J. (1995) 'Static measurements of the total vapor pressure of water + methanol mixtures at temperatures between 243 and 313 K', The International Electronic Journal of Physico-Chemical Data, 1.

Mokhatab, S., Poe, William, A. and Mak, J.Y. (2015) Handbook of Natural Gas Transmission and Processing. 3rd edn. Elsevier. Available at: https://doi.org/10.1016/C2013-0-15625-5.

Moore, C.W., Zielinska, B., Pétron, G. and Jackson, R.B. (2014) 'Air Impacts of Increased Natural Gas Acquisition, Processing, and Use: A Critical Review', Environmental Science & Technology, 48, pp. 8349–8359. Available at: https://doi.org/10.1021/es4053472.

Moosavi, M. and Rostami, A.A. (2017) 'Densities, Viscosities, Refractive Indices, and Excess Properties of Aqueous 1,2-Etanediol, 1,3-Propanediol, 1,4-Butanediol, and 1,5-Pentanediol Binary Mixtures', Journal of Chemical & Engineering Data, 62, pp. 156–168. Available at: https://doi.org/10.1021/acs.jced.6b00526.

Mostafazadeh, A.K., Rahimpour, M.R. and Shariati, A. (2009) 'Vapor−Liquid Equilibria of Water + Triethylene Glycol (TEG) and Water + TEG + Toluene at 85 kPa', Journal of Chemical & Engineering Data, 54, pp. 876–881. Available at: https://doi.org/10.1021/je800675u.

Mühlbauer, A.L. and Raal, J.D. (1993) 'High-pressure vapor-liquid equilibria in the propane-1-propanol system', AIChE Journal, 39, pp. 677–688. Available at: https://doi.org/10.1002/aic.690390416.

Mukelabai, M.D., Wijayantha, U.K.G. and Blanchard, R.E. (2022) 'Renewable hydrogen economy outlook in Africa', Renewable and Sustainable Energy Reviews, 167, p. 112705. Available at: https://doi.org/10.1016/j.rser.2022.112705.

Naicker, S. (2017) Development of a new static synthetic apparatus for phase equilibrium measurements. Durban University of Technology. Master Thesis, Available at: https://doi.org/10.51415/10321/2494.

Narasigadu, C. (2006) Phase equilibrium investigation of the water and acetonitrile solvent with heavy hydrocarbons. University of Kwa-Zulu Natal. Master Thesis Available at: https://researchspace.ukzn.ac.za/xmlui/handle/10413/1539.

Nasrifar, K., Alavi, F. and Javanmardi, J. (2017) 'Prediction of water content of natural gases using the PC-SAFT equation of state', Fluid Phase Equilibria, 453, pp. 40–45. Available at: https://doi.org/10.1016/j.fluid.2017.08.023.

Neagu, M. and Cursaru, D.L. (2017) 'Technical and economic evaluations of the triethylene glycol regeneration processes in natural gas dehydration plants', Journal of Natural Gas Science and Engineering, 37, pp. 327–340. Available at: https://doi.org/10.1016/j.jngse.2016.11.052.

Nelson, W.M., Naidoo, P. and Ramjugernath, D. (2021) 'A new high pressure phase equilibrium cell featuring the static-combined method: Equipment commissioning and data measurement', The Journal of Supercritical Fluids, 176, p. 105291. Available at: https://doi.org/10.1016/j.supflu.2021.105291.

Nelson, W.M. and Ramjugernath, D. (2017) 'Experimental Solubility Data for Binary Mixtures of Ethane and 2,2,4-Trimethylpentane at Pressures up to 6 MPa Using a New Variable-Volume Sapphire Cell', Journal of Chemical & Engineering Data, 62, pp. 3915–3920. Available at: https://doi.org/10.1021/acs.jced.7b00613.

Ng, H. joo and Robinson, D.B. (1983) Equilibrium Phase Composition and Hydrating Conditions in Systems Containing Methanol, Light Hydrocarbons, Carbon Dioxide, and Hydrogen Sulfide.

O'Brien, D., Mejorada, J. and PE, L.A. (2016) 'No Title', in Adjusting Gas Treatment Strategies to Resolve Methanol Issues. Norman.

Ohgaki, K., Sano, F. and Katayama, T. (1976) 'Isothermal vapor-liquid equilibrium data for binary systems containing ethane at high pressures', Journal of Chemical & Engineering Data, 21, pp. 55–58. Available at: https://doi.org/10.1021/je60068a016.

de Oliveira Cavalcanti Filho, V., Chapoy, A. and Burgass, R. (2021) 'Phase Behavior in Natural Gas + Glycol Systems, Part 1: Tri(ethylene glycol) (TEG) and Its Aqueous Solutions', Journal of Chemical & Engineering Data, 66, pp. 4075–4093. Available at: https://doi.org/10.1021/acs.jced.1c00313.

Olsen, R., Kvamme, B. and Kuznetsova, T. (2016) 'Free energy of solvation and Henry's law solubility constants for mono-, di- and tri-ethylene glycol in water and methane', Fluid Phase Equilibria, 418, pp. 152–159. Available at: https://doi.org/10.1016/j.fluid.2015.10.019.

Paiva, A., Gerasimov, K. and Brunner, G. (2008) 'Phase equilibria of the ternary system vinyl acetate/(R,S)-1-phenylethanol/carbon dioxide at high pressure conditions', Fluid Phase Equilibria, 267, pp. 104–112. Available at: https://doi.org/10.1016/j.fluid.2008.02.010.

Pálinkás, G., Hawlicka, E. and Heinzinger, K. (1991) 'Molecular dynamics simulations of water-methanol mixtures', Chemical Physics, 158, pp. 65–76. Available at: https://doi.org/10.1016/0301-0104(91)87055-Z.

Peng, D.-Y. and Robinson, D.B. (1976) 'A New Two-Constant Equation of State', Industrial & Engineering Chemistry Fundamentals, 15, pp. 59–64. Available at: https://doi.org/10.1021/i160057a011.

Peters, L., Hussain, A., Follmann, M., Melin, T. and Hägg, M.-B. (2011) 'CO2 removal from natural gas by employing amine absorption and membrane technology—A technical and economical analysis', Chemical Engineering Journal, 172, pp. 952–960. Available at: https://doi.org/10.1016/j.cej.2011.07.007.

Pfohl, O., Petersen, J., Dohrn, R. and Brunner, G. (1997) 'Partitioning of carbohydrates in the vapor-liquid-liquid region of the 2-propanol + water + carbon dioxide system', The Journal of Supercritical Fluids, 10, pp. 95–103. Available at: https://doi.org/10.1016/S0896-8446(97)00010-7.

Qvistgaard, D., Trancoso, J., Solbraa, E., Danielsen, M.V., Panteli, E., Kontogeorgis, G.M. and von Solms, N. (2023) 'Multicomponent vapor-liquid equilibrium measurements and modeling of triethylene glycol, water, and natural gas mixtures at 6.0, 9.0 and 12.5 MPa', Fluid Phase Equilibria, 565, p. 113660. Available at: https://doi.org/10.1016/j.fluid.2022.113660.

Raal, J.D. and Mühlbauer, A.L. (1997) Phase Equilibria: Measurements and computations. 1st edn. Taylor & Francis.

Raal, J.D., Motchelaho, A.M., Perumal, Y., Courtial, X. and Ramjugernath, D. (2011) 'P–x data for

binary systems using a novel static total pressure apparatus', Fluid Phase Equilibria, 310, pp. 156–165. Available at: https://doi.org/10.1016/j.fluid.2011.08.009.

Raeissi, S. and Peters, C.J. (2005) 'Experimental determination of high-pressure phase equilibria of the ternary system carbon dioxide+limonene+linalool', The Journal of Supercritical Fluids, 35, pp. 10–17. Available at: https://doi.org/10.1016/j.supflu.2004.12.004.

Rastorguew, Y, L. and Gazdiev, M.A. (1969) 'Study of the thermal conductivity of manyatomic alcohols.', (17), pp. 72–79.

Reddy, P. (2006) Development of Novel Apparatus for Vapour-liquid Equilibrium Measurements at Moderate Pressures. Univeristy of KwaZulu-Natal.

Reid, R.C., Praysbutz, J.M. and Sherwood, T.K. (1989) The Properties of Gas and Liquids. 4th edn.

Rufford, T.E., Smart, S., Watson, G.C.Y., Graham, B.F., Boxall, J., Diniz da Costa, J.C. and May, E.F. (2012) 'The removal of CO2 and N2 from natural gas: A review of conventional and emerging process technologies', Journal of Petroleum Science and Engineering, 94–95, pp. 123–154. Available at: https://doi.org/10.1016/j.petrol.2012.06.016.

Safarov, J., Kul, I., Talibov, M., Shahverdiyev, A. and Hassel, E. (2015) 'Vapor Pressures and Activity Coefficients of Methanol in Binary Mixtures with 1-Hexyl-3-methylimidazolium Bis(trifluoromethylsulfonyl)imide', Journal of Chemical & Engineering Data, 60, pp. 1648–1663. Available at: https://doi.org/10.1021/je501033z.

Saffari, H. and Zahedi, A. (2013) 'A New Alpha-function for the Peng-Robinson Equation of State: Application to Natural Gas', Chinese Journal of Chemical Engineering, 21, pp. 1155–1161. Available at: https://doi.org/10.1016/S1004-9541(13)60581-9.

Samie, N.N. (2016) Practical Engineering Management of Offshore Oil and Gas Platforms. 1st edn. Elsevier. Available at: https://doi.org/10.1016/C2014-0-04721-1.

Schlichting, H., Langhorst, R. and Knapp, H. (1993) 'Saturation of high pressure gases with low volatile solvents: experiments and correlation', Fluid Phase Equilibria, 84, pp. 143–163. Available at: https://doi.org/10.1016/0378-3812(93)85121-2.

Seneviratne, K.N., Hughes, T.J., Johns, M.L., Marsh, K.N. and May, E.F. (2017) 'Surface tension and critical point measurements of methane + propane mixtures', The Journal of Chemical Thermodynamics, 111, pp. 173–184. Available at: https://doi.org/10.1016/j.jct.2017.03.002.

Sentenac, P., Bur, Y., Rauzy, E. and Berro, C. (1998) 'Density of Methanol + Water between 250 K and 440 K and up to 40 MPa and Vapor−Liquid Equilibria from 363 K to 440 K', Journal of Chemical & Engineering Data, 43, pp. 592–600. Available at: https://doi.org/10.1021/je970297p.

Silva-Oliver, G., Eliosa-Jiménez, G., García-Sánchez, F. and Avendaño-Gómez, J.R. (2006) 'High-pressure vapor–liquid equilibria in the nitrogen–n-pentane system', Fluid Phase Equilibria, 250 pp. 37–48. Available at: https://doi.org/10.1016/j.fluid.2006.09.018.

Smith, J.M., Van Ness, H C., Abbott, M.M., Swihart, M.T, (2019) Introduction to Chemical Engineering Thermodynamics. 8th edn. McGraw Hill.

Software, C.S. (2023) Chemical Safety Software. Available at: https://chemicalsafety.com/sds-search/ (Accessed: 6 March 2023).

von Solms, N., Kouskoumvekaki, I.A., Michelsen, M.L. and Kontogeorgis, G.M. (2006) 'Capabilities, limitations and challenges of a simplified PC-SAFT equation of state', Fluid Phase Equilibria, 241, pp. 344–353. Available at: https://doi.org/10.1016/j.fluid.2006.01.001.

Soo, C.-B. (2011) 'Experimental thermodynamic measurements of biofuel-related associating compounds and modeling using the PC-SAFT equation of state'. Available at: https://pastel.archives-ouvertes.fr/pastel-00666125/document.

Sun, T. and Teja, A.S. (2003) 'Density, Viscosity, and Thermal Conductivity of Aqueous Ethylene, Diethylene, and Triethylene Glycol Mixtures between 290 K and 450 K', Journal of Chemical & Engineering Data, 48, pp. 198–202. Available at: https://doi.org/10.1021/je025610o.

Tafazzol, A.H. and Nasrifar, K. (2011) 'Thermophysical Properties Of Associating Fluids In Natural Gas Industry Using Pc-Saft Equation Of State', Chemical Engineering Communications, 198, pp. 1244–1262. Available at: https://doi.org/10.1080/00986445.2010.525207.

Tanaka, H. and Gubbins, K.E. (1992) 'Structure and thermodynamic properties of water–methanol mixtures: Role of the water–water interaction', The Journal of Chemical Physics, 97(4), pp. 2626–2634. Available at: https://doi.org/10.1063/1.463051.

Teixeira, A.M., Arinelli, L. de O., de Medeiros, J.L. and Araújo, O. de Q.F. (2018) 'Recovery of thermodynamic hydrate inhibitors methanol, ethanol and MEG with supersonic separators in offshore natural gas processing', Journal of Natural Gas Science and Engineering, 52, pp. 166–186. Available at: https://doi.org/10.1016/j.jngse.2018.01.038.

Tshibangu, Mulamba, M. (2010) High Pressure Vapour-Liquid Equilibrium Data Of Fluorochemical Systems For Various Temperatures Using A New Static Apparatus. Master Thesis University of Kwa-Zulu Natal.

Tsivintzelis, I. and Kontogeorgis, G.M. (2012) 'Capabilities and Limitations of an Association Theory for Chemicals in Liquid or Supercritical Solvents', Industrial & Engineering Chemistry Research, 51, pp. 13496–13517. Available at: https://doi.org/10.1021/ie301388d.

Ukai, T., Kodama, D., Miyazaki, J. and Kato, M. (2002) 'Solubility of Methane in Alcohols and Saturated Density at 280.15 K', Journal of Chemical & Engineering Data, 47, pp. 1320–1323. Available at: https://doi.org/10.1021/je020108p.

Vetere, A. (1986) 'Vapor-liquid equilibria with supercritical gases calculated by the excess Gibbs energy method', Fluid Phase Equilibria, 28, pp. 265–281. Available at: https://doi.org/10.1016/0378-3812(86)80032-2.

Walas, S.M. (1991) Modeling with differential equations in chemical engineering. 1st edn. Boston: Butterworth-Heinemann.

Wang, L.-K., Chen, G.-J., Han, G.-H., Guo, X.-Q. and Guo, T.-M. (2003) 'Experimental study on the solubility of natural gas components in water with or without hydrate inhibitor', Fluid Phase Equilibria, 207, pp. 143–154. Available at: https://doi.org/10.1016/S0378-3812(03)00009-8.

Wise, M. and Chapoy, A. (2016) 'Carbon dioxide solubility in Triethylene Glycol and aqueous solutions', Fluid Phase Equilibria, 419, pp. 39–49. Available at: https://doi.org/10.1016/j.fluid.2016.03.007.

Wise, M., Chapoy, A. and Burgass, R. (2016) 'Solubility Measurement and Modeling of Methane in Methanol and Ethanol Aqueous Solutions', Journal of Chemical & Engineering Data, 61, pp. 3200–3207. Available at: https://doi.org/10.1021/acs.jced.6b00296.

Wu, J. and Prausnitz, J.M. (1998) 'Phase Equilibria for Systems Containing Hydrocarbons, Water, and Salt: An Extended Peng−Robinson Equation of State', Industrial & Engineering Chemistry Research, 37, pp. 1634–1643. Available at: https://doi.org/10.1021/ie9706370.

Wu, Y., Tang, D., Verploegh, R.J., Xi, H. and Sholl, D.S. (2017) 'Impacts of Gas Impurities from Pipeline Natural Gas on Methane Storage in Metal–Organic Frameworks during Long-Term Cycling', The Journal of Physical Chemistry C, 121, pp. 15735–15745. Available at: https://doi.org/10.1021/acs.jpcc.7b03459.

Yang, C., Feng, X., Sun, Y., Yang, Q. and Zhi, J. (2015) 'Isobaric Vapor–Liquid Equilibrium for Two Binary Systems{Propane-1,2-diol + Ethane-1,2-diol and Propane-1,2-diol + Butane-1,2-diol} at p = (10.0, 20.0, and 40.0) kPa', Journal of Chemical & Engineering Data, 60, pp. 1126–1133. Available at: https://doi.org/10.1021/je5010824.

Yarym-Agaev, N., Sinyavskaya, R.P., Koliushko, I.I. and Levinton, L.Y. (1985) 'Phase equilibria in th water-methane and methanol-methane binary systems under high pressures', 58, p. 158.

Yoon, J.H., Lee, H.S. and Lee, H. (1993) 'High-pressure vapor-liquid equilibria for carbon dioxide + methanol, carbon dioxide + ethanol, and carbon dioxide + methanol + ethanol', Journal of Chemical &

Engineering Data, 38, pp. 53–55. Available at: https://doi.org/10.1021/je00009a012.

Zeck, S. and Knapp, H. (1986) 'Vapor—liquid and vapor—liquid—liquid phase equilibria for binary and ternary systems for nitrogen, ethane and methanol: Experiment and data reduction', Fluid Phase Equilibria, 25, pp. 303–322. Available at: https://doi.org/10.1016/0378-3812(86)80006-1.

Zhang, X., Gao, N., Wu, Y. and Chen, G. (2018) 'Vapor Pressure Measurement for the Ternary System of Water, Lithium Bromide, and 1-Ethyl-3-methylimidazolium Acetate', Journal of Chemical & Engineering Data, 63, pp. 781–786. Available at: https://doi.org/10.1021/acs.jced.7b00951.

Zvawanda, P., Naidoo, P., Nelson, W.M. and Moodley, K. (2022 a) 'P-T-x Measurement and Modeling of Methane + Propane + Methanol or 2,2′-[Ethane-1,2-diylbis(oxy)] Di(ethan-1-ol) and Methane + Propane + Methanol + 2,2′-[Ethane-1,2-diylbis(oxy)] Di(ethan-1-ol) Systems', Journal of Chemical & Engineering Data [Preprint]. Available at: https://doi.org/10.1021/acs.jced.2c00776.

Zvawanda, P., Naidoo, P., Nelson, W.M. and Moodley, K. (2022 b) 'P–T–x Measurement and Modeling of Methane or Carbon Dioxide + Methanol +2,2′-[Ethane-1,2-diylbis(oxy)] di(ethan-1-ol) Systems from T = 298 to 323 K', Journal of Chemical & Engineering Data, 67, pp. 1174–1187. Available at: https://doi.org/10.1021/acs.jced.2c00061.

Zvawanda, P. (2022 c) Phase Equilibria Studies On Chemical Mixtures Encountered In The Natural Gas Industry. PhD Thesis, University of Kwa-Zulu Natal.

Appendix A : Additional Literature

This appendix includes additional literature that was researched and documented but not included in the literature review to ensure a concise and focused literature review in the main body.

A.1. Natural Gas Treatments

This section of the review details with the natural gas treatment process, adding greater context and relevance to the topic studied and the experimental results obtained. The complexity of the process for extraction of the gas to the final treated product supports the need for further research, as conducted in this study.

Natural gas treatment is essential in ensuring a final product that is safe and has a high caloric value. The compositions of natural gas can vary depending on the source location and the depth of extraction, but usually the constituents of the gas are similar (hydrocarbons, water, non-hydrocarbon impurities) but with varying relative quantities (Faramawy et al., 2016). Thus, the purification steps are generally uniform, entailing removing the non-hydrocarbons from the valuable hydrocarbons. Figure A.1 depicts a block flow diagram of the overall treatment of natural gas from extraction to pipeline quality.

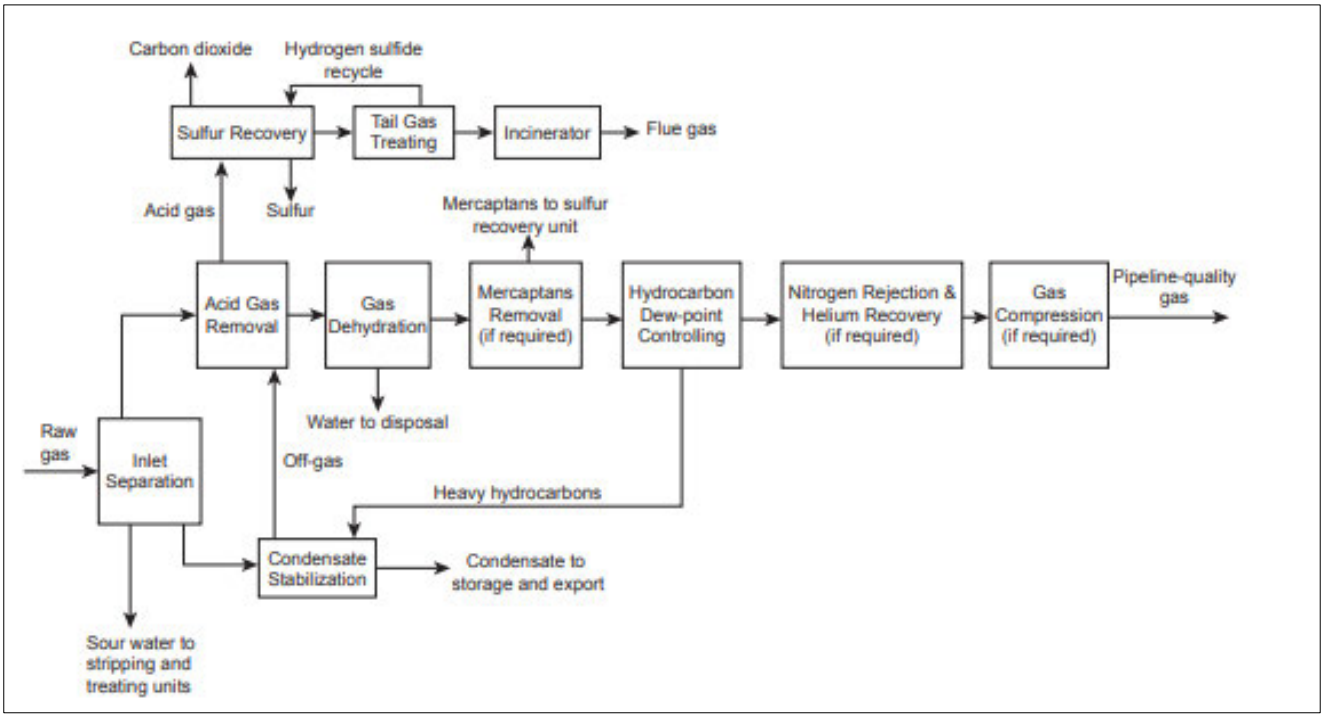

Figure A.1 Overall process for natural gas treatment extracted from (Mokhatabv 2015).

A.1.1. Liquid removal

When natural gas is extracted, it is not completely in the gaseous state. Another valuable component that can be removed is liquid petroleum gas (LPG). These are heavier hydrocarbons (C3 alkenes, C4 alkanes, etc.) that remain in the liquid phase under extraction conditions. In addition to this liquid, water and crude oil comprise the fluid that accompanies natural gas during extraction (Faramawy et al., 2016). Crude oil can be refined and sold while the liquid water must be removed to prevent clathrate hydrates from forming and corrosion. Even though the liquid water is removed, the natural gas is likely saturated with water vapour. A scrubber is usually used to separate these phases. The type, shape and size of the scrubbing can vary depending on the amount of liquid present. This can vary from large qualities to fine mists, and the equipment must be tailored to deal with these conditions. The amount of liquid, however, rarely exceeds 4 vol% (Austrheim, 2006). The basic principles of the scrubbing step remain the same; the scrubber removes the liquids from the gas through gravity, mechanical mesh pads and particle filters. This process should result in an entirely gaseous mixture leaving the top of the scrubber and all liquids leaving the bottom.

A.1.2. Hydrogen sulphide (H_2S) and Carbon Dioxide (CO_2) removal

In addition to the natural gas hydrocarbons, other non-hydrocarbon gases are also contained within the natural gas. The most dangerous of these for human health and equipment safety is hydrogen sulphide (H_2S). This acid gas is highly toxic and, when exposed to water, forming a weak acid with corrosive properties. The concentrations of hydrogen sulphide in the natural gas can vary depending on the natural gas source. Thus, no single method is universally implemented. These methods can vary from chemical and physical absorption to membranes and cryogenic fractionation (Kidnay et al., 2019). An additional consideration when choosing an appropriate method is whether CO_2 is being removed with the hydrogen sulphide. Some gas treatment plans treat CO_2 as a waste gas, while others may use it in other chemical processes, thus attempting to extract it at a later stage. It is advantageous to remove CO_2 if it is in high concentration, as the CO_2 additionally forms a weak corrosive acid when exposed. Despite all the considerations, absorption is the most conventional method used for this removal (Austrheim, 2006). Once treated, the amount of acid gas should not exceed 4ppm by volume (Mokhatab et al., 2015).

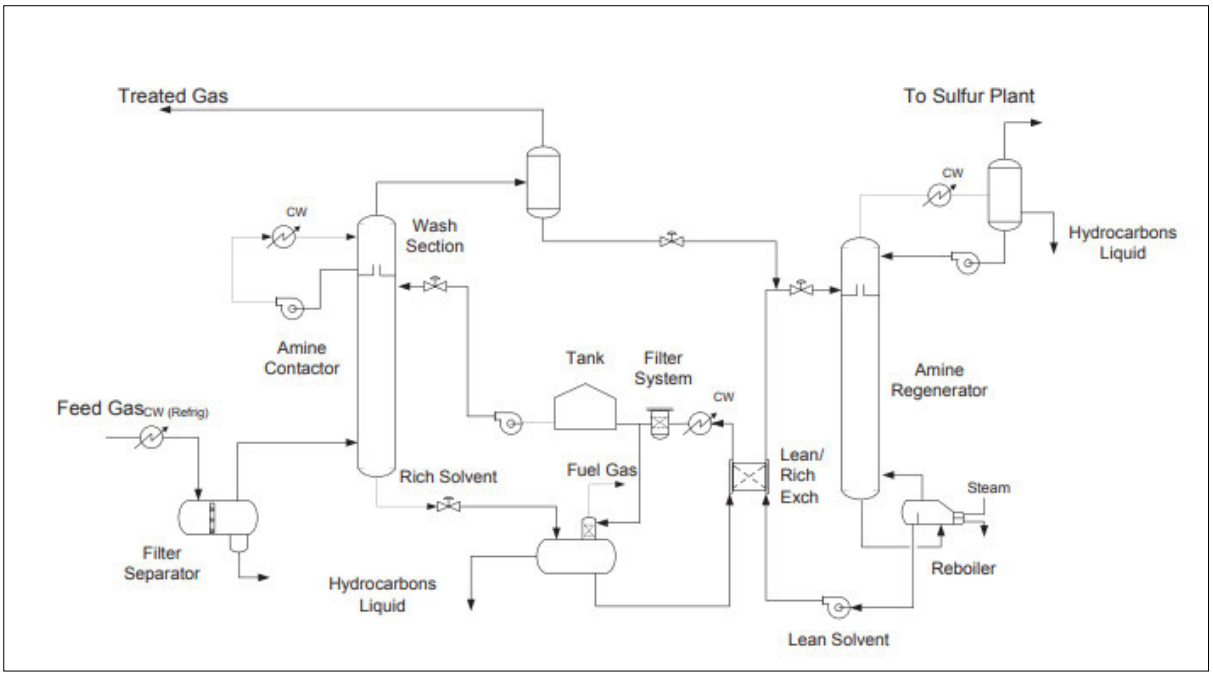

Figure A.2 Amine process plant for the extraction of H_2S from untreated natural gas extracted from (Mokhatab et al., 2015).

Figure A.2 depicts a typical amine process plant where an aqueous amine solution is a solvent used for the absorption of hydrogen sulphide and carbon dioxide from natural gas feeds. The amine absorbs the H_2S and CO_2 from the filtrated natural gas, allowing a treated natural gas to leave the top of the absorber and a rich amine solution recovered at the bottom. These process conditions are selected such that H_2S removal is prioritised, thus, as much as 2 mol % of CO_2 can be found in the treated gas stream (Mokhatab et al., 2015). The rich amine is passed through a regulator, which removes the absorbed H_2S allowing for the recycling of a lean amine solution back to the absorber. Additional modifications can be added to this process for specialised conditions. A second absorption step can be added if the concentration of H_2S is difficult to reduce. It should be noted that the amine process is the most traditional method, however, when CO_2 content is high, other methods, such as implementing physical solvents and solid bed absorption, is preferred (Peters et al., 2011).

A.1.3. Additional and optional processes

Natural gas compositions can vary from different locations, making additional treatments necessary depending on the circumstances. For instance, in the US Midwest, North Sea, Eastern Europe and South East Asia, the natural gas deposits have a higher nitrogen concentration (Mokhatab et al., 2015). The natural gas extracted from these reserves must have the excess nitrogen removed as this causes several issues such as increased compression costs and lower recovery of LPG. This is also true for compounds such as helium and mercaptans, which both require additional processes for separation from the valuable hydrocarbons(Rufford et al., 2012).

A.2. Chemical Interactions

Understanding intermolecular forces between specific molecules are imperative as these forces are the causes of non-ideal behaviour in chemical systems, and affect parameters such as pure component and mixture melting and boiling points(Hunter, 2004). These intermolecular forces are either repulsive or attractive and can vary in strength depending on the type of molecule, the electronegativity of the molecule and the distance between molecules. At low pressures and high temperatures intermolecular forces are more prominent in liquids and solids due to the relative closeness of molecules as opposed to gas which has a greater distance between them (Ahlrichs et al., 1977).

There are 3 main types of intermolecular forces, dispersion forces, dipole-dipole interactions and hydrogen bonding.

Table A.1 Strength comparison for the respective intermolecular forces (Liu, 2022).

Types of Forces	**Applied to**	**Force strength**
Dispersion Forces	All molecules	0.1-5 kJ/mol
Dipolar Forces	Polar Molecules	5-20 kJ/mol
Hydrogen bonding	Polar molecules typically with Hydrogen bonded to Nitrogen, oxygen or fluorine	5-50 kJ/mol

These intermolecular forces are not present in all molecules but depend on the molecule arrangement. As seen in Table A.1., these forces also differ in strength, where hydrogen bonding is the strongest while dispersion forces are the weakest. Despite being the weakest, dispersion forces are the most prevalent and thus make up the vast majority of attractive forces in most interactions (Soo, 2011)

A.2.1. Dispersion forces

Dispersion forces, also known as London forces, are the most prevalent despite being the weakest intermolecular forces. These forces form from the instantaneous and induced dipoles that non-polar molecules experience, as shown in Figure A.3. These usually occur as the electron density for all molecules constantly shifts, and in these brief moments, an instantaneous dipole is formed (Liu, 2022). This instantaneous dipole polarises nearby molecules, forming an induced dipole within the molecule structure. This causes a short-lived attractive force between the two molecules. The strength of this force depends on the ease of polarisation and the relative surface area of a molecule. Larger molecules are easier polarised as the electrons surrounding the nucleus are freer. Additionally, more linear molecules, as opposed to more branched molecules, have stronger dispersion forces (Liu, 2022).

Despite being the weakest of the Van der Waals forces in most cases, except in the case of highly polar molecules, dispersion forces are the most dominant (Kontogeorgis and Folas, 2010).

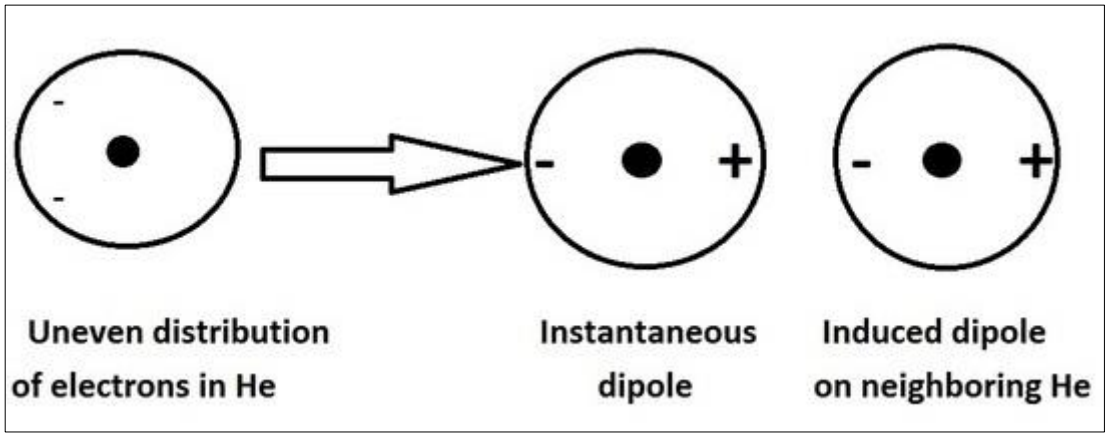

Figure A.3 Dispersion forces causing instantaneous dipole extracted from (LibreTexts, 2022).

A.2.2. Dipole-Dipole forces

Dipole-Dipole forces are another type of Van der Waals force experienced by polar molecules. Polar molecules have a permanent dipole, forming an attraction between itself and other polar molecules. These forces are more significant than a dispersion force as the electromagnetic force is more permanent. The strength of dipole-dipole forces is dependent on the dipole moment, which measures a molecule's overall polarity. The effect of dipole-dipole forces can be quite significant when molecules have a dipole moment above 1 Debye (Kontogeorgis and Folas, 2010).

It should be noted that there is a variation of Van der Wall force known as Dipole-induced Dipole forces. This is caused by a polar molecule causing a non-polar molecule to polarise, leading to an attractive force between the two molecules. However, these forces make up the most minor contribution when it comes to Van der Waals attractive forces, rarely making up more than 7 % (Kontogeorgis and Folas, 2010).

A.2.3. Hydrogen bonding

Hydrogen bonding is the strongest intermolecular force and is experienced between molecules with a hydrogen bonded to an oxygen, nitrogen or fluorine atom. The high electronegativity of these elements allows for polarisation to occur with the hydrogen side becoming positive and the O, N or F side becoming negative. This results in an attraction between the positive side of one molecule and the negative side of another.

For this study, hydrogen bonding features prominently in the mixtures studied. Due to the inclusion of water, TEG and methanol which are known as oxygenated molecules. These molecules can self-

associate, which is a type of hydrogen bonding that occurs when a molecule can behave as an electron acceptor and donor, such as diols, alcohols and acids (Soo, 2011). Additionally, molecules cross-associate, which is when they hydrogen bond with molecules that are either electron acceptors or donors, typical of ketones and aldehydes (Soo, 2011). In this study, molecule combinations such as Water-TEG, Water-Methanol and Methanol-TEG would cross-associate.

A.3. Component interactions

With multicomponent systems, the interactions between the various components can become very complex. This can be somewhat simplified by looking at individual members and their interactions.

A.3.1. Methanol Interactions

A.3.1.1. Methanol with Light Hydrocarbons (Methane, Ethane, Propane)

The mixing of light hydrocarbons and methanol is a well-known process occurrence in the natural gas industry, however, detailed information on their intermolecular interactions during the dehydration process with TEG is limited. Methane, ethane and propane are non-polar molecules due to their symmetrical shape and lack of atoms with strong electronegativities. This results in only London forces and induced dipole-dipole forces being present between the methanol and light hydrocarbon molecules.

However, a number of studies investigate other aspects of mixtures, including methanol and light hydrocarbons. The study by (Kondori et al., 2019) investigated the dissociation of methane hydrate, including interactions between the inhibitor methanol and the hydrate. The study concluded that introducing methanol into the methane hydrate system resulted in new hydrogen bonds between the water and methanol. This caused an earlier decomposition of the hydrate lattice than without methanol. This was due to the stronger forces between the methanol and water as compared to the methane and water interactions. A similar study by (Dai et al., 2020) investigated the effect structural properties of alcohols had on the decomposition of natural gas hydrates. The study found that the rate of decomposition was inversely proportional to the chain length. This was due to longer chains having a lower polarity and, thus, weaker hydrogen bonds between the methanol and water molecule. And finally, a study by (Frost et al., 2014) conducted VLE experiments with a methane, water and methanol mixture. The study used the Cubic Plus Association EoS which is typically used due to its ability to predict association in chemical equilibrium systems. The CPA model showed a good relationship between the predictive and experimental data showing the importance of accounting for associating components. These studies show the strong effect methanol has on light hydrocarbons and the importance of accounting for their interactions.

A.3.1.2. Methanol with water

The interactions between water and methanol are of great interest due to methanol's inhibiting properties for clathrate formation. Methanol and water are both associating molecules (with hydrogen bonding) and these interactions facilitate the inhibiting of clathrate hydrate. The study by (Tanaka and Gubbins, 1992) examined methanol-water mixtures with specific detail about how water-water interactions influence the mixture behaviour. This study focused on the structure and thermodynamic properties of these mixtures. The main conclusion drawn was that water-water interactions, which include hydrogen bonding, are just as important as methanol-water interactions when determining the thermodynamic behaviour of the mixtures. Another study by (Pálinkás et al., 1991) simulated the dynamics of water-methanol mixtures. The study used mole fractions of 0.1 and 0.9 methanol to water in-order to investigate the difference between a pure component and a mixture. The study found that the methanol rich-mixture caused the water molecules within it to act more like a methanol molecule than a water molecule. This was due to the water molecule building linear structures. Opposed to this, the water-rich mixture caused some defects in the hydrogen bond network as methanol molecules filled the spaces that water molecules would typically inhabit. Finally, a study by (Besford et al., 2022) investigated the dipolar dispersion forces in methanol-water mixtures. The study accomplished this by simulating the interactions and concluded that the addition of methanol causes greater self-associating between water molecules. In addition, water molecules had greater dipole interactions within a mixture, increasing in strength with higher concentrations of methanol. In contrast, methanol interactions become weaker as the pure component was diluted with water. These studies highlight a fairly complicated set of interactions between the methanol and water in mixture.

A.3.2. Tri-ethylene glycol interactions

A.3.2.1.Tri-Ethylene glycol and light hydrocarbons

The mixture of light hydrocarbons and tri-ethylene glycol is commonly encountered in the natural gas industry however, detailed information on their intermolecular interactions during the dehydration process is limited in the literature. Methane, ethane and propane are non-polar molecules due to their symmetrical shape and lack of atoms with strong electronegativities. This results in only London forces and induced dipole-dipole forces being present between the triethylene glycol and light hydrocarbon molecules.

However, a number of studies have investigated other aspects of mixtures, including TEG and light hydrocarbons. The study by (Olsen et al., 2016) investigated the free energy of solvation and Henry's law solubility constants between TEG and methane. The study simulated the molecular dynamics between the respective components and found the free energy of solvation was negative. This meant TEG was more energetically favourable to reside in methane or water as a solvent. Another study by (de Oliveira et al., 2021) investigated the phase behaviour of natural gas in a glycol system. The study

accomplished this by modelling the interactions using the CPA, SRK, NRTL and PR models. The study found that the CPA model had the most consistent prediction ability, highlighting the importance of accounting for the association compounds.

A.3.2.2.Tri-Ethylene glycol and water

The interactions between water and tri-ethylene are of great interest due to TEG's hygroscopic nature. TEG and water are both associating molecules. The interaction between these two molecules allows for the absorption of water. TEG and water are associating molecules due to the hydrogen bond between them. This results in the molecules experiencing all three types of molecular forces. There is very limited information on the interactions between ethylene glycol and water, with the majority available for solubility measurements. However, other studies investigating different aspects of these mixtures can be used to evaluate some assumptions. A study by (Kruger et al., 2018) measured and modelled an ethylene glycol, water and methane system. The system was investigated at high pressures and used the Cubic Plus Association (CPA) equation of state to model the experimental data. The CPA model fit absolute average relative deviation ranged from 5-40%, with the model usually overestimating the experimental values. The study shows the limitation associated with the CPA model and the difficulty of accurately describing the interactions of associating systems. A similar study by (Folas et al.,2007) conducted HPVLE experiments of an ethylene glycol, water and methane system with modelling. The study focused on the CPA and Soave-Redlich-Kwong equation of state using a Huron Vidal mixing rule. It concluded that both models adequately modelled the data with the CPA model requiring just binary interaction parameters. This study differs in conclusions from (Kruger et al., 2018), however, each study used differing molar compositions and pressures. This shows the variability in intermolecular interactions depending on the conditions and concentrations of each component. It should be noted that these studies used ethylene glycol and not tri-Ethylene glycol, which as mentioned is not well studied in the literature. As these components have similar characteristics and behaviours and are constituted of similar functional groups, it is assumed that they exhibit broadly similar intermolecular forces with water.

A.3.2.3.Tri-Ethylene Glycol and Methanol

As mentioned, depending on natural gas composition and climate conditions, it may be necessary for the gas processing steps to include methanol injection upon extraction to inhibit clathrate formation, with down-stream dehydration by TEG. Hence the interaction between methanol and TEG becomes important, especially within natural gas mixtures. Both TEG and methanol are polar molecules due to asymmetrical shape and high electronegativity difference between the oxygen and hydrogen atoms. This results in both molecules experiencing all three types of major intermolecular forces. Studies dealing with these interactions directly are scarce thus, the studies previously mentioned such as (Kruger et al., 2018) and (Folas et al.,2007) are used to accentuate these intermolecular interactions by

considering other aspects. Through the modelling and experimental work, these studies showed the fairly complex and hard-to-predict interactions between methanol and TEG, warranting further study of these interactions in the natural gas setting.

A.4. Phase equilibria and thermodynamic modelling

The fundamental understanding of the thermodynamic properties of various fluid mixtures is imperative for a number of reasons. This allows for the design of methodologies for highly accurate thermodynamic data to be measured, modelled and interpreted, and enables for better design and optimisation of various chemical process, units which is a costly and labour-intensive practice. the inter-molecular forces between the constituent species of the process can be achieved via studying this mixture combination which helps develop an improved perception of the results obtained and trends shown in the results of a chemical thermodynamics study.

A.4.1. Principles of Phase Equilibrium

Equilibrium is a state in which no macroscopic changes occur within the properties of an isolated system over a given period (Smith et al., 2019). During this condition, all drivers for change are balanced; thus, the state of the system is consistent. These include the pressure, temperature and phase compositions remaining consistent at the macroscopic scale (Smith et al., 2019). However, at the microscopic scale, there are constant changes with individual molecules changing phase, energy states and locations. This, however, results in a fixed state for various properties when all molecules are considered.

The concept of phase equilibrium is useful when looking theoretically and practically at various systems, as it allows for simplifying reasonably complex systems into ordered behavioural structures. However, it should be noted that true phase equilibrium is never achieved in a practical setting as it is impossible to have a totally isolated system in reality. The practical goal in experimental phase equilibrium studies is to observe and measure the system at conditions as close to equilibrium as possible within the uncertainty limitations of the experimental design.

A.4.2. Criterion for phase equilibrium

This state of phase equilibrium can be shown mathematically through the implementation of various equations. These equations are expressed in terms of thermal, mechanical and chemical equilibrium. Assuming a closed system at equilibrium with two known phases α and β and making assumptions that the systems are constant in terms of pressure and temperature, the following equations indicate equilibrium conditions (Smith et al., 2019):

$$T^{\alpha} = T^{\beta} = T^{\boldsymbol{\pi}} \qquad \text{Thermal Equilibrium} \qquad \text{(A-1)}$$

$$P^{\alpha} = P^{\beta} = P^{\boldsymbol{\pi}} \qquad \text{Mechanical Equilibrium} \qquad \text{(A-2)}$$

For chemical equilibrium, the concept of Gibbs energy which is related to temperature and pressure through the following equation, must be evaluated:

$$d(nG) = (nV)dP - n(S)dT \tag{A-3}$$

When considering that a system is a single phase and open, meaning molecules can enter or leave the system at will from the surrounding, the Gibbs energy equations becomes a function of n_i Which is the number of a known chemical species i. The equation is now represented by the following:

$$nG = g(P, T, n_i) \tag{A-4}$$

The differential of which is shown below:

$$d(nG) = (nV)dP - (nS)dT + \sum_i \mu_i dn_i \tag{A-5}$$

In the equation μ_i represents the chemical potential of the species i which is given by:

$$\left[\frac{\partial(nG)}{\partial n_i}\right]_{P,T,n_i} = \mu_i \tag{A-6}$$

The last criterion for phase equilibrium, the chemical equilibrium, can now be expressed:

$$\mu^{\alpha} = \mu^{\beta} = \mu^{\boldsymbol{\pi}} \qquad \text{Chemical Equilibrium} \quad (i=1,2\ldots.N) \tag{A-7}$$

A.4.3. Fugacity and vapour-liquid equilibrium (pure and mixtures)

The use of chemical potential as a criterion for phase equilibrium is beneficial theoretically. However, due to the relation chemical potential has with immeasurable variables which have unknown absolute values, an absolute value for chemical potential is impossible, (Narasigadu, 2006), Thus it is an excellent theoretical representation of equilibrium but proves to be difficult to apply mathematically.

For this reason, the quantity termed fugacity was developed, which is related to chemical potential using the following equation assuming constant temperature (Smith et al., 2019):

$$\mu_i = \Gamma_i(T) + RT\ ln(f_i) \tag{A-8}$$

Fugacity can be defined as the likelihood of the transfer of molecules from one phase of a system into the other (Ahmed, 2010). The components of a system can thus be identified as phases with high component fugacity and low component fugacity, where there is defusal between these phases until there is equal fugacity in each of the different phases. Once this condition of stable and equal fugacity is reached, the system can be considered in thermodynamic equilibrium. This can be expressed as:

$$f_i^{\alpha} = f_i^{\beta} = f_i^{\boldsymbol{\pi}} \tag{A-9}$$

The fugacity coefficient of a known component *i* is depicted as (φ_i). This variable is used to determine the non-ideality and magnitude of departure for a molecule of component (*i*) towards its surrounding molecules. This is depicted by the term($\frac{\hat{f}_i}{P_i}$). For a vapor and liquid phase, the fugacity coefficient can be depicted using the following equation:

$$\hat{\varphi}_i^{\,Vapour} = \frac{\hat{f}_i}{p_i} = \frac{\hat{f}_i}{y_i P} \quad \text{Vapour Relations} \tag{A-10}$$

Where $\hat{\varphi}_i^{\,Vapour}$ is the fugacity coefficient in the vapour phase of component *i*; P is the pressure of the system and y_i is the mole fraction of component *i* in the vapour phase.

$$\hat{\varphi}_i^{\,liquid} = \frac{\hat{f}_i}{p_i} = \frac{\hat{f}_i}{x_i P} \quad \text{Liquid Relations} \tag{A-11}$$

Where $\hat{\varphi}_i^{\,Liquid}$ is the fugacity coefficient in the liquid phase of component *i*; P is the pressure of the system and y_i is the mole fraction of component *i* in the liquid phase.

These Equations 2.10 and 2.11 can be related to each other to produce the following relation:

$$P y_i \varphi_i^{vapour} = P x_i \varphi_i^{liq} \tag{A-12}$$

This can be simplified to:

$$y_i = K_i x_i \tag{A-13}$$

Where $K_i = \frac{\varphi_i^{liq}}{\varphi_i^{vapour}}$ Which is the equilibrium ratio

Mixtures

Hydrocarbon gases are usually extracted in mixtures, thus the phase behaviour of these mixtures is relevant to this study. The gas mixture, at a specific temperature and pressure, can be in equilibrium with a liquid hydrocarbon mixture, the absorbing liquid, water etc. This equilibrium is unlikely to have the same molar composition in each phase due to differences in volatilities of the respective components. The fugacity of a component *i* in a mixture can be defined using the following equation:

$$d\mu_i = RT\ d\ ln\hat{f}_i \tag{A-14}$$

Where the $d\mu_i$ represents the change in chemical potential of component *i* within the specified mixture; R represents the universal gas constant; T is temperature, and $d\ l\hat{f}_i$ represents the change in the natural logarithm of fugacity of component *i* in a mixture.

By substituting the pure component chemical potential with the pure component excess molar Gibbs free energy the following equation can be derived:

$$\mu_i(T,P,x) = G^E + RTln\left[\frac{\hat{f}_i(T,P,x)}{f_i(T,P)}\right] = \overline{G}_\iota \tag{A-15}$$

Where $\overline{G}_\iota$ is the partial molar Gibbs free energy of component *i* within a mixture.

Using equation A.15, the ability to model VLE Data becomes possible using the concepts ideal gas for the vapour phase and the ideal solution for the liquid phase.

Ideal gas and ideal solution approaches.

If a gas is assumed to behave like an ideal gas, then its behaviour can be characterised by the ideal gas fugacity. Ideal gas behaviour is only truly approached when a substance is at high temperatures and low pressures. The ideal gas chemical potential is the same as the ideal gas partial molar Gibbs free energy in respect to component *i*. The ideal gas fugacity can be expressed in the following equation using computations from (Dahm and Visco, 2014).

$$\hat{f}_i^{\,ig}(T,P,y) = y_i f_i^{ig}(T,P) \tag{A-16}$$

Where the superscript *ig* represents the ideal gas.

The fugacity of a liquid can similarly be represented as an ideal solution for low to moderate pressures. This is known as the Lewis-Randall rule and is expressed as:

$$\hat{f}_i^{\,id}(T,P,x) = x_i f_i^{id}(T,P) \tag{A-17}$$

Where the super script *id* reflects the ideal solution.

Using equation A.15 the system pressure can be equated to the pure component fugacity for an ideal gas. Thus, the fugacity of the specified component *i* can be expressed as an ideal gas:

$$\hat{f}_i^{\,ig}(T,P,y) = P_i \tag{A-18}$$

Gases generally do not behave ideally, thus residual properties are used to quantify the deviations from ideal gas, and excess properties are used to quantify the deviations from ideal solution behaviour.

Therefore the excess chemical potential of component *i* in a mixture can be shown using the following equation (Dahm and Visco, 2014):

$$\mu_i^E(T,P,x) = RT\ln\left[\frac{\widehat{f_i}(T,P,x)}{f_i(T,P)}\right] = RT\ln\gamma_i \tag{A-19}$$

Where $\gamma_i$is the activity coefficient of component *i* in the mixture; μ_i^E represents the excess chemical potential.

The residual properties are used to represent the deviation from ideal gas in the vapour phase. This is represented by the following formula where the residual chemical potential of component *i* in solution can be determined:

$$\mu_i^R(t,P,y) = RT\ln\left[\frac{\widehat{f_i}(T,P,x)}{Py_i}\right] = RT\ln\hat{\varphi}_i \tag{A-20}$$

Where $\hat{\varphi}_i$ is the fugacity coefficient of component *i* in the solution.

The ratio of the fugacity coefficient of component *i* in a mixture to its ideal solution value is known as the activity coefficient. Thus, the fugacity coefficient accounts for deviations from the ideal solution, expressed as:

$$\hat{f}_i(T,P,x) = \hat{f}^{id}{}_i\,\gamma_i = x_i f_i(T,P)\gamma_i \tag{A-21}$$

Finally the fugacity coefficient and activity coefficient are sufficient to model the VLE for low to moderate pressure systems. Thus, the mixture chemical equilibrium condition is equal to the fugacity mixture conditions.

$$\widehat{f}_i(T,P,x)^{Phase\ 1} = \widehat{f}_i(T,P,x)^{Phase\ 2} \tag{A-22}$$

Using equations (A-21) and (A-22), the following expressions are obtained.

$$\widehat{f}_i(T,P,z)^{Phase\ 1} = \widehat{f}_i(T,P,z)^{Phase\ 2} \tag{A-23}$$

$$z_i^{Phase\ 1} P\hat{\varphi}_i^{Phase\ 1} = z_i^{Phase\ 2} P\hat{\varphi}_i^{Phase\ 2} \tag{A-24}$$

Where z can be either the liquid or vapour phase composition.

At equilibrium the phases will have the same pressure thus equation (A.24) can be determined to be:

$$z_i^{Phase\ 1}\hat{\varphi}_i^{Phase\ 1} = z_i^{Phase\ 2}\hat{\varphi}_i^{Phase\ 2} \tag{A-25}$$

Thus when using the fugacity coefficient in a mixture , the mole fraction will be included at chemical equilibrium (Dahm and Visco, 2014). The mole fraction will thus not be equal unless an azeotrope is present. Reducing the fugacity expressions into pressure, composition and temperature equations is still an issue; however, different approaches can be used to remedy this.

A.4.4. Phase equilibria fundamentals and thermodynamic modelling

The fundamental understanding of thermodynamic properties of various fluid mixtures and their relation to one another is imperative for a number of reasons. These include correctly predicting their behaviour at various conditions such as temperature and pressure which is accomplished using first principles and appropriate models such as equations of states.

A.4.5. Fugacity and vapour-liquid equilibrium (pure and mixtures)

The use of chemical potential as a criterion for phase equilibrium as shown in Appendix A, is beneficial theoretically. However, due to the relation chemical potential has with immeasurable variables which have unknown absolute values, an absolute value for chemical potential is impossible, (Narasigadu, 2006). Thus, it is an excellent theoretical representation of equilibrium but proves to be difficult to apply mathematically.

For this reason, the quantity termed fugacity was developed, which is related to chemical potential using the following equation assuming constant temperature (Smith et al., 2019).:

$$\mu_i = \Gamma_i(T) + RT\ ln(f_i) \tag{A-26}$$

Fugacity can be defined as the likelihood of the transfer of molecules from one phase of a system into the other (Ahmed, 2010). The components of a system can thus be identified as phases with high component fugacity and low component fugacity, where there is defusal between these phases until there is equal fugacity in each of the different phases. Once this condition of stable and equal fugacity is reached, the system can be considered in thermodynamic equilibrium. This occurs at thermal, mechanical and chemical equilibrium. This can be expressed as:

$$f_i^{\alpha} = f_i^{\beta} = f_i^{\boldsymbol{\pi}} \tag{A-27}$$

The fugacity coefficient of a known component *i* is denoted as (φ_i). This variable is used to determine the non-ideality (magnitude of departure) for a molecule of component (*i*) from its surrounding molecules. This is depicted by the term ($\frac{\hat{f}_i}{P_i}$). For a vapor and liquid phase, the fugacity coefficient can be denoted using the following equation:

$$\hat{\varphi}_i^{\,Vapour} = \frac{\hat{f}_i}{p_i} = \frac{\hat{f}_i}{y_i P} \quad \text{Vapour Relations} \tag{A-28}$$

Where $\hat{\varphi}_i^{\,Vapour}$ is the fugacity coefficient in the vapour phase of component *i*; P is the pressure of the system and y_i is the mole fraction of component *i* in the vapour phase.

$$\hat{\varphi}_i^{\,liquid} = \frac{\hat{f}_i}{p_i} = \frac{\hat{f}_i}{x_i P} \quad \text{Liquid Relations} \tag{A-29}$$

Where $\hat{\varphi}_i^{\,Liquid}$ is the fugacity coefficient in the liquid phase of component *i*; P is the pressure of the system and y_i is the mole fraction of component *i* in the liquid phase.

Equations A.28 and A.29 can be related to each other to produce the following relation:

$$Py_i\varphi_i^{vapour} = Px_i\varphi_i^{liq} \tag{A-30}$$

This can be simplified to:

$$y_i = K_i x_i \tag{A-31}$$

Where $K_i = \frac{\varphi_i^{liq}}{\varphi_i^{vapour}}$ which is the equilibrium ratio

A.4.6. Gamma- Phi (Combined method) modelling

The gamma-phi ($\gamma - \Phi$) method uses an activity coefficient model to express the non-idealities found in the liquid phase and generally apply to low to moderate pressure systems. The non-idealities in the vapour phase are usually expressed using a suitable equation of state, (Liwanth, 2014).

In-order to model mixtures in phase equilibrium, a component found in the mixture must have the same fugacities in both phases. Thus the following equation can be expressed (Dahm and Visco, 2014):

$$\hat{f}_i^{liq} = \hat{f}_i^{vap} \tag{A-32}$$

Using the gamma-phi approach, the deviations from an ideal solution are accounted for by the activity coefficient (known as γ_i). This is presented by the following equation:

$$\hat{f}_i^{liq}(T, P, x) = x_i f_i(T, P)\gamma_i \tag{A-33}$$

In addition, the deviations from an ideal gas are accounted for by the fugacity coefficient (known as phi) for component *i* in a mixture.

$$\hat{f}_i^{vap}(T, P, y) = y_i f_i \hat{\varphi}_i \tag{A-34}$$

Equating equation 2.8 and 2.9 yields for the following equation:

$$x_i f_i(T, P)\gamma_i = y_i f_i \hat{\varphi}_i \tag{A-35}$$

This equation allows for a more realistic modelling of VLE behaviour in mixtures at low to moderate pressures (Dahm and Visco, 2014). In modelling software such as Aspen Plus ®, there are in-inbuilt algorithms to execute the gamma-phi formulation to obtain the modelling parameters by regression. These modelling parameters minimise the deviation between the experimental data and model values, allowing for a better fit.

A.4.7. phi-phi Modelling

The phi-phi ($\varphi - \varphi$) model approach uses an equation of state to represent both the vapour and liquid phase non-idealities. These deviations are represented through fugacity coefficients. The following equations represent this:

$$\hat{f}_i^{vap}(T, P, y) = y_i P_i \hat{\varphi}_i^{vap} \tag{A-36}$$

$$\hat{f}_i^{liquid}(T, P, y) = x_i P_i \hat{\varphi}_i^{liquid} \tag{A-37}$$

Equating these two equations results in the following equation:

$$x_i P_i \hat{\varphi}_i^{liquid} = y_i P_i \hat{\varphi}_i^{vap} \tag{A-38}$$

The pressures for both phases at equilibrium are the same. Thus, the equation becomes:

$$x_i \hat{\varphi}_i^{liquid} = y_i \hat{\varphi}_i^{vap} \tag{A-39}$$

An appropriate equation of state is usually required to calculate the $\hat{\varphi}_i^{liquid}$and $\hat{\varphi}_i^{vap}$ for accurate modelling.

A.5. Property methods used in this study

The intermolecular forces between the respective components result in the non-ideal behaviour of specific systems (Kontogeorgis and Folas, 2010). The non-ideal behaviour makes it challenging to predict system behaviours at various compositions, particularly the non-idealities caused by the hydrogen bonding. At moderate temperatures and low pressures, these non-ideal behaviours are minimal. However, most natural gas processes occur at high pressure and low temperatures where the non-ideality is most prevalent (Mokhatab et al., 2015). Thus, to accurately model these systems, an equation of state is required to describe the mixture behaviour when operating at high pressures. When specifically considering non-polar hydrocarbons, the Peng and Robinson and Soave-Redlich-Kwong (SRK)equations of state are the most popular and commonly used (Mokhatab et al., 2015). However, the Peng-Robinson EoS does not specifically consider hydrogen bonding, which makes it poor at estimating systems that have water, TEG or methanol (Soo, 2011). The Cubic Plus Association (CPA) EOS and PC-SAFT model do possess this consideration and are commonly used for systems that include water, glycols and methanol (Mokhatab et al., 2015).

For these reasons, this study focused on describing the phase behaviours of the measured systems with CPA EoS, PC-SAFT model and Peng-Robinson as a comparative reference, to demonstrate both the abilities and limitations of these models compared to experiential data. SRK was omitted because the

CPA is an extension of this model by including an association term and has proved to be superior than conventional SRK for natural gas dehydration systems (Kontogeorgis and Folas, 2010).

A.5.1. Peng and Robinson Equation of state

The Peng and Robinson equation of state (1976) (Lopez-Echeverry et al., 2017) has become one of the most successful models applied to phase equilibria (Walas, 1991). It improved the predictions for liquid phase behaviour by implementing an expression for volume dependency. The Peng Robinson equation of state is as follows (Kontogeorgis and Folas, 2010):

$$P = \frac{RT}{V-b} - \frac{a(T,w)}{V(V+b)+b(V-b)} \quad \text{(A-40)}$$

Where the constant, b, depends on the molecular size and is temperature-independent:

$b = 0.07790(\frac{RT_c}{P_c})$

And the constant, a, is temperature dependent and related to the intermolecular forces of attraction:

$$a(T,w) = a_c\alpha(T,w) \quad \text{(A-41)}$$

A.5.2. Association models

The PC-SAFT and CPA models are known as association models due to their ability to model systems with hydrogen bonding generally and accurately. These include systems that have glycols, alcohols, water, acids, amines and other molecules with hydrogen bonding (Kontogeorgis and Folas, 2010). The PC-SAFT and CPA models were used in this work due to the association model ability and common use for modelling natural gas systems.

A.5.2.1.1 The Perturbed-Chain Statistical Associating Fluid Theory (PC-SAFT) model

The PC-SAFT EoS is an extension of the SAFT EoS, which uses statistical mechanical method such as perturbation theory. There are several variations of the SAFT EoS. However, the PC-SAFT EoS differs from these by treating fluids as being connected by complex chained structures as opposed to unbound spherical particles (Kontogeorgis and Folas, 2010).

Despite this difference, the variants of the SAFT EoS use the same common chain and association terms as contributions to the Helmholtz energy:

$$a^{res} = a^{sg} + a^{chn} + a^{as} \tag{A-42}$$

Where the a^{res} is the residual Helmholtz energy; a^{sg} is the Helmholtz energy of the dispersion and unbound spherical term; a^{chn} is the contribution for chain formation and a^{as} is the association's contribution

The expressions for the chain and association terms are as follows:

$$\frac{a^{chain}}{RT} = \sum_i x_i\,(1 - m_i)\ln(g_{ii}(d_{ii})^{hs}) \tag{A-43}$$

$$\frac{a^{assoc}}{RT} = \sum_i x_i\,[\sum_{A_i}(lnX_i^A - \frac{X^{A_i}}{2}) + \frac{1}{2}M_i] \tag{A-44}$$

Where the $X_{A_i}$is the fraction of molecules of compound *i* not bonded to site A; and M_i is the number of association sites. X_{A_i} can be defined as(Kontogeorgis and Folas, 2010):

$$X_{A_i} = \frac{1}{1 + \sum_j \rho_j x_j \sum_{B_j} X_{B_i}\,\Delta^{A_iB_j}} \tag{A-45}$$

Where the ρ_j is the molar density of compound *j*; and $\Delta^{A_iB_j}$ is the association strength between two sites from two different associating molecules. This association strength is expressed using the following formula:

$$\Delta^{A_iB_j} = d_{ij}^3 g_{ij}\big(d_{ij}\big)^{seg} K^{A_iB_j}[exp\left(\frac{\varepsilon^{A_iB_j}}{KT}\right) - 1] \tag{A-46}$$

Where $g(\rho)$ is the radial distribution function:

$g(\rho) = \frac{1}{1-1.9\eta}$; $\eta = \frac{1}{4}b\rho$;while $b_{ij} = \frac{b_i+b_j}{2}$

Where, η is the reduced fluid density; and b is the co-volume parameter

The different variations of the SAFT EoS employ either a temperature-dependent or temperature-independent diameter in the association strength expression. The PC-SAFT EoS uses a temperature-independent diameter (Soo, 2011). This just replaces the $d_{ij.}$in equation (A.46)

A simplified version of the PC-SAFT model is typically used for the mixing rules as it allows for lower computing power. This allows for the hard-sphere and association terms to be reduced to:

$$g^{hs}(d^{+}) = \frac{2-\eta}{2(1-\eta)^3} \tag{A-47}$$

And

$$a^{-hs} = \frac{4\eta - 3\eta^2}{(1-\eta)^2} \tag{A-48}$$

These reduced forms affect the chain and association terms allowing for more straightforward determination of the association strength term.

A.5.2.1.2 Dispersion Terms

The dispersion term for the PC-SAFT EoS differs from other variations by accounting for dispersion attraction as whole chains rather than individual hard spheres. Thus the Helmholtz energy for the dispersion attraction is expressed as (Kontogeorgis and Folas, 2010):

$$\frac{a^{dispersion}}{kTN} = \frac{A_1}{kTN} + \frac{A_2}{kTN} \tag{A-49}$$

Where:

$$\frac{A_1}{kTN} = -2\pi\rho m^2 \left(\frac{\varepsilon}{kT}\right)\sigma^3 \int_1^{\infty} \tilde{u}(x) g^{hc}\left(m; \frac{x\sigma}{d}\right) x^2 dx \tag{A-50}$$

$$\frac{A_2}{kTN} = -\pi\rho m \left(1 + Z^{hc} + \rho\frac{\delta Z^{hc}}{\delta\rho}\right)^{-1} m^2 \left(\frac{\varepsilon}{kT}\right)^2 \sigma^3 \frac{\delta}{\delta\rho}\left[\rho \int_1^{\infty} \tilde{u}(x) g^{hc}\left(m; \frac{x\sigma}{d}\right) x^2 dx\right] \tag{A-51}$$

Where $x = r/\sigma$ and $\tilde{u}(x) = u(x)/\varepsilon$ which is the reduced intermolecular potential.

A.5.2.1.3 Mixing Rules

The mixing rules for the PC-SAFT EoS are only required for the dispersion term and not the chain or association (Kontogeorgis and Folas, 2010). This is true for all variants of the SAFT EoS, which use combining rules for the volume and segment energy parameters. The Lorentz-Berthelot rules are typically used and are presented as follows:

$$\varepsilon_{ij} = \sqrt{\varepsilon_i \varepsilon_j}(1 - k_{ij}) \tag{A-52}$$

$$\sigma_{ij} = \frac{\sigma_i + \sigma_j}{2} \tag{A-53}$$

Where the k_{ij} is the interaction parameter which corrects dispersion energies caused by unlike molecules (Kontogeorgis and Folas, 2010).

The Elliot combining rule is applied to the cross-association strength:

$$\Delta^{A_i B_j} = \sqrt{\Delta^{A_i B_i} \Delta^{A_j B_j}} \tag{A-54}$$

A.5.2.2. Cubic Plus Association (CPA) EOS

The CPA model combines the Soave-Redlich-Kwong (SRK) Equation of State and an association term similar to that in the SAFT model (Kontogeorgis and Folas, 2010). The model's development allows for predicting multicomponent hydrocarbon systems, including highly polar molecules such as water, glycols and alcohols. Further targets were (Kontogeorgis and Folas, 2010):

- Accurate calculations for multicomponent systems using only parameters estimated from binary data
- Simplify mathematical formulas for describing complex compound systems.

The CPA EoS can be expressed for mixtures as follows:

$$P = \frac{RT}{V_m - b} - \frac{a(T)}{V_m(V_m + b)} - \frac{1}{2}\frac{RT}{V_m}\left(1 + \frac{\rho \delta lng}{\delta \rho}\right)\sum_i x_i \sum_{A_i}(1 - X_{A_i}) \tag{A-55}$$

Where the b is the co-volume; a_0 is the attractive energy term; R is the Universal Gas constant; T is the temperature, V_m is the molar volume and ρ is the molar density.

This expression can be broken up into the respective forces, with the first two terms representing the SRK Repulsion and SRK attractive forces and the final term representing the SAFT association term.

The most important of these terms is the association term for this study. The X_{A_i} is the most important element in this term, it represents the fraction of sites A on a molecule *i* that don't form bonds with other active sites (Kontogeorgis and Folas, 2010). This is represented by the following term:

$$X_{A_i} = \frac{1}{1 + \rho \sum_j x_j \sum_{B_j} X_{B_i} \Delta^{A_i B_j}} \tag{A-56}$$

Where $\Delta^{A_i B_j}$ is association strength between two sites of different molecules expressed as:

$$\Delta^{A_i B_j} = g(\rho) \left[exp\left(\frac{\varepsilon^{A_i B_j}}{RT}\right) - 1 \right] b_{ij} \beta^{A_i B_j} \tag{A-57}$$

Where $g(\rho)$ is the radial distribution function:

$g(\rho) = \frac{1}{1-1.9\eta}$; $\eta = \frac{1}{4} b\rho$;while $b_{ij} = \frac{b_i + b_j}{2}$

b_{ij} and $\varepsilon^{A_i B_j}$ are the volume parameter and association energy for the CPA model and b is the co-volume parameter. These parameters are only used for associating components and form part of the five pure component parameters for the CPA model (Kontogeorgis and Folas, 2010).

The energy parameter of the CPA EOS is given temperature-dependent Soave-type a(T) expressed as follows:

$$a(T) = a_o \left(1 + c_1 \left(1 - \sqrt{T_r}\right)\right)^2 \tag{A-58}$$

Where the $T_r = T/T_c$

It should be noted that the b is temperature independent.

A.5.2.2.1 Mixing rules

The CPA model uses the conventual mixing rules where the energy parameter a_{ij} utilities the geometric mean rule while the interaction parameter k_{ij} is generally required for self-association compounds such as glycols, alcohols and water. These parameters are expressed as follows:

$$a = \sum_i \sum_j x_i x_j a_{ij} \; ; b = \sum_i x_i b_i \tag{A-59}$$

Where $a_{ij} = \sqrt{a_i a_j}(1 - k_{ij})$

A.5.2.2.2 Associating terms

A.5.2.2.3 Cross associating mixtures

The Association term within the CPA EOS doesn't include a mixing term, however, when two association parameters are present, combining of rules is needed. This is especially needed when there is a mixing between two associating compounds, which requires combining the association energy and association volume terms in-order to calculate the association strength ($\Delta^{A_iB_j}$)(Kontogeorgis and Folas, 2010). Thus the CR-1 rule and Elliot combining rules were most commonly used to accurately predict mixing properties(Kontogeorgis and Folas, 2010). Thus, the expressions using the CR-1 rule are given by:

$$\varepsilon^{A_iB_j} = \frac{\varepsilon^{A_iB_i} + \varepsilon^{A_jB_j}}{2} \tag{A-60}$$

$$\beta^{A_iB_j} = \sqrt{\beta^{A_iB_i}\beta^{A_jB_j}} \tag{A-61}$$

The cross -association strength is expressed using the Elliot combining rule as follows:

$$\Delta^{A_iB_j} = \sqrt{\Delta^{A_iB_i}\Delta^{A_jB_j}} \tag{A-62}$$

A.5.2.2.4 Solvation mixtures

Induced association occurs between self-associating compounds and inert compounds. In (Kontogeorgis and Folas, 2010), these are known as solvating mixtures, and a modification of the CR-1 rule is applied. In this modification, the cross-association volume is determined from experimental data and the cross-associating energy is equal to half the value of the association compound in said mixture:

$$\varepsilon^{A_iB_j} = \frac{\varepsilon_{associating}}{2} \tag{A-63}$$

$$\beta^{A_iB_j} = Fitted\ from\ data \tag{A-64}$$

The associating strength is determined using the equation (2.52). This method showed accurate results for a system where glycols, alcohols and water are present (Kontogeorgis and Folas, 2010)

A.6. VLE Modelling

The Models used in this study, namely the cubic plus association (CPA), Peng Robinson (PR) and perturbed-chain statistical association fluid theory (PC-SAFT) were implemented using the Aspen plus V12 software. The maximum-likelihood objective function was used for the data correlations using the Deming or New Britt-luecke algorithm. The Deming or weighted least squares were used for the initialization method. The maximum likelihood objective functions for the expression can be found in the equations A-65 and A-66 below.

$$Obj\ F = \sum_{n=1}^{NDG} w_n \sum_{i=1}^{N} \left[\left(\frac{T_{Calc,i} - T_{Exp,i}}{\sigma_{T,i}} \right)^2 + \left(\frac{P_{Calc,i} - P_{Exp,i}}{\sigma_{P,i}} \right)^2 + \sum_{j=1}^{NC-1} \left(\frac{x_{Calc,i,j} - x_{Exp,i,j}}{\sigma_{x,i,j}} \right)^2 \right] \quad \text{(A-65)}$$

$$Obj\ F = \sum_{n=1}^{NDG} w_n \sum_{i=1}^{N} \left[\left(\frac{T_{Calc,i} - T_{Exp,i}}{\sigma_{T,i}} \right)^2 + \left(\frac{P_{Calc,i} - P_{Exp,i}}{\sigma_{P,i}} \right)^2 + \sum_{j=1}^{NC-1} \left(\frac{x_{Calc,i,j} - x_{Exp,i,j}}{\sigma_{x,i,j}} \right)^2 + \sum_{j=1}^{NC-1} \left(\frac{y_{Calc,i,j} - y_{Exp,i,j}}{\sigma_{y,i,j}} \right)^2 + \right] \quad \text{(A-66)}$$

Where: *Obj F* is the objective function minimised used for data regression

NDG is the number of data groups in the regression case

w_n is the weight of the data group n

N is the number of data points in group n

NC is the number of components present in the data group

T, P,x,y represents the temperature, pressure, liquid mole fraction and vapour mole fraction

Calc represents calculated data

Exp represents experimentally measured data

i is data for data point *i*

j is fraction data for component *j*

σ is the standard deviation of the data.

Appendix B : Model Parameters

B.1. Pure component parameters

Relevant properties for components of interest in this study.

Table B.1 Critical properties and acentric factors for components of interest in this study. (Aspen Plus V12, DB PURE 38)

Parameter	Units	CO_2	CH_3OH	H_2O	TEG	CH_4	C_2H_6	C_3H_8
Omega		0.22362	0.56583	0.34486	0.75595	0.01155	0.013257	0.15229
P critical	MPa	7.38	8.08	22.06	3.32	4.60	4,41	4.25
T critical	K	304.21	512.50	647.10	769.50	190.56	310.159	369.83

Table B.2 Pure component parameters for the CPA and PC-SAFT models

Chemical component	Methane	Ethane	Propane	Water	TEG (4C association)	Methanol	Carbon dioxide (2B association)
CPA							
CPATC (K)	193.162[e]	310.159[d]	378.644[d]	303.409[d]	747.054[d]	364.17[c]	309.935[d]
CPAAT	-	-	-	4	4	2	1004
CPAAC	-	-	-	0.0692[d]	0.0188[d]	0.0161[c]	-
CPAAI (K)	-	-	-	2003.2[d]	1724.4[d]	2957.78[c]	-
CPAPC (Bar)	47.8142[e]	52.0782[d]	47.1602[d]	150.726[d]	40.7359[d]	84.8085[c]	82.0785[d]
CPAM	0.45172[e]	0.591946[d]	0.642975[d]	0.380371[d]	1.13257[d]	0.340423[c]	0.772821[d]
PC-SAFT							
PCSFTM	1[a]	1.6069[e]	2.002[e]	1.5[a]	3.18092[a]	1.9107[b]	2.7852[a]
PCSFTV	3.7039[a]	3.5206[e]	3.6184[e]	2.6273[a]	4.0186[a]	3.0633[b]	2.0729[a]
PCSFTU (K)	150.03[a]	191.42[e]	208.11[e]	180.3[a]	333.17[a]	231.57[b]	169.21[a]
PCSFAT	-	-	-	4	4	2	1004
PCSFAU (K)	-	-	-	1804.22[a]	2080.03[a]	2283.6[b]	-
PCSFAV	-	-	-	0.0942[a]	0.0235[a]	0.041[b]	-

a:(Grenner et al., 2007)**; b:**(Tafazzol and Nasrifar, 2011)**; c:**(Folas et al., 2006)**; d:** (Qvistgaard et al., 2023)**; e:**(Reid et al., 1989)

B.2. Binary interaction parameters

Table B.3 Binary parameters used for the CPA model.

Component i	Component j	AIJ	BIJ	Pressure Limits (Bar)	Temperature Limits (K)
METHANE	ETHAN-01	0	0	-	-
ETHAN-01	PROPA-01	0	0	-	-
METHANE	PROPA-01	0	0	-	-
WATER	METHANE	0.7988	0	0.07 - 1334	274.19-483.15
WATER	ETHAN-01	0.54729	0	3.2-49.5	274.26-373.15
WATER	PROPA-01	0.1135	0	-	278-366
TRIET-01	WATER	-0.211	0	0.85	371-417
TRIET-01	METHANE	0.13574	0	1.1-202	298-398
TRIET-01	ETHAN-01	0.135	0	1.1-204.8	298-398
TRIET-01	PROPA-01	0.153	0	0.2-64.5	298-398
METHANOL	WATER	-0.094	0	0.04-85.1	298.15-523.15
METHANOL	METHANE	0.0134	0	6.9-2935	274.19-483.15
METHANOL	PROPA-01	0.059	0	-	-

(Qvistgaard et al., 2023)

B.3. Raw vapour pressure with model predictions experimental data

Table B.4 Experimental and calculated vapour pressure data with experimental uncertainty for methanol.

T_{exp} (K)[a]	P_{exp} (MPa)	$U_c(P)$ (MPa)	P_{lit} (MPa)[b]	P (MPa) Antoine	P (MPa) CPA	P (MPa) PC-SAFT	P (MPa) PR
303.24	0.023	0.0001	0.022	0.022	0.022	0.022	0.021
313.29	0.037	0.0002	0.036	0.037	0.036	0.035	0.035
318.06	0.045	0.0002	0.045	0.045	0.044	0.045	0.044
323.01	0.057	0.0003	0.056	0.056	0.058	0.056	0.055
328.05	0.069	0.0004	0.070	0.070	0.069	0.069	0.069

[a]$U_c(T) = 0.04$ (K) [b](Safarov et al., 2015)

Table B.5 Vapour pressure data and uncertainty for water.

T_{exp} (K)[a]	P_{exp} (MPa)	$U_c(P)$ (MPa)	P_{lit} (MPa)[b]	P (MPa) Antoine	P (MPa) CPA	P (MPa) PC-SAFT	P (MPa) PR
303.19	0.004	0.00002	0.004	0.004	0.004	0.005	0.004
313.31	0.008	0.00004	0.007	0.007	0.007	0.008	0.006
323.26	0.012	0.00006	0.013	0.012	0.012	0.013	0.011
333.40	0.020	0.0001	0.021	0.020	0.020	0.021	0.018

[a]$U_c(T) = 0.04$(K) [b](Zhang et al., 2018)

Table B.6 Vapour pressure data and uncertainty for CO_2.

T_{exp} (K)[a]	P_{exp} (MPa)	$U_c(P)$ (MPa)	P_{lit} (MPa)[b]	P (MPa) CPA	P (MPa) PC-SAFT	P (MPa) PR
282.80	4.47	0.015	4.46	4.68	4.66	4.45
287.92	5.07	0.015	5.08	5.04	5.05	5.06
293.04	5.71	0.015	5.71	5.69	5.74	5.72
298.27	6.44	0.015	6.48	6.39	6.48	6.46
303.19	7.18	0.015	7.19	7.12	7.25	7.22

[a]$U_c(T) = 0.06$ (K) [b](Kim and Kim, 2005)

Table B.7 Vapour pressure data for CH_4

T_{exp} (K)	P_{lit} (MPa)[a]	P (MPa) CPA	P (MPa) PC-SAFT	P (MPa) PR
112	0.10	0.10	0.10	0.11
118	0.17	0.17	0.17	0.17
124	0.25	0.25	0.25	0.25
130	0.37	0.37	0.37	0.37
136	0.52	0.52	0.52	0.52
142	0.71	0.71	0.71	0.72
148	0.95	0.95	0.95	0.96
154	1.24	1.24	1.24	1.25
160	1.59	1.59	1.60	1.61
166	2.01	1.99	2.02	2.03
172	2.50	2.47	2.51	2.53
178	3.07	3.02	3.09	3.10
184	3.74	3.65	3.75	3.77

[a](Haselden, 1979)

Table B.8 Vapour pressure data for C_2H_6

T_{exp} (K)	P_{lit} (MPa)[a]	P(MPa) CPA	P(MPa) PC-SAFT	P(MPa) PR
274.62	2.47	2.46	2.47	2.49
279.17	2.75	2.73	2.75	2.77
283.79	3.06	3.03	3.06	3.08
291.25	3.62	3.57	3.60	3.64
293.15	3.76	3.71	3.75	3.79
294.16	3.85	3.79	3.83	3.87
295.04	3.92	3.86	3.90	3.94
297.19	4.11	4.04	4.08	4.13
299.14	4.28	4.20	4.25	4.30
301.26	4.47	4.38	4.44	4.49
303.11	4.65	4.55	4.60	4.66

Table B.9 Vapour pressure data for C_3H_8

T_{exp} (K)	P_{lit} (MPa)[a]	P (MPa) Antoine	P (MPa) CPA	P (MPa) PC-SAFT	P (MPa) PR
270.51	0.44	0.44	0.44	0.44	0.44
271.77	0.46	0.45	0.45	0.45	0.45
280.13	0.58	0.59	0.59	0.58	0.58
285.35	0.68	0.68	0.68	0.68	0.68
287.35	0.72	0.72	0.72	0.72	0.72
289.65	0.76	0.77	0.76	0.76	0.76
291.75	0.81	0.81	0.81	0.81	0.80
297.98	0.95	0.95	0.95	0.95	0.95
300.92	1.02	1.02	1.01	1.01	1.02
303.37	1.08	1.09	1.08	1.08	1.09
314.06	1.40	1.40	1.39	1.39	1.40

[a](Seneviratne et al., 2017)

B.4. Raw system data

Table B.10 Experimental and regressed isothermal VLE Data (P-x) for the CH_4(1) + CH_3OH (2) system at 303.15 K.

Liquid mole composition (x_1)	Pressure (MPa)			
	P_{exp} (MPa)	CPA	PC-SAFT	PR
0.019	2.41	2.27	2.22	2.22
0.022	2.72	2.57	2.51	2.51
0.029	3.66	3.50	3.44	3.44
0.051	6.46	6.26	6.21	6.22
0.065	7.99	8.21	8.21	8.23
0.075	9.61	9.73	9.81	9.82
0.085	10.65	11.12	11.29	11.27
0.102	13.06	13.95	14.37	14.27

Table B.11 Isothermal VLE Data (P-x) for the CO_2 (1) + TEG (2)-water (3) (96.5/3.5 wt.%) system at 322.04 K with comparison to regressed property models.

Liquid mole composition (x_1)	Pressure (MPa)			
	P_{exp} (MPa)	Pressure CPA	Pressure PC-SAFT	Pressure PR
0.019	2.41	2.27	2.22	2.22
0.022	2.72	2.57	2.51	2.51
0.029	3.66	3.16	3.44	3.44
0.051	6.46	3.51	6.21	6.22
0.065	7.99	6.27	8.21	8.23
0.075	9.61	8.22	9.81	9.82
0.085	10.65	7.61	11.29	11.27
0.102	13.06	9.76	14.37	14.27

Table B.12 Experimental isothermal VLE Data (P-x) and modelling results for the CH_4 (1) + (CH_3OH (2) /TEG (3)/Water (4) 3.33/91.84/4.83 wt%) system at 303.15 K

Experimental				Model		
T_{exp} (K)[a]	Liquid mole composition (x_1)	P_{exp} (MPa)	U_c (P) (MPa)	Pressure (MPa)		
				Pressure CPA	Pressure PC-SAFT	Pressure PR
303.16	0.006	2.25	0.02	1.52	1.52	1.54
303.15	0.013	4.11	0.03	3.76	3.74	3.85
303.14	0.015	4.49	0.03	4.42	4.39	4.53
303.16	0.017	5.32	0.03	5.10	5.08	5.24
303.14	0.018	5.40	0.07	5.45	5.43	5.61
303.15	0.020	6.06	0.06	6.03	6.01	6.22
303.15	0.021	7.01	0.06	6.65	6.63	6.87
303.14	0.024	8.00	0.08	7.75	7.73	8.03
303.14	0.025	8.33	0.07	8.15	8.15	8.47
303.13	0.028	9.07	0.03	9.45	9.48	9.87
303.13	0.029	9.56	0.06	9.78	9.80	10.21
303.14	0.032	10.74	0.03	11.31	11.39	11.88
303.14	0.037	12.27	0.05	14.12	14.35	14.98

[a] $U_c(T) = 0.06$ (K) ; [b] $U_c(x_3) = 0.002$;

Table B.13 Experimental isothermal VLE Data (P-x) and modelling results for the CH_4 (1) + (CH_3OH (2) /TEG (3)/Water (4) 3.33/91.84/4.83 wt%) system at 313.15 K

Experimental				Model		
T_{exp} (K)[a]	Liquid mole composition (x_1)	P_{exp} (MPa)	U_c (P) (MPa)	Pressure (MPa)		
				Pressure CPA	Pressure PC-SAFT	Pressure PR
313.15	0.013	3.70	0.08	3.72	3.70	3.66
313.14	0.015	4.34	0.06	4.36	4.33	4.29
313.15	0.017	5.19	0.04	5.02	4.99	4.95
313.16	0.020	5.91	0.03	5.91	5.89	5.85
313.15	0.021	6.64	0.05	6.51	6.48	6.44
313.16	0.024	7.81	0.04	7.55	7.52	7.48
313.15	0.025	8.17	0.03	7.94	7.91	7.87
313.15	0.028	8.68	0.03	9.16	9.16	9.10
313.15	0.029	9.17	0.06	9.46	9.46	9.40
313.16	0.032	10.56	0.04	10.87	10.91	10.84
313.14	0.037	11.76	0.03	13.42	13.54	13.42

[a] $U_c(T) = 0.06$ (K) ; [b] $U_c(x_3) = 0.002$

Table B.14 Experimental isothermal VLE Data (P-x) and modelling results for the CH_4 (1) + (CH_3OH (2) /TEG (3)/Water (4) 3.33/91.84/4.83 wt%) system at 323.15K

Experimental				Model		
T_{exp} (K)[a]	Liquid mole composition (x_1)	P_{exp} (MPa)	U_c (P) (MPa)	Pressure (MPa)		
				Pressure CPA	Pressure PC-SAFT	Pressure PR
323.14	0.006	2.16	0.03	1.52	1.51	1.43
323.15	0.013	3.50	0.03	3.68	3.66	3.49
323.16	0.015	4.17	0.04	4.30	4.27	4.08
323.15	0.017	5.03	0.04	4.94	4.92	4.70
323.14	0.018	5.47	0.03	5.27	5.25	5.01
323.14	0.020	58.0	0.13	5.81	5.78	5.53
323.16	0.021	6.49	0.03	6.38	6.35	6.07
323.15	0.024	7.70	0.03	7.38	7.34	7.02
323.15	0.025	8.02	0.03	7.74	7.71	7.37
323.15	0.028	8.50	0.03	8.90	8.88	8.48
323.15	0.029	8.83	0.04	9.18	9.16	8.75
323.15	0.032	10.13	0.03	10.50	10.51	10.02
323.15	0.037	11.36	0.03	12.84	12.91	12.25

[a] $U_c(T) = 0.06$ (K) ; [b] $U_c(x_1) = 0.002$

Table B.15 Experimental isothermal VLE Data (P-x) and modelling results for the (CH_4 (1)/C_2H_6 (2)/C_3H_8 (3) 3.68/0.22/96.10 wt%) + (CH_3OH (4)/TEG (5)/Water (6) 3.33/91.84/4.83 wt%) system at 303.15 K

Experimental				Model		
T_{exp} (K)[a]	Liquid mole composition (x_3)	P_{exp} (MPa)	U_c (P) (MPa)	Pressure (MPA)		
				Pressure CPA	PC-SAFT	PR
303.15	0.020	1.02	0.03	0.91	0.95	0.97
303.15	0.021	1.09	0.03	0.98	1.02	1.05
303.16	0.033	1.64	0.03	1.51	1.56	1.60
303.15	0.044	2.07	0.03	2.05	2.09	2.16
303.14	0.056	2.60	0.04	2.62	2.64	2.75
303.15	0.061	2.86	0.05	2.85	2.85	2.97
303.14	0.063	2.94	0.03	2.93	2.94	3.05
303.15	0.071	3.27	0.04	3.35	3.32	3.46
303.16	0.084	3.89	0.03	4.02	3.93	4.14
303.14	0.096	4.52	0.03	4.61	4.47	4.70

[a]$U_c(T) = 0.06$ (K) ; [b] U_c (x_3) = 0.002

Table B.16 Experimental isothermal VLE Data (P-x) and modelling results for the (CH_4 (1)/C_2H_6 (2)/C_3H_8 (3) 3.68/0.22/96.10 wt%) + (CH_3OH (4) /TEG (5)/Water (6) 3.33/91.84/4.83 wt%) system at 313.15 K

Experimental				Model		
T_{exp} (K)[a]	Liquid mole composition (x_3)	P_{exp} (MPa)	U_c (P) (MPa)	Pressure (MPa)		
				Pressure CPA	PC-SAFT	PR
313.16	0.020	1.02	0.03	0.94	0.97	0.96
313.16	0.021	1.10	0.06	1.01	1.04	1.03
313.16	0.033	1.53	0.03	1.54	1.59	1.56
313.16	0.044	1.99	0.03	2.09	2.12	2.10
313.16	0.056	2.53	0.06	2.67	2.68	2.68
313.15	0.061	2.91	0.07	2.90	2.90	2.89
313.15	0.063	3.02	0.04	2.99	2.99	2.97
313.16	0.071	3.28	0.03	3.40	3.38	3.36
313.15	0.084	3.99	0.03	4.07	4.00	4.01
313.15	0.096	4.72	0.03	4.66	4.56	4.55

[a]$U_c(T) = 0.06$ (K) ; [b] $U_c(x_3) = 0.002$

Table B.17 Experimental isothermal VLE Data (P-x) and modelling results for the (CH_4 (1)/C_2H_6 (2)/C_3H_8 (3) 3.68/0.22/96.10 wt%) + (CH_3OH (4) /TEG (5)/Water (6) 3.33/91.84/4.83 wt%) system at 323.15 K

Experimental				Model		
T_{exp} (K)[a]	Liquid mole composition (x_3)	P_{exp} (MPa)	U_c (P) (MPa)	Pressure (MPa)		
				Pressure CPA	Pressure PC-SAFT	Pressure PR
323.15	0.020	1.01	0.03	0.97	1.00	0.95
323.15	0.021	1.13	0.05	1.04	1.08	1.02
323.14	0.033	1.51	0.02	1.59	1.62	1.54
323.16	0.044	1.95	0.02	2.15	2.17	2.07
323.16	0.056	2.68	0.03	2.74	2.74	2.63
323.15	0.061	2.89	0.03	2.97	2.96	2.84
323.15	0.071	3.48	0.03	3.47	3.45	3.29
323.15	0.084	4.05	0.03	4.15	4.09	3.93
323.16	0.096	5.03	0.03	4.74	4.66	4.45

[a]$U_c(T) = 0.06$ (K) ; [b] $U_c(x_3) = 0.00$

Appendix C : Uncertainty calculations

C.1.1. Uncertainty Classification

The measured values determined by any experiment are only complete once the uncertainty results are included. Uncertainty is the quantifiable confidence of the experimental measured values and represents the margin by which the true value of an experiment could be found. This uncertainty determination followed the method outlined in the JCGM guidelines, where the following could be taken as sources of uncertainty(JCGM/WG, 2008)

a) incomplete definition of the measurand.

b) imperfect realisations of the definition of the measurand.

c) nonrepresentative sampling — the sample measured may not represent the defined measurement.

d) inadequate knowledge of the effects of environmental conditions on the measurement or imperfect measurement of environmental conditions.

e) personal bias in reading analogue instruments.

f) finite instrument resolution or discrimination threshold.

g) inexact values of measurement standards and reference materials.

h) inexact values of constants and other parameters obtained from external sources and used in the data-reduction algorithm.

i) approximations and assumptions incorporated in the measurement method and procedure.

j) variations in repeated observations of the measurand under apparently identical conditions.

The uncertainty of a measurement is broken up into types A, and B. Type A is the uncertainty that occurs from the observations from repeated experiments. Type B is the uncertainty that occurs from other sources of uncertainty, such as calibration reports. The following formulas represent the Type A and Type B uncertainties formulas:

Type A

$$u(\theta) = \frac{\sigma}{\sqrt{N}} \tag{C-1}$$

Where the θ is the parameter measure, σ is the standard deviation of the data, and N is the number of repeated data points.

Type B

$$u_i(\theta) = \frac{b}{\sqrt{3}} \tag{C-2}$$

Where $u_i(\theta)$ is the standard uncertainty of a parameter being evaluated, b is the maximum error induced by the type B uncertainty. This was determined assuming a rectangular distribution as there was 100% likelihood the value lay between this distribution.

C.1.1. Standard Uncertainty

The sources of uncertainty that make up an experiment's overall uncertainty is best presented by a calculated standard uncertainty u_i. This is equal to the positive square root of the standard variance. The standard uncertainties for this work can be found in Table A.1

C.1.2. Combining standard uncertainties.

The combined standard uncertainties represented the combination of all A and B-type standard uncertainties. The following equation determined the combined standard uncertainties:

$$\theta = f(\alpha_1, \alpha_2 \ldots . \alpha_n)$$

$$u(\theta) = \sqrt{\left[\left(\frac{\partial\theta}{\partial\alpha 1}\right)_{\alpha_{i\neq 1}} u\alpha 1\right]^2 + [(\frac{\partial\theta}{\partial\alpha 2})_{\alpha_{i\neq 2}} u\alpha 2]^2 + \cdots + [(\frac{\partial\theta}{\partial\alpha n})_{\alpha_{i\neq n}} u\alpha n]^2} \tag{C-3}$$

The following equation shows a simplified combined standard uncertainty of a parameter (θ):

$$u_c(\theta) = \pm\sqrt{\sum_i u_i(\theta)^2} \tag{C-4}$$

Where $u_i(\theta)$ is the standard uncertainty of a parameter being evaluated, where the uncertainty is due to repeatability, uncertainty induced by calibration standards or references, errors in calibration polynomials and so on.

Table C.1 Values of standard uncertainties for equipment used in this study.

Source of uncertainty	**Estimate**
Temperature(T)	
Calibration uncertainty T(K) for probes used in this work	0.05
Calibration uncertainty T(K) for liquid vapour pressure equipment	0.01
T standard (K), CTH 6500	0.02
Pressure(P)	
P standard (MPa), CPC Mensor 8000 (25 MPa gauge)	0.01%

Standard uncertainty (MPa) induced by the pressure transducer (0-35 MPa)	0.02
Composition uncertainty (x_i), Bubble point measurements	
Mass balance uncertainty	
Mass balance model PA423C (1) uncertainty (g) (liquid solution preparation)	0.003
Mass balance model PX5202 (2) uncertainty (g)	0.01

C.1.3. Coverage factor k

The combined standard uncertainty can be multiplied by the coverage factor in-order to include a confidence level for the data. This can be determined using the following formula:

$$U_c = \pm[k * u_c] \quad \text{(C-5)}$$

A value of k=1.65 was chosen as this allows a 95% level of confidence assuming a rectangular distribution, whereas the assumption of a normal distribution would require a coverage factor of k=2 for a 95% confidence level.

C.2. Temperature Uncertainty

The combined standard uncertainty for temperature $u_c(T)$ was determined using the following formula:

$$u_c(T) = \pm\sqrt{u_{rep}(T^2) + u_{calib}(T^2)} \quad \text{(C-6)}$$

Where u_{rep} is the standard uncertainty due to measurement repeatability (Type A), and u_{calib} is the uncertainty due to the calibration polynomial and method.

$$u_{calib}(T) = \pm\sqrt{u_{calib\ cor}(T^2) + u_{std}(T^2)} \quad \text{(C-7)}$$

Where $u_{calib\ cor}(T)$ is the standard uncertainty due to calibration correlation (Type B), and $u_{std}(T)$ is standard uncertainty induced by the standard temperature probe (Type B).

$u_{calib\ cor}(T)$, b was taken as the maximum calibration error of the temperature probes used

$u_{std}(T)$, b was 0.02 K obtained using data from calibration data sheet of the temperature standard.

C.3. Pressure Uncertainty

The combined standard uncertainty of pressure for all pressure measurements was determined using the following formula:

$$u_c(P) = \pm\sqrt{u_{calib\ cor}(P^2) + u_{std}(P^2) + u_{atm}(P^2) + u_{rep}(P^2)} \quad \text{(C-8)}$$

Where:

u_{atm} *(P)* is the standard uncertainty of the CPC Mensor (barometer), (Type B). and b, in this case, is 0.001 MPa.

$u_{calib\ corr}$ *(P)* is the standard uncertainty due to calibration correlation (Type B).

u_{std} *(P)* is standard uncertainty induced by the pressure transducer (Type B)

u_{rep} *(P)* is the standard uncertainty due to measurement repeatability (Type A)

C.4. Molar Composition Uncertainty Bubble point (*TPx*) measurements

The combined standard uncertainty is determined using the respective individual standard uncertainty of the mass balance, masses of respective components, their mole fractions and manufacturer uncertainties. These are type B uncertainties.

The combined standard uncertainty u_{ci} is given by

$$u_{ci} = \pm\sqrt{ub_{xi}\ ^2} \tag{C-9}$$

Where ub_{xi} is uncertainty of the mass balance, combined with uncertainty of the manufacturer.

ub_{xi} is determined using the following equation:

$$ub_{Xi} = \pm\sqrt{[\frac{dx_1}{dm_1} * u(m_1)]^2 + [\frac{dx_1}{dm_2} * u(m_2)]^2 + [\frac{dx_1}{dm_3} * u(m_3)]^2}\ldots\ldots \tag{C-10}$$

Where: If mm_1, mm_2 and mm_3 are the masses of the respective components and MM_1, MM_2 and MM_3 are the molecular masses of the same components, respectively, then applying the root-sum-squared method. This method can be multiplied depending on the number of components in the system.

For the gas components of a system the following formula should be used for $u(m_i)$:

$$u(m_i) = \left[\frac{c * m_i + ub * o}{\sqrt{3}}\right] \tag{C-11}$$

Where:

c is the gas composition uncertainty provided by the manufacturer; and *b* represents the mass balance precision, o represents composition of the gas in the mixture

For the liquid components of a systems the following formula should be used for $u(m_i)$:

$$um_i = [\frac{u\ prep\ mix * mi + ub * wt\%}{\sqrt{3}} \tag{C-12}$$

Where and *ub (precision)* represents the mass balance precision; *u prep mix* represents uncertainty induced by preparing the liquid-liquid solution; $wt\%_i$ represents the weight percent of component *i* in the liquid-liquid solution.